NORTHWESTERN UNIVERSITY

Biomolecule Assembly and Metal Nanostructures

A DISSERTATION

SUBMITTED TO THE GRADUATE SCHOOL
IN PARTIAL FULFILLMENT OF THE REQUIREMENT

for the degree

DOCTOR OF PHILOSOPHY

Field of Chemistry

By

Raymond Jose de Guia Sanedrin

EVANSTON, ILLINOIS

December 2007

@ Copyright by Raymond Jose de Guia Sanedrin

All rights reserved.

ABSTRACT

Biomolecule Assembly and Metal Nanostructures

Raymond Jose de Guia Sanedrin

This dissertation describes the use of alkanethiols and polymers for the development of lithographic affinity and resist array templates that can be utilized for directing the assembly of biological molecules, for building up multilayered polyelectrolyte thin films, and for fabricating metal solid-state nanostructures. The first two chapters of the work described in this dissertation are focused on the use of nanoarrays, in conjunction with various protein immobilization schemes, to probe fundamental biological processes that cannot be addressed by macro- and microarray methodologies. Covalent and divalent metal ion coordination chemistries are utilized to tether biological molecules onto nanoaffinity templates generated using Dip-pen nanolithography (DPN). This high-resolution lithographic technique enables the fabrication of lithographic arrays of alkanethiol self-assembled monolayers (SAMs) with different functional head groups (carboxylate and N-hydroxysuccinimide), which can be used to coordinate Zn (II) ions and covalently bind protein A/G, respectively. The bound metal ions or small proteins specifically bind to the Fc region of antibodies. Biological molecules that are immobilized in such a fashion exhibit high activity and specificity for antigens and virus particles. Site isolation of single virus particles can be further accomplished by controlling the dot diameter features of the DPN-generated templates.

Other “soft” materials that can be assembled onto the DPN-generated alkanethiol templates are polyelectrolytes. Taking advantage of the charged functional pendant groups, these polymers can be electrostatically adsorbed onto the written SAMs. Sequential exposure of the generated alkanethiol SAM templates to oppositely charged polyions afford the fabrication polyelectrolyte multilayer films. The ease of use of the Layer-by-Layer (LbL) assembly in conjunction with the DPN approach offers the ability to tailor and control important parameters such as the sizes and thicknesses of the generated polyelectrolyte multilayer assemblies, and also the chemical functionality at the top most layer of the multilayer films. In principle, any charged materials other than polymers can be immobilized onto the polyelectrolyte multilayered arrays.

Raised and recessed metal nanostructures are generated using a combination of DPN and wet-chemical etching methodology. Polyethylene glycol is used either as a resist or sacrificial material to generate positive or negative patterns, respectively. In the case of positive nanostructure fabrication, the DPN-generated PEG nano size features are used to protect the underlying gold films from oxidization by chemical etching solutions. Negative nanostructure fabrication, on the other hand, is accomplished through passivation of the areas surrounding the DPN-generated PEG patterns with 1-ocatadecanethiol (ODT), dissolution of polymer templates using a simple washing step, and oxidation of the gold areas originally occupied by PEG. The positive and negative nanostructures have well defined shape features, and they can be easily scaled-up using parallel-DPN.

Finally, this dissertation describes a seed mediated approach for synthesizing Au/Ag core-shell prisms with smooth and corrugated surfaces. The shapes, sizes, and optical properties of these core-shells nanostructures can be tailored using various stoichiometric ratios of silver

and gold. Nanoparticles with thicker gold shells and roughened surfaces are produced with decreasing ratios of Au^{3+} and Ag^{+}, and their corresponding surface plasmon bands are red shifted to the near-IR region of the spectrum.

Thesis Advisor: Professor Chad A. Mirkin

ACKNOWLEDGEMENTS

I am very grateful to the following individuals who have contributed in the accomplishment of my goals during my graduate career at Northwestern University.

I thank my advisor, Professor Chad A. Mirkin, for giving me the opportunity to become a part of his research group. I applied at Northwestern University with the sole purpose of joining his group. Chad has always been an excellent mentor; he has given me the freedom to pursue and explore my interest in nanoscience. His guidance has steered me in the right direction, which in return has enabled me to achieve my goals in both research and education.

To my committee members, Professor George Schatz and Professor Peter Stair, I extend my appreciation for all their excellent advice during the various stages of my graduate career.

I extend my deepest appreciation to my family, especially my mom who has always been there encouraging me to pursue my goals. To her I dedicate this dissertation. I also thank Jun, Splong, and Bog for being the best brother and sisters a person could ever have. I would like to acknowledge Ira, Bopeep, and Lala for all the support that they have given me.

To Bobby who has been here with me since the journey from Los Angeles to Chicago, I greatly appreciate his kindness and generosity. He has always encouraged me to do my very best and to never give up on my goals.

I extend my appreciation to all the individuals with whom I had the pleasure of collaborating. To Dr. Seung Woo Lee, Dr. Dimitra Georganopoulou, Dr. Sungho Park, Dr. Jae Won Jang, Dr. Ling Huang, Dr. Steve Wolinsky, Dr. Eunyoung Kim, and Derick Bogadan, I thank them for all the help and advices given to me during my graduate career. Because of them

I am a better scientist. Lastly, I thank the past and present members of the Mirkin group who have been there to lend a helping hand. They have always contributed to the betterment of my graduate career.

TABLE OF CONTENTS

LIST OF FIGURES AND SCHEMES

Page

CHAPTER ONE

CHAPTER TWO

CHAPTER THREE

CHAPTER FOUR

CHAPTER FIVE

CHAPTER SIX

LIST OF TABLES

Page

CHAPTER 3

CHAPTER 6

CHAPTER ONE

Biomolecule Assembly, Metal Nanostructures, and Thesis Overview

1.1. INTRODUCTION

Many scientists around the globe continuously venture in the field of nanoscience to find answers to fundamental questions that arise from studying processes in the nanoscale regime. Scientific breakthroughs in this area have been significant in the past decades and have been the sources for the creation of many novel nanotechnologies, which now greatly impact the macroscopic world. For instance, nanostructured materials, whose at least one spatial dimension is in the size range of 1-100 nm, have been of interest because they exhibit remarkable physical properties, such as surface plasmons, near-field optical effects, quantum effects, electron tunneling, and superparamagnetic phenomena.[1-2] Various synthetic methods and materials have been used to produce highly uniform nanostructures with very interesting shapes. Depending on their compositions, features (sizes and shapes), and properties, these materials can have further applications in catalysis, electronics, optical devices, drug delivery and biosensing.[3-11]

The interface between nanoscience, chemistry, and biology is another area that is of interest because nature has shown how highly functional materials can be synthesized from nanoscale building blocks. The "bottom-up" approach in biological material synthesis can be seen in processes involving cells, which in themselves are a collection of nanoscale systems and structures (enzymes, lipid bilayers, vacuoles, DNA, RNA, and proteins).[2, 12] As an example, most proteins have sizes in the range of 6 to 15 nm, while other biomolecules such as DNA and RNA have diameter features of 2 and 1 nm, respectively. Because of the inherent dimensions of these nano biomaterials, their bioactivities and biomolecular interactions also occur at the nanometer length scale. As a consequence, highly sophisticated tools and techniques are

necessary to characterize such biological systems at the molecular level. In many cases, researchers often times develop and reconfigure instruments to suit such demands.

Many of the advancements in nanoscience and nanotechnology existing today can be attributed to the substantial sophisticated innovations made in the development of tools and methods suitable for characterizing nanomaterials and nanoprocesses. For example, uv-vis spectroscopy had been very useful to many researchers in characterizing and understanding the surface plasmon resonance properties of various metal nanoparticles, such as Ag and Au.[4, 6-8, 13-14] Scanning probe microcopy (SPM) and electron microscopy (EM) had been excellent imaging tools that can elucidate structural details of surface bound adsorbates. Lithography-based methods, on the other hand, are very useful techniques to probe processes at the nanoscale level (i.e. biomolecule interactions)

1.2. LITHOGRAPHIC METHODS

There are a variety of patterning techniques that have been developed over the years. Because of the high-throughput capabilities of photolithography[16-17] and the ability to produce features with high resolution and registration of electron beam lithography,[17] these conventional lithographic techniques have been widely used in industrial applications. They rely on the use of resists and etching protocols that are often times cumbersome because of multiple processing steps. Microcontact printing,[1-2, 18-19] on the other hand, which was developed by the Whitesides group, relies on the use of elastomeric stamps to directly pattern molecules onto a substrates surface. The ease of use of this technique affords the patterning over large areas with resolution

limit approaching 100 nm. It is limited, however, in its ability to generate multiple and chemically diverse patterns.

Since the invention of the STM[20] and AFM,[21] both instruments have had far reaching impacts in various fields including chemistry, biology, and material science. While these instruments are often used as surface imaging tools, their capabilities as lithographic instruments had been realized. In fact, the earliest report on the use of STM as a writing tool was on the transfer of an atom from tip to surface.[22] On the other hand, the first lithographic pattern generated using STM was reported by Schweizer and co-workers wherein single Xe atoms were intentionally positioned on a nickel surface to spell IBM.[23]

The use of an AFM cantilever tip as a tool to deliver organic molecules from tip to surface was first demonstrated by Jaschke and Butt,[24] where they reported on the formation of 1-octadecanethiol (ODT) aggregates on a mica surface. The authors claim that these molecules were only physisorbed on the substrate surface owing to the irregularly shaped appearance and measured heights of the written ODT. The mechanism involved in the transport of molecules was not discussed, and failure to write the ODT molecules on glass and Au surfaces convinced the authors that the organic molecule could only be deposited on the high-energy surfaces of mica.

Similarly, reports on the transport of water to and from an AFM cantilever tip and substrate surface were investigated by the Mirkin group.[25] The authors concluded that the transfer of water from tip to surface was a dynamic process that was dependent on several factors, such as humidity, chemical nature of the substrate surface, and dynamics of the tip motion. Although the focus of the research work was on how lateral force microscopy (LFM)

measurements were affected by water formation, the possibility of using this effect (meniscus formation) as a medium to transfer molecules was also realized. This work was the starting point in the development of the Dip-pen Nanolithography (DPN) methodology and many other variants, such as nanografting, nanoshaving, and nanofountain pen (NFP). Until recently, Weeks and DeYoreo[26] confirmed the formation of a meniscus by monitoring the accumulation of water between an AFM cantilever tip and substrate surface using an environmental scanning electron microscope (ESEM).

Writing water on mica substrates prompted the realization that the possible combinations of molecular inks and substrates that can be used for lithography are limitless given the correct chemistries, parameters, and environmental conditions. The DPN (**Figure 1.1**) technique, which is a direct-write nanolithographic method, is a powerful tool that can deliver diverse materials on a surface with high resolutions and registration. The methodology started as a serial process wherein one single cantilever tip is used for delivering inks from tip to surface. Typically, an AFM cantilever tip (conventional silicon nitride cantilever) is coated with the molecular inks of choice either by immersing the whole AFM cantilever tip assembly in the molecule solution, selectively dipping the silicon nitride tip in a custom designed microwell containing the sample, or depositing volatile materials using high temperature ovens. Upon contact of the coated AFM cantilever tip to a substrate surface, a water meniscus is formed which serves as a medium for molecule transport. Ink molecules are delivered from AFM cantilever tip, through the water meniscus, and to the substrate. A key requirement for writing molecules is that there is some interaction between the ink and the surface. Molecules can either be chemically or physically adsorbed onto the substrate surface. For example, arrays of stable alkanethiols SAMS on Au

Figure 1.1. Schematic representation of the Dip-pen Nanolithography Process

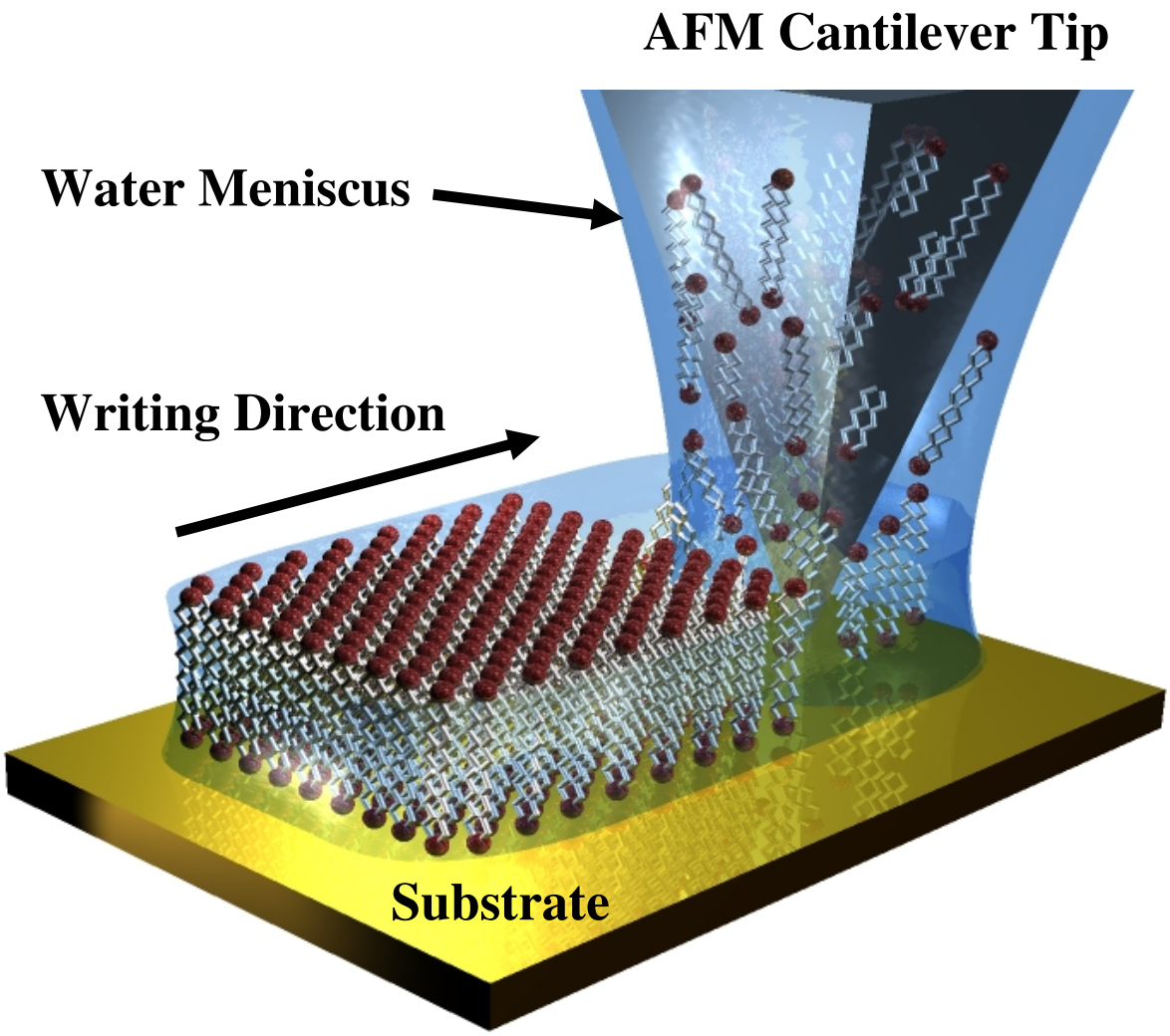
AFM Cantilever Tip
Water Meniscus
Writing Direction
Substrate

surfaces can be generated using DPN owing to the formation of coordination bonds between the thiol moiety of the organic molecule and the metal surface. The generality of this approach makes DPN a very versatile technique that allows the delivery of a variety of inks, such as alkanethiols, silanes, polymers, phospholipids, oligonucleotides, peptides, proteins, polymers, and dendrimers, onto various substrates (SiO, Au, GaAs, Ag and mica).[27-40] Furthermore, multiple functionalities and various features (shapes and sizes) can be written on a single substrate using the described writing methodology. Although the serial DPN process has proven to be an excellent technique owing to its many excellent attributes, very limited number of features can be generated because the writing area of DPN is dictated by the scanning window of most SPM based methods (90 x 90 microns) (**Figure 1.2A**).

Recent advances in AFM cantilever tip fabrication circumvented the writing limitation of DPN. An AFM cantilever with 26 tips (A-26)[41] (**Figure 1.2B**) extended the writing area of the once serial DPN process to millimeter scale patterning with writing time scales similar to that of using a single AFM cantilever tip. The DPN technique has evolved into a parallel process that exceeds the throughput capabilities of other serial lithographic methods. A more impressive innovation was the development of the 2D cantilever pen array, which consisting of 55,000 tips[42] (**Figure 1.2C**). With this invention, rapid prototyping of similar features can be accomplished over a centimeter scale area.

Figure 1.2. (A) Serial and (B-C) parallel Dip-pen Nanolithography process.

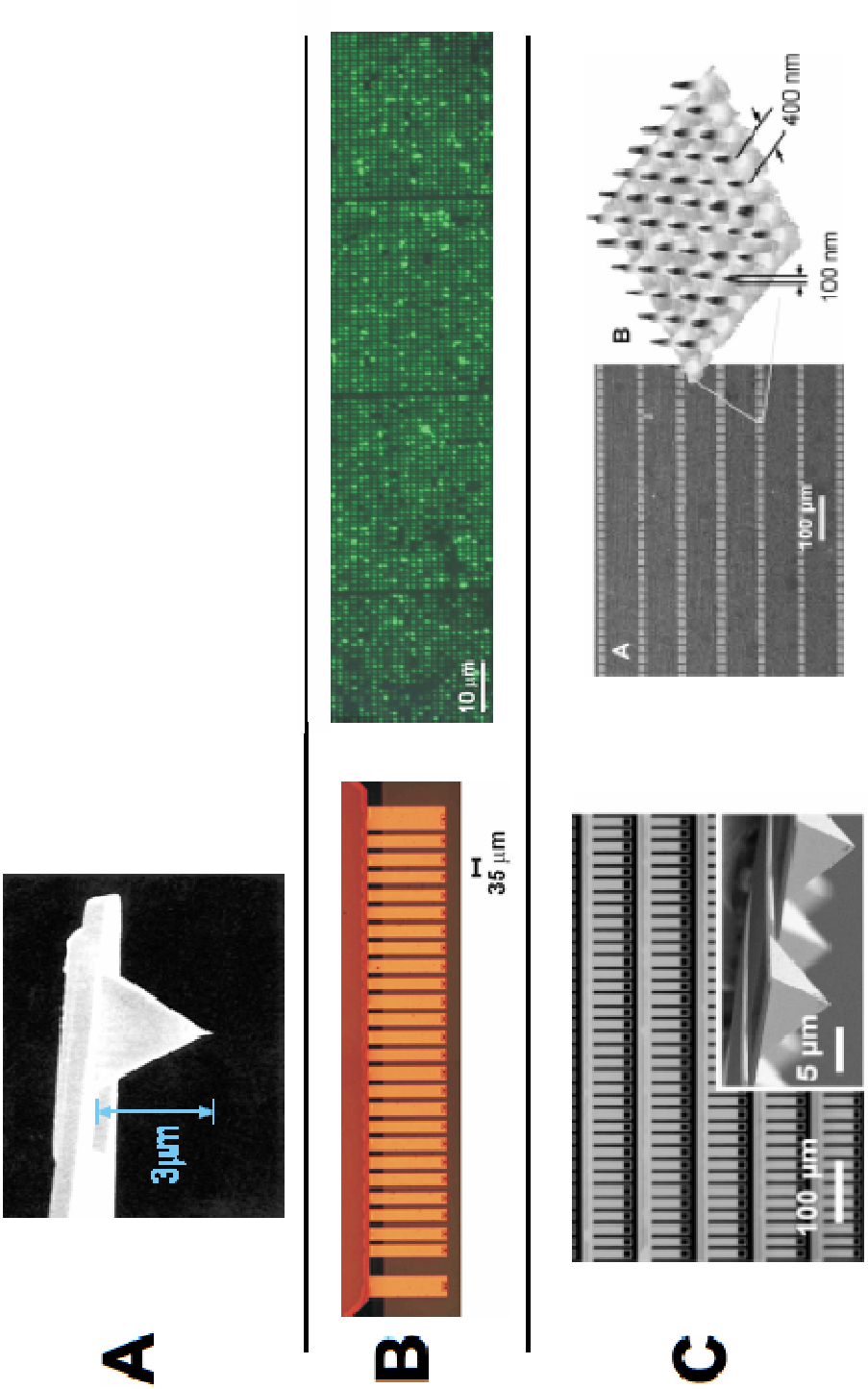
A
3µm
B
10 µm
35 µm
C
400 nm
100 nm
100 µm
5 µm
100 µm

1.3. SURFACE-BASED ASSEMBLIES

1.3.1. Biomolecule Array Assembly

The use of an array format for biomolecule patterning has proven to be a powerful tool for biological studies. Although this technology is very diverse in terms of formats and protocols that can be chosen depending on the research goals of an investigator, they share a common feature which is the ability to perform multiplexed analyses. Significant advances in the areas of biology and medicine have been made since the inception of the array methodology, and are continuously opening up many avenues that are now beginning to be explored. The most commonly studied biomolecules using arrays are nucleic acids and proteins.[43-44] The development of protein arrays, however, is slow compared to that of DNA because of the complex nature of proteins. DNAs are very stable molecules that have uniformly structured hydrophilic backbones. Moreover, they have one single binding site and orientation for hybridizing with complementary DNAs. Proteins, on the other hand, have many different structures, have multiple binding sites, have hydrophobic and hydrophilic domains, and have biological activities that are dependent on the retention of their native structure. Furthermore, it is essential that the functional domains of the proteins (once tethered on a surface) are in the correct orientation in order for binding with target molecules to occur. Because of this a variety of oriented immobilization schemes have been developed. For instance, antibody and carbohydrate binding proteins have been shown to bind with high specificity to the F_c region and carbohydrate moieties at the same region of the antibodies.[45-47]

Powerful tools such as DPN have been shown to indirectly bind antibodies onto nanosize templates. DPN-generated nanosize features of various organic molecules, such as 16-mercaptohexadecanoic acid (MHA) and 11-mercaptoundecanoyl-N-hydroxysuccinimide ester, have been shown to electrostatically[31] and covalently[48] bind antibodies, respectively. Recent reports have shown that antibodies bound to Zn (II) ion nanoarray templates display high binding activities for specific antigens and virus particles.[49]

1.3.2. Layer-by-Layer Assembly

The layer-by-Layer (LbL) assembly is a very simple and inexpensive technique for generating multi-component thin films. As early as 1966, alternate layers of anionic and cationic colloids were fabricated using this technique.[50] The concept of LbL growth was then extended to the multilayer build-up of polyelectrolytes by Decher and co-workers.[51-52] This methodology is based upon the sequential adsorption of polyions on surfaces. Typically, a substrate with a positively charged surface is immersed in a solution containing anionic polyelectrolytes. Upon adsorption, the substrate surface charge is reversed from positive to negative. Exposing the substrate in a cationic polyelectrolyte solution adsorbs the positively charged polymer, which in this case restores the original surface charge. Polyelectrolyte multilayer films are obtained by repeating the immersion cycle. A wide variety of charged species in combination with polyions have been assembled using this technique, including polymers, biomolecules, clays, nanoparticles, and modified zeolites crystals, just to name a few.[53-58] Since most biomolecules bear multiple surface charge, they can be easily co-adsorbed with an oppositely charge polyelectrolyte. For example, Lvov and co-workers[59] have shown that the LbL technique can be

used to immobilize a monolayer of spherical carnation mottle virus. Shi and co-workers[60] reported on the sequential adsorption of polylysine and single stranded oligonucleotides. The simplicity of this methodology affords the precise tailoring of the generated film depending on the molecules used and the number of deposition cycles. Furthermore, using this technique in conjunction with DPN affords the control over shape, size, and composition of pattern features, which will be discussed in chapter 3.

1.4. METAL NANOSTRUCTURES

1.4.1. Metal Nanostructure Fabrication using Alkanethiols

A variety of resist, such as polymers and alkanethiol SAMs (n > 16), in conjunction with various etching methods (i.e. dry, wet, and electrochemical) and lithographic techniques have been used to direct the patterning of underlying metal films.[1-2, 41-42, 62] For Au, Cu, Pt, and Ag surfaces, alkanethiols are the most widely used resist because SAMs of these materials have been demonstrated to effectively protect the underlying metal surface from various etching materials. The quality and critical dimensions of the generated metal nanostructures are dictated by composition of the alkanethiol SAM, presence and density of defects (pinholes), the morphology of the thin film, and the etchant solution. Typically, patterns of alkanethiol SAMs on Au or Ag are generated using various lithographic methods. Incubation of the substrate to etchant solutions generates positive nanostructures (raised features). Since alkanethiols are one of the easiest molecules to use as DPN inks, the Mirkin group has explored the resist capabilities of these materials for generating metal solid state nano features. For example, Au nanostructures

on silicon surfaces can be generated using a combination of ODT SAMs as the resist and cyanide solution as the etchant.[41-42]

Interestingly, the features that can be generated using alkanethiol SAMs are not limited to positive features. Negative features (holes or recessed features) can be generated using a modified procedure that requires the use of an electrochemical set-up.[63] Alkanethiols SAMs are initially patterned onto a metal surface. The surrounding exposed metal regions are backfilled with different kind alkanethiol molecules. Depending on the applied electrochemical potential, the patterned alkanethiols can be selectively desorbed from a surface leaving lithographic patterns of exposed Au regions. Incubation of the substrate to etching solutions generates negative nanostructures.

1.4.2. Seed-Mediated Nanoparticle Synthesis

The seed-mediated growth approach, which was pioneered by Murphy and co-workers,[64] was initially used for synthesizing Ag and Au nanorods and nanowires with controllable aspect ratios. This methodology involves the use of 3-4 nm spherical nanoparticles that acts as seeds for nanoparticle growth. The nanoparticles are added to growth solutions containing metal salts, a weak reducing agent (ascorbic acid), and a surfactant (cetyltrimethylammonium bromide (CTAB)). The authors believe that the CTAB plays significant role in the resulting shape of the growing nanoparticles.[65] The aspect ratios of the synthesized rods and wires can be controlled by varying the chain length of the surfactant material. Interestingly, slight changes in the reaction condition results to the synthesis of other shaped nanoparticles, such as cubes, blocks, and tetrapods. Recent reports from the Mirkin group[66] showed that prism shaped Au

nanoparticles with average edge length and thickness of 144 and 8 nm, respectively, can be synthesized using the seed-mediated growth approach. Furthermore, this synthetic method is also amenable for the synthesis of core-shell nanostructures, which will be discussed in chapter 6.

1.5. DISSERTATION OVERVIEW

1.5.1. Chapter 2: Biologically Active Protein Nanoarrays Generated via Parallel Dip-pen Nanolithography

This chapter describes the fabrication of biologically active protein nanoarrays using parallel-DPN. Amine reactive N-hydroxysuccinimide terminated alkyl thiol templates were generated using a cantilever with 26 tips via parallel-DPN with feature sizes ranging from 150 to 650 nm. The N-hydroxysuccinimide moieties were used to covalently couple protein A/G. The generated protein nanoarrays are used to capture antibodies through affinity binding while preserving their biological recognition properties. Moreover, I describe the versatility of the parallel-DPN method for making many similar structures in a relatively high throughput manner (14,000 dots in 10 min).

1.5.2. Chapter 3: Probing the Activity of Antibodies for HIV in the Context of Nanoarrays Generated Via Dip-Pen Nanolithography

CD4-dependent and independent antibodies against HIV were immobilized onto Dip-Pen Nanolithography (DPN) generated templates using Zn (II) mediated coordination chemistry, and were used to bind HIV particles onto the surface. Virus binding onto the DPN-generated antibody templates is highly dependent on the feature size of the templates and the type of

antibody bound to the metal ion dot features. Single or a collection of virus particles can be bound onto size features of 200–300 and >300 nm, respectively. Among the antibodies used, the CD4-independent 2F5 antibody templates exhibited the most bound viruses while the CD4-dependent antibody templates displayed the least.

1.5.3. Chapter 4: Nanostructured Polyelectrolyte Multilayer Organic Thin Films Generated via Parallel Dip-pen Nanolithography

Polyelectrolyte multilayer (PEM) organic thin films with diameters ranging from 80 to 200 nm were generated from dip-pen nanolithography (DPN) fabricated templates. The PEM films upon adsorption of each polyelectrolyte layer exhibited a linear height increase. Through the use of multi-pen AFM cantilever probes, parallel fabrication of the PEM features with nanoscale resolution can be achieved. This capability demonstrates the versatility of the parallel DPN approach and its applicability to building nano- and micro-structures in conjunction with the LBL method.

1.5.4 Chapter 5: Polyethylene Glycol as Resist and Sacrificial Material for Generating Positive and Negative Nanostructures

This chapter describes the fabrication of positive and negative nanostructures using a combination of Dip-pen Nanolithography and wet-chemical etching methodology. Polyethylene glycol, which is a polymer often used to block the non-specific binding of biomolecules onto surfaces, is used either as a resist or sacrificial material to generate raised metal features or recessed patterns, respectively. In the case of positive nanostructure fabrication, the DPN-

generated PEG nano size features are used to protect the underlying gold film from oxidization by chemical etching solutions. Negative nanostructure fabrication, on the other hand, is accomplished by the passivation of the areas surrounding the DPN-generated PEG patterns with 1-ocatadecanethiol, dissolution of the polymer lithographic feature using a simple washing step, and oxidation of the gold areas originally occupied by PEG. The positive and negative nanostructures have well defined shape features, and they can be easily scaled-up using parallel-DPN.

1.5.5. Chapter 6: Seed Mediated Growth of Bimetallic Prisms

This chapter describes the synthesis of prism, corrugated surface, and spherical shaped bimetallic core-shell nanoparticles. The optical properties and physical attributes (sizes and shapes) of these core-shells can be tailored using various stoichiometric ratios of gold and silver. Decreasing ratios of Au^{3+} and Ag^{+} results in nanoparticles with thicker gold shells and roughened surfaces, and surface plasmon bands that are red shifted from the visible to the near-IR region of the spectrum.

CHAPTER 2

Biologically Active Protein Nanoarrays Generated via Parallel Dip-pen Nanolithography

2.1. INTRODUCTION

Proteins immobilized on surfaces have been extensively investigated because of their importance in drug screening, protein analysis, and medical diagnostics.[1-3] Several methods for protein immobilization on various surfaces have been reported, including photolithography,[4] microcontact printing (μ-CP),[5] e-beam lithography,[6] and certain scanning probe microscope (SPM) based lithographies.[7] Of these techniques, SPM based lithography methods provide access to the smallest features which, in principle, allow for a smaller chip size with many more reactive sites than conventional microscale techniques. Among the SPM based lithographies, Dip-Pen Nanolithography (DPN), in particular, is the only one with the demonstrated capability of generating arrays with over hundreds of features. Importantly, bio-molecular arrays with extremely small features open the door for single-particle (proteins, virus, and cells) studies in biology.[8]

Unfortunately, most single probe methods are limited with respect to scaling (typically 90 x 90 μm) or the ability to directly deposit soft matter, two essential capabilities for realizing highly miniaturized biomolecular nanoarrays.[7, 9] DPN, however, can be used to deliver many types of soft matter reagents to nanoscopic regions of a target substrate with high resolution and registration.[10] Importantly, DPN has been used to immobilize biomolecules such as proteins [9a-9d], DNA [9e] and more recently single viruses [9f] on a variety of substrates with indirect or direct-write methods. To address the (90 x 90) μm pattern area limitation of DPN, centimeter-scale and sub-100 nm resolution patterning through the use of multiple pen cantilever arrays has been reported by our group in the context of small molecules used as a resist to fabricate highly

miniaturized solid-state structures.[11] This capability allows one to make many similar structures that span macroscopic distances (cm) in a relatively high throughput manner.[12]

Using DPN, proteins have been deposited on gold, nickel oxide, and pretreated glass substrates from chemically modified single cantilever tips.[9] A variety of protein-surface interactions have been used in DPN, such as chemisorption [9c,9d] or electrostatic attraction.[9b] Often times, however, adsorption leads to full or partial denaturation of the proteins and therefore a loss of function.

To generate biologically active immobilized antibodies, protein A, protein G, and protein A/G have been used to optimize antibody orientation and minimize denaturation.[13] It is well known that protein A and protein G have the affinity to bind to the Fc (Fragment crystallizable) region, which is the tail region of a Y-shaped antibody.[13] Their binding affinities, however, are relatively weaker compared to that of monoclonal antibodies and their respective antigens. Protein A/G, on the other hand, is a genetically engineered protein that is designed to contain four Fc binding domains from protein A and two from protein G, which allow for enhanced binding affinity.[13] By using this property and coupling it with the parallel DPN patterning technique, we demonstrate centimeter-scale protein patterning which exhibits enhanced binding properties. In particular, we present an indirect approach to fabricating features with biologically active antibodies using templates made by the covalent attachment of protein A/G to arrays of DPN-generated 11-mercaptoundecanoyl-N-hydroxysuccinimide ester ($NHSC_{11}SH$, ProChimia, Co., Gdansk, Poland) on gold surfaces. This is the first example of the use of parallel SPM capabilities to generate arrays of protein structures.

2.2. EXPERIMENTAL

2.2.1. Materials

11-mercaptoundecyl-tri(ethylene glycol) and $NHSC_{11}SH$ were purchased from ProChimia Co., Poland. Antibodies (anti-β-galactosidase, anti-ubiquitin, anti-human IgG), proteins (protein A/G, ubiquitin, galactosidase, and human IgG) were purchased from Sigma-Aldrich. All chemicals and biomaterials were used as received.

2.2.2. Fabrication of $NHSC_{11}SH$ lithographic patterns via DPN

All DPN patterning was done with an Nscriptor™ AFM (NanoInk, Inc., Chicago, IL) driven by custom lithography software (NanoInk, Inc., Chicago, IL) and passive multi-probe arrays (k = 0.097 N/m, NanoInk, Inc., Chicago, IL). Au substrates were prepared via thermal evaporation with a 10 nm Ti adhesion layer and subsequently coated with 50 nm Au under vacuum conditions (pressure $< 1 \times 10^{-7}$ Mbar). The obtained Au substrates were used immediately for DPN experiments. The multi-pens were coated with $NHSC_{11}SH$ and were used to generate dot features with various sizes ranging from 100 to 1000 nm under ambient conditions (22 - 24 °C, 30 - 36 % relative humidity) (**Scheme 2.1**). The substrates containing the DPN-generated dot features were then immersed in a 10 mM ethanol solution of 11-mercaptoundecyl-tri(ethylene glycol) (PEG, ProChimia, Co., Gdansk, Poland) for 20 min, rinsed with ethanol, and then dried with nitrogen. PEG has previously been used to prevent the nonspecific adsorption of proteins onto unpatterned gold areas.[14]

Scheme 2.1. Schematic representation of the process used to obtain biologically active antibodies on protein A/G which is covalently bound to 11-mercaptoundecanoyl-*N*-hydroxysuccinimide ester (NHSC11SH) nanoscale features patterned using DPN.

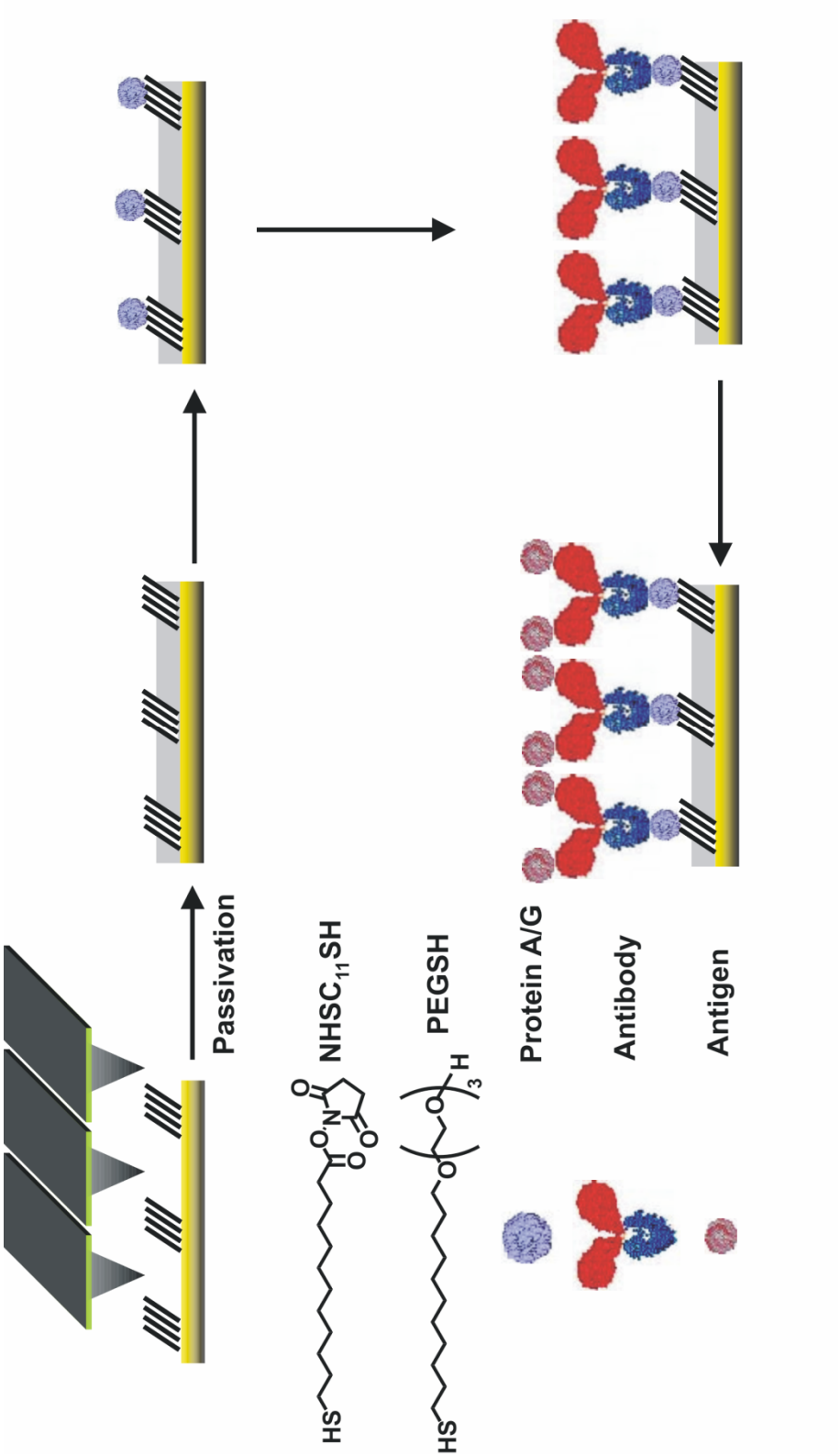
Passivation
NHSC11SH
PEGSH
Protein A/G
Antibody
Antigen

2.2.3. Antibody immobilization and antigen binding

Antibodies were immobilized onto the DPN generated $NHSC_{11}SH$ patterns by subsequent incubation of the Au substrate in a 15 μg/mL protein A/G solution (phosphate-buffered saline (PBS) buffer, pH 7.4, 1 hr.) and then in a 15 μg/mL antibody (anti-ubiquitin, anti-human IgG, or anti-β-galactosidase) solution (PBS buffer pH 7.4, 1 hr.). Antigens were bound to the immobilized antibodies through exposure of the Au substrate in a 15 μg/mL antigen (ubiquitin, human IgG, or β-galactosidase protein) solution (PBS buffer, pH 7.4, 1 hr). Tapping mode images were obtained using Nanoscope IIIa and MultiMode microscope (Digital Instruments, Santa Barbara, CA) and the fluorescence images were taken using Zeiss Axiovert 100 microscope (Carl Zeiss Inc., Thornwood, NY).

2.3 RESULTS AND DISCUSSION

The DPN-generated $NHSC_{11}SH$ dot arrays served as a template for the immobilization of protein A/G. Self-assembled monolayers (SAMs) of *N*-hydroxysuccinimide (NHS) ester have been widely used for the immobilization of the biomolecules, such as nucleic acids, enzymes, and proteins, because of their high reactivity with the primary amine groups of biomolecules.[15] However, direct patterning of molecules containing NHS ester moieties has not been explored using μ-CP or DPN. Because of the abundance of lysine side chains and terminal amine groups in protein A/G, attachment onto the DPN patterned SAMs can be achieved through covalent coupling. This is accomplished by immersing the $NHSC_{11}SH$ patterned substrates in an aqueous protein A/G solution. Nanoscale arrays of the covalently attached protein A/G were imaged by tapping mode atomic force microscopy (TMAFM). Although the height difference between

$NHSC_{11}SH$ features coupled to protein A/G and the as-prepared $NHSC_{11}SH$ features are very small (approximately 0.5 nm), the phase image shows a large contrast between protein A/G covered features and PEG passivated non-patterned areas (**Figure 2.1**). This can be attributed to the difference in stiffness and viscoelasticity of the passivating molecule and the covalently attached protein.[16]

To generate nanoscale antibody-based arrays, DPN-generated highly dense dot arrays (23,400 dots with 1 μm dot-to-dot spacing) of $NHSC_{11}SH$ covalently coupled to protein A/G were incubated in a solution of Alexa Fluor 594-labeled human IgG solution (15 μg/mL, PBS buffer, pH 7.4) for 1 hr. The substrates were subsequently rinsed with PBS buffer, Tween-20, and NANOpure water in an ultrasonic bath for 10 sec to remove loosely adsorbed human IgG. The obtained nanoarrays of human IgG were then investigated by TMAFM and fluorescence microscopy (**Figure 2.2**). Importantly, the feature size of IgG nanoarrays can be adjusted from 100 to 650 nm by simply adjusting the tip-surface contact time. Regardless of the dot diameter, the patterned human IgG nanoarrays are 8.0 nm in height, which is comparable to values previously reported in the literature (**Figure 2.3**).[7a,7c,13f,17] Furthermore, the fluorescence microscopy images confirm the adsorption of Alexa Fluor 594-labeled human IgG immobilized on the generated protein A/G arrays (**Figure 2.2b and 2.3b**). Both the height profile and the fluorescence images suggest that the antibodies were adsorbed onto the DPN-generated protein array templates.

In order to demonstrate the generality of this approach to protein patterning, anti-*β*-galactosidase and anti-ubiquitin nanoarrays (14,000 dots with 2 μm dot-to-dot spacing) were prepared in a similar manner to that used for human IgG. The patterned anti-*β*-galactosidase

Figure 2.1. (a) Topography and (b) phase tapping mode AFM (TMAFM) images of nine protein A/G dots with successively decreasing diameters generated by using different contact times between an AFM cantilever tip and a gold substrate. [650 nm:8 sec, 580 nm:7 sec, 510 nm:6 sec, 450 nm:5 sec, 390 nm:4 sec, 320 nm:3 sec, 260 nm:2 sec, 200 nm:1 sec, 150 nm:0.5 sec].

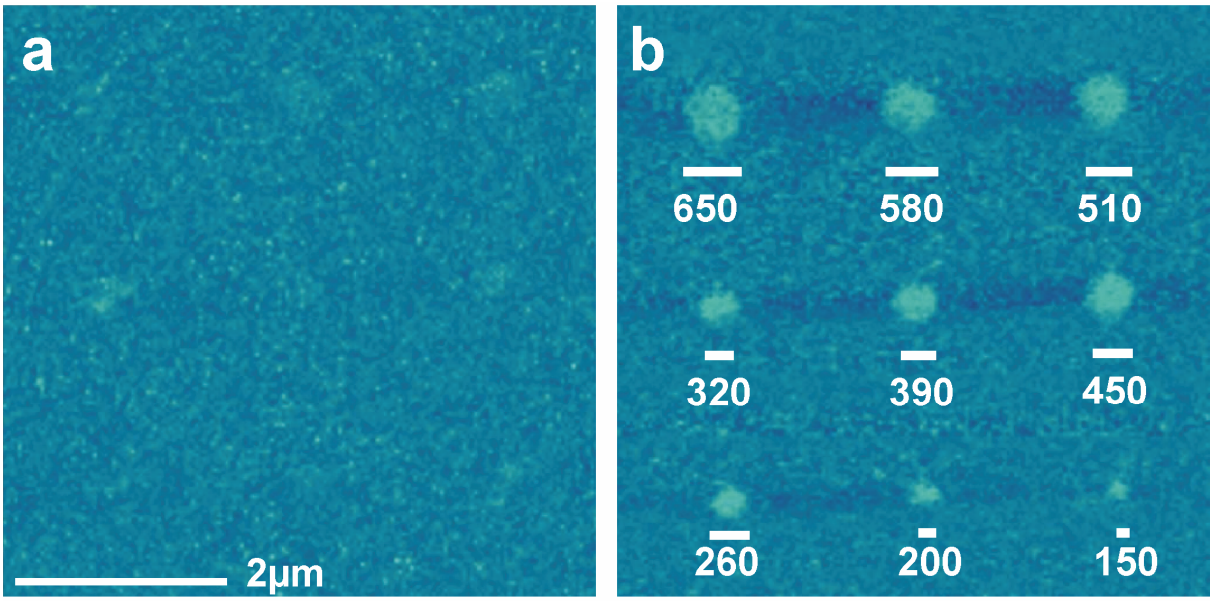
a
2µm
b
650
580
510
320
390
450
260
200
150

Figure 2.2. (a) Topographical TMAFM image and its corresponding height profile of fluorescein isothiocyanate Alexa Fluor 594-labeled human IgG nanoarrays immobilized onto protein A/G templates. (b) Representative fluorescence microscopy image of Alexa Fluor 594-labeled antibody nanoarray patterns. The patterns span a distance of 1 cm.

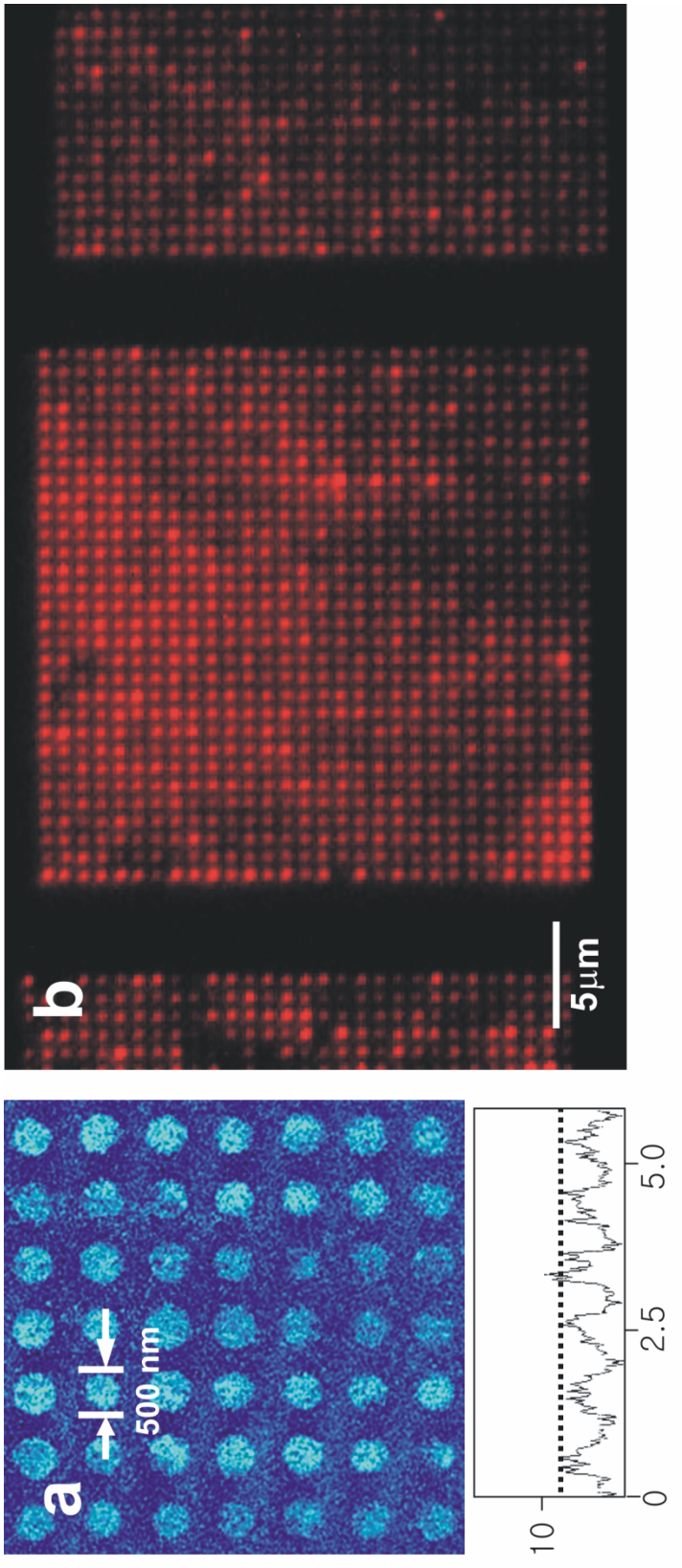
a
500 nm
b
5μm
10
0
2.5
5.0

Figure 2.3. (a) Topographical TMAFM image and its corresponding height profile of fluorescein isothiocyanate (FITC)-labeled human IgG nanoarrays immobilized onto protein A/G templates. (b) Representative fluorescence microscopy image of FITC-labeled human IgG antibody nanoarray patterns (Inset shows zoomed image).

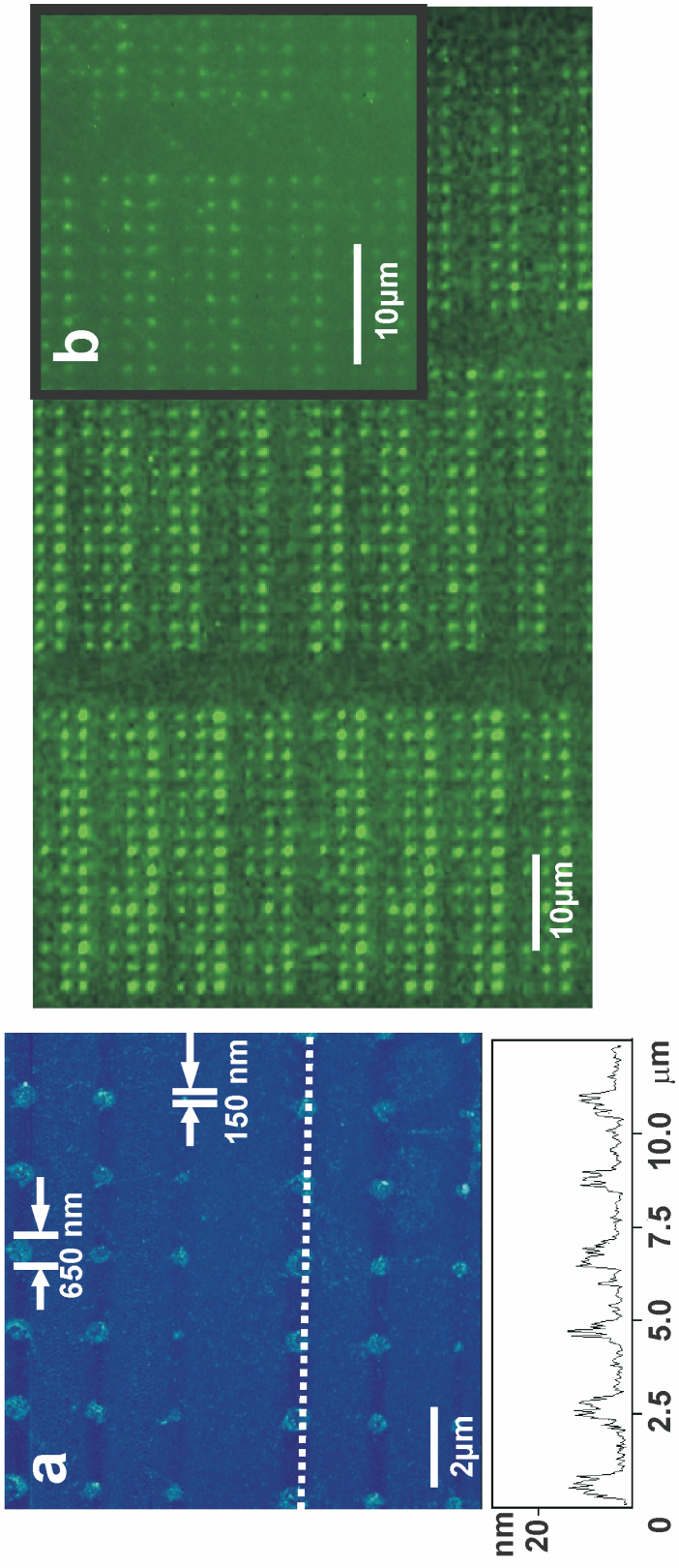
a
650 nm
150 nm
2µm
b
10µm
10µm
nm
20
0
2.5
5.0
7.5
10.0
µm

(**Figure 2.4a**) and anti-ubiquitin (**Figure 2.5a**) nanoarrays are approximately 6.8 nm and 6.5 nm in height, respectively. The biological activity of the patterned antibodies on protein A/G were evaluated by incubating the substrates in a solution containing either Alexa Fluor 594 labeled *β*-galactosidase (15 μg/mL) or Alexa Fluor 488 labeled ubiquitin (15 μg/mL) in PBS buffer with pH 7.4 for 2 hr. After washing the substrates with PBS buffer solution and Tween-20, they were sonicated for 10 sec in an ultrasonic bath. The substrates were then imaged using TMAFM and fluorescence microscopy. The binding of the Alexa Fluor 594 labeled *β*-galactosidase molecules to the anti-*β*-galactosidase increased the height of the patterned features from 6.8 nm to 9.5 nm (**compare Figure 2.4a and 2.4b**). Uniform *β*-galactosidase binding can be observed from the fluorescence images, (**Figure 2.4c**). Importantly, no binding was observed when the arrays were exposed to fluorophore-labeled ubiquitin protein. On the other hand, the binding of the FITC labeled ubiquitin molecules to the anti-ubiquitin increased the height of the patterned features from 6.5 nm to 8.5 nm (**Figure 2.5a and 2.5b**). Uniform ubiquitin binding can be observed from the fluorescence images (**Figure 2.5c**). No binding was observed when the arrays were exposed to fluorophore-labeled BSA protein. These demonstrate that the arrays of immobilized antibodies retained their biological activity after immobilization.[9c,18]

Figure 2.4. Topographical TMAFM images and their corresponding height profiles of anti-β-galactosidase nanoarrays immobilized on protein A/G templates (a) before and (b) after incubation in β-galactosidase protein solution. (c) Fluorescence microscopy image of the Alexa 594-labeled b-galactosidase complexes nanoarrays.

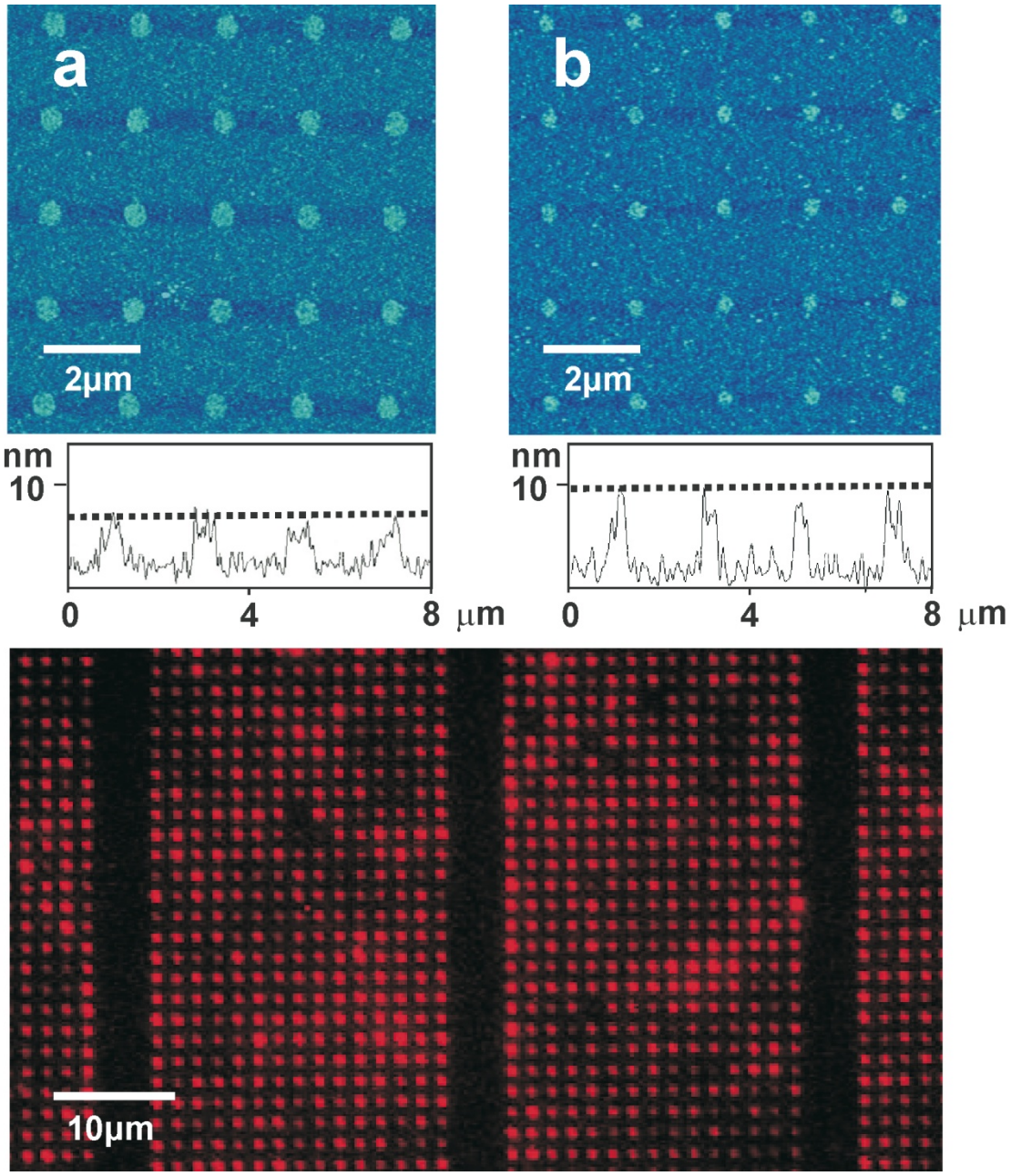
a
2μm
b
2μm
nm
10
0
4
8 μm
nm
10
0
4
8 μm
10μm

Figure 2.5. Topographical TMAFM images and their corresponding height profiles of anti-ubiquitin nanoarrays immobilized on protein A/G templates (a) before and (b) after incubation in ubiquitin protein solution. (c) Fluorescence microscopy image of the Alexa 488-labeled ubiquitin complexes nanoarrays.

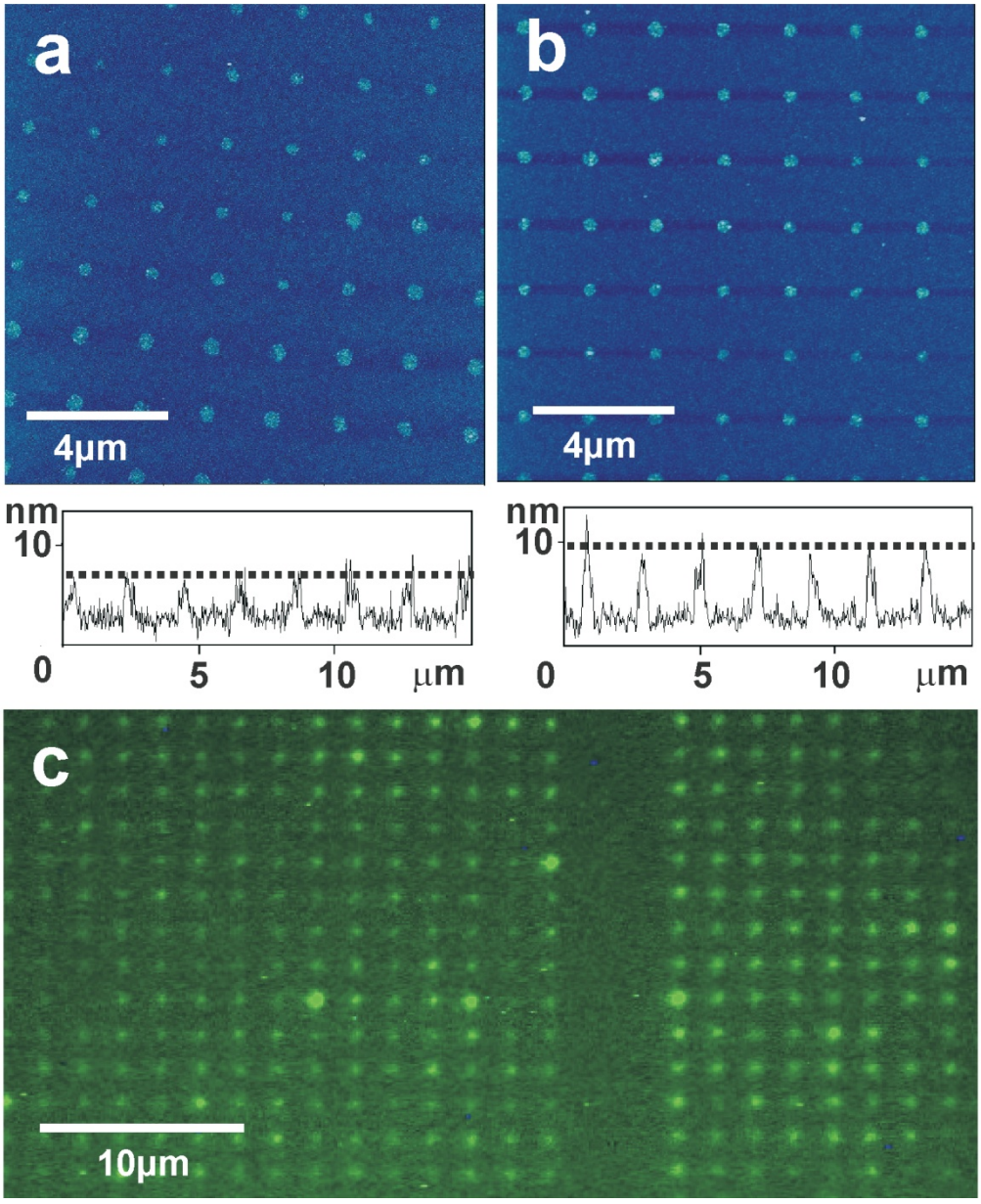
a
4µm
b
4µm
nm
10
0
5
10
µm
nm
10
0
5
10
µm
c
10µm

2.4. CONCLUSION

We have demonstrated that the amine-reactive alkylthiol molecule, $NHSC_{11}SH$, can be used as a template molecule for high-throughput DPN-based protein patterning. Through the use of the affinity binding of the antibodies on protein A/G, biologically active antibody nanoarrays can be generated over macroscopic distances through parallel DPN, demonstrating the versatility of the approach for making many similar antibody structures in a relatively high throughput manner. Although this approach is currently limited to the deposition of only one type of protein, this work is a crucial first step toward building massive biomolecular libraries with feature sizes that are unattainable by other methods and on par with or smaller than the size of many important biological structures (e.g. virus, spores, and cells). This work will challenge researchers in nanoscience and biology to consider new ways of using such patterned interfaces to probe biological systems.

CHAPTER 3

Probing the Activity of Antibodies for HIV in the Context of Nanoarrays Generated Via Dip-Pen Nanolithography

3.1. INTRODUCTION

Recent advances in the development of nanolithographic tools such as Dip-Pen Nanolithography (DPN) point towards ways of manipulating viruses at the single particle level by using nanoarrays for virus immobilization.[1-2] Indeed, with Tobacco Mosaic Virus (TMV), it has been shown that one can immobilize and manipulate the virus at the single particle level.[1] In the TMV studies, metal ions were used as bridging groups for the carboxylate terminated nanofeatures and the virus particles. Another common way of immobilizing viruses is through the use of surface-confined antibodies. However, when one utilizes templates with nanoscale features, the antibody orientation and activity becomes critical. Indeed, surface immobilization of antibodies can lead to a variety of antibody sites and orientations, some of which are active and others inactive. With microscale or larger features, there is typically enough surface area to ensure the immobilization of the antibody in an active state or orientation. With smaller features, one does not always have a large enough area to ensure the immobilization of the antibodies at each feature site in active form. Therefore, an excellent assay for the activity of an antibody immobilized via a particular strategy is to evaluate its performance in the context of both micro- and nanoarrays. An inefficient antibody immobilization strategy may yield good activity in the context of a microarray but not a nanoarray, while an efficient strategy will exhibit high activity regardless of feature size.

In this study, we use DPN-generated nanoarray templates of a variety of antibodies to probe their activity towards HIV-1 and their ability to manipulate the virus at the small collection of, or individual, particle level. HIV is one of the most important viruses in the infectious disease arena because of its enormous worldwide impact. Many techniques have

been developed to study its structure and composition in a variety of environments.[3-13] This has catalyzed the development of several diagnostic systems for the disease, including ones based upon polymerase chain reaction (PCR) and a nanoarray based assay that relies on using antibodies to HIV p 24 gag for the detection of the gag protein in serum and plasma samples of HIV patients.[14] This nanoarray system utilizes a three-component sandwich assay that employs gold nanoparticles modified with polyclonal HIV anti-p24 IgG as probes and uses a scanning probe microscope (SPM) or reverse transcriptase polymerase chain reaction (RT-PCR) as the readout device. In the study presented herein, we utilize an indirect approach to fabricate virus nanoarrays through the use of antibodies that are adsorbed onto nanoarray templates through Zn^{2+}-coordination chemistry. This is a new and very effective approach to antibody immobilization.[15] We use the immobilization process to examine the relationship between feature size and activity for a variety of antibodies down to the single virus particle level.

In a typical experiment, lithographic patterns of 16-mercaptohexadecanoic acid (MHA) were generated using either serial or parallel-DPN methods (**Scheme 3.1**). Briefly, a single cantilever or an array of cantilevers was coated with MHA by dipping them into a 10 mM MHA solution for 10 seconds. The coated tips were then used as pens in a DPN experiment to make dot features with diameters ranging from 200 to 1000 nm on a gold substrate. The exposed gold areas of the substrates were then passivated with 11-mercaptoundecyl-tri(ethylene glycol) (PEG) by immersing them into an ethanolic solution of the PEG adsorbate for 1 hr. The patterned structures were rinsed with copious amounts of ethanol and then immersed in a 5 mM ethanolic solution of zinc nitrate hexahydrate ($Zn(NO_3)_2 \cdot 6H_2O$) for at least 12 hours. The substrates were washed with ethanol, dried with nitrogen, and subsequently incubated with 100

μg/mL antibody solution in a humidity chamber at ambient temperature for 2 hrs. The substrates were then rinsed with 0.1 M PBS buffer solution and incubated with aldrithiol-2 (AT-2) treated HIV-MN[10] (provided by Jeffrey Lifson, NCI, Frederick) at 37 ˚C for 2 hrs. The substrates were then dip washed in a PBS buffer solution, dried, and characterized by tapping mode atomic force microscopy (TMAFM) and fluorescence microscopy.

3.2. EXPERIMENTAL

3.2.1. Materials

16-mercaptohexadecanoic acid (MHA) and 11-mercaptoundecyl-tri(ethylene glycol) (PEG) were purchased from Sigma Aldrich and Prochimia, Corporation respectively. Antibody and HIV solutions were either purchased from Cliniqa or generously provided by NIH. All chemicals and antibodies were used as received. Virus particles were treated with aldrithiol-2 (AT-2) to render them not infectious.

3.2.2. Zn(II) Mediated Approach for Antibody and Virus Particle Immobilization

Lithographic patterns of MHA were generated using either serial or parallel-DPN methods, Scheme 1. Briefly, a single cantilever or an array of cantilevers was coated with MHA by dipping them into a 10 mM MHA solution for 10 seconds. The coated tips were then used as pens in a DPN experiment to make dot features with diameters ranging from 200 to 1000 nm on a gold substrate. The exposed gold areas of the substrates were then passivated with PEG by immersing them into an ethanolic solution of the PEG adsorbate for 1 hr. The patterned structures were rinsed with copius amounts of ethanol and immersed in a 5 mM

Scheme 3.1. Schematic representation of the binding of HIV-1 molecules on antibodies adsorbed via metal ion coordination.

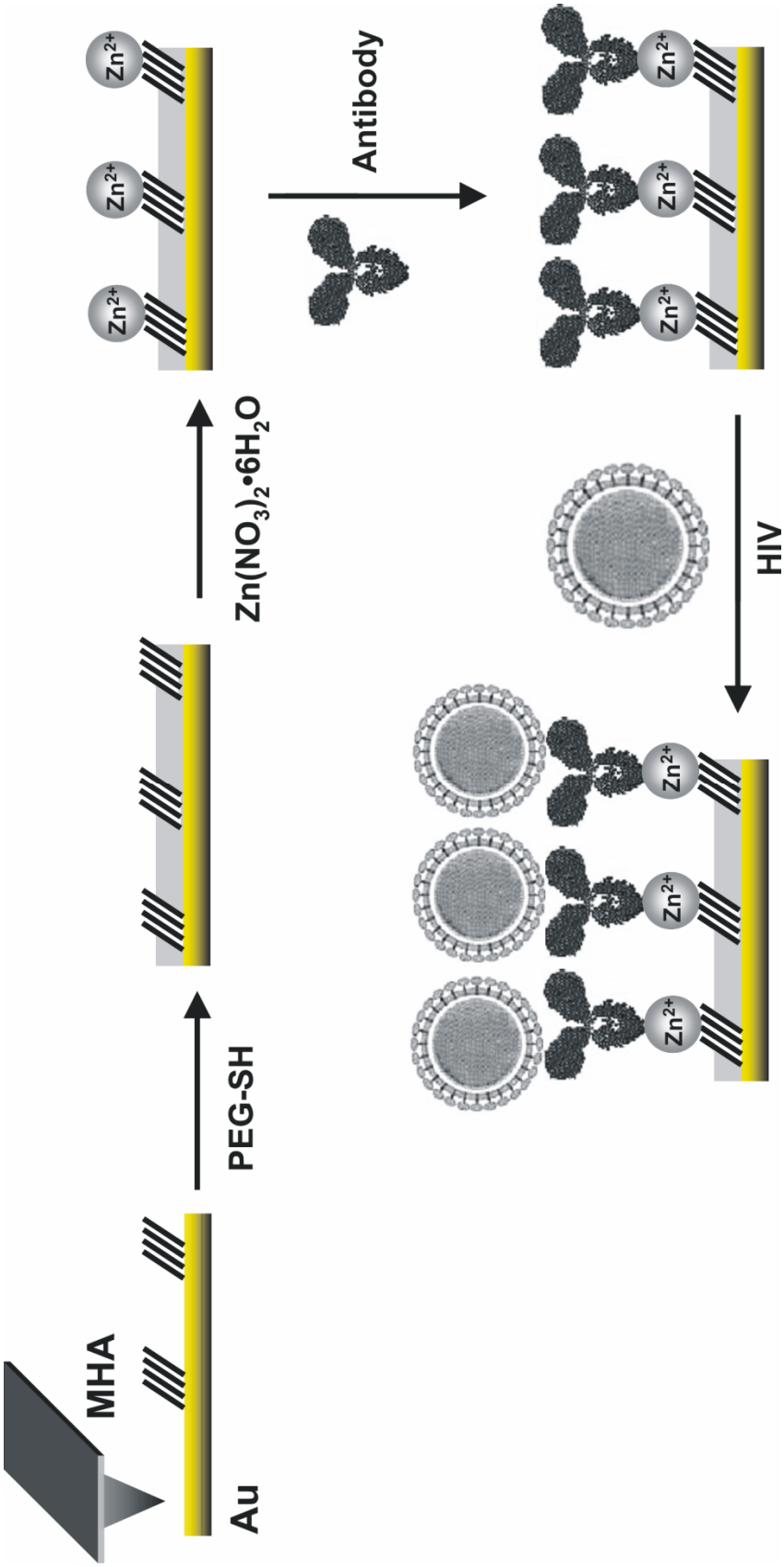
MHA
Au
PEG-SH
$Zn(NO_3)_2 \cdot 6H_2O$
Antibody
HIV
Zn^{2+}

ethanolic solution of zinc nitrate hexahydrate (Zn(II)) for at least 12 hours. The substrates were washed with ethanol, dried with nitrogen, and subsequently incubated in a 100 μg/mL antibody solution (2 hrs, room temperature). They were then rinsed with 0.1 M PBS buffer solution and exposed to a solution of HIV-1 (2 hrs, 37˚ C). The substrates were then dip washed in a PBS buffer solution, dried with Kimwipes™, and characterized by tapping mode atomic force microscopy (TMAFM) and fluorescence microscopy.

3.3. RESULTS AND DISCUSSION

In order to investigate how various antibodies can effect HIV-1 capture onto DPN-generated templates, mono- and polyclonal antibodies, specific to epitopes of the gp120 and gp41 proteins on the surface of an HIV particle, were adsorbed onto Zn (II) modified MHA templates. Our group has shown recently that Zn ions are excellent linkers for protein immobilization, and that immobilized antibodies are often highly active with respect to antigen-antibody binding.[9] All antibodies that were used in this work show excellent binding as evidenced by TMAFM images (**Figure 3.1**). Height profiles are consistent with a monolayer of the antibodies adsorbed onto the DPN-generated templates. 2F5 (**Figure 3.1A**), 2G12 (**Figure 3.1B**), and polyclonal anti-gp120 (**Figure 3.1C**) exhibit an average of 6.8±0.8, 5.6±0.2, and 7.3±0.9 nm height increase upon antibody adsorption, respectively. Moreover, the adsorption of the fluorophore (alexa fluor 594) labeled polyclonal gp120 antibody confirms the immobilization of the antibody on the DPN-generated templates, Figure 1D. Templates that were exposed only to the dye solution did not fluoresce, showing that the measured fluorescence is due to the dye labeled immobilized antibodies.

Figure 3.1. TMAFM images and corresponding height profiles of (A) 2F5, (B) 2G12, and (C) polyclonal gp-120 antibodies immobilized on Zn(II)-MHA generated DPN templates. (D) Fluorescence images of Alexa fluor labeled polyclonal gp-120 antibody adsorbed onto the generated templates. The inset shows antibody arrays that were generated using an array of 26 cantilevers (although only two nanoarrays are shown, a total of 26 arrays with 5200 dots were generated in ~20 min).

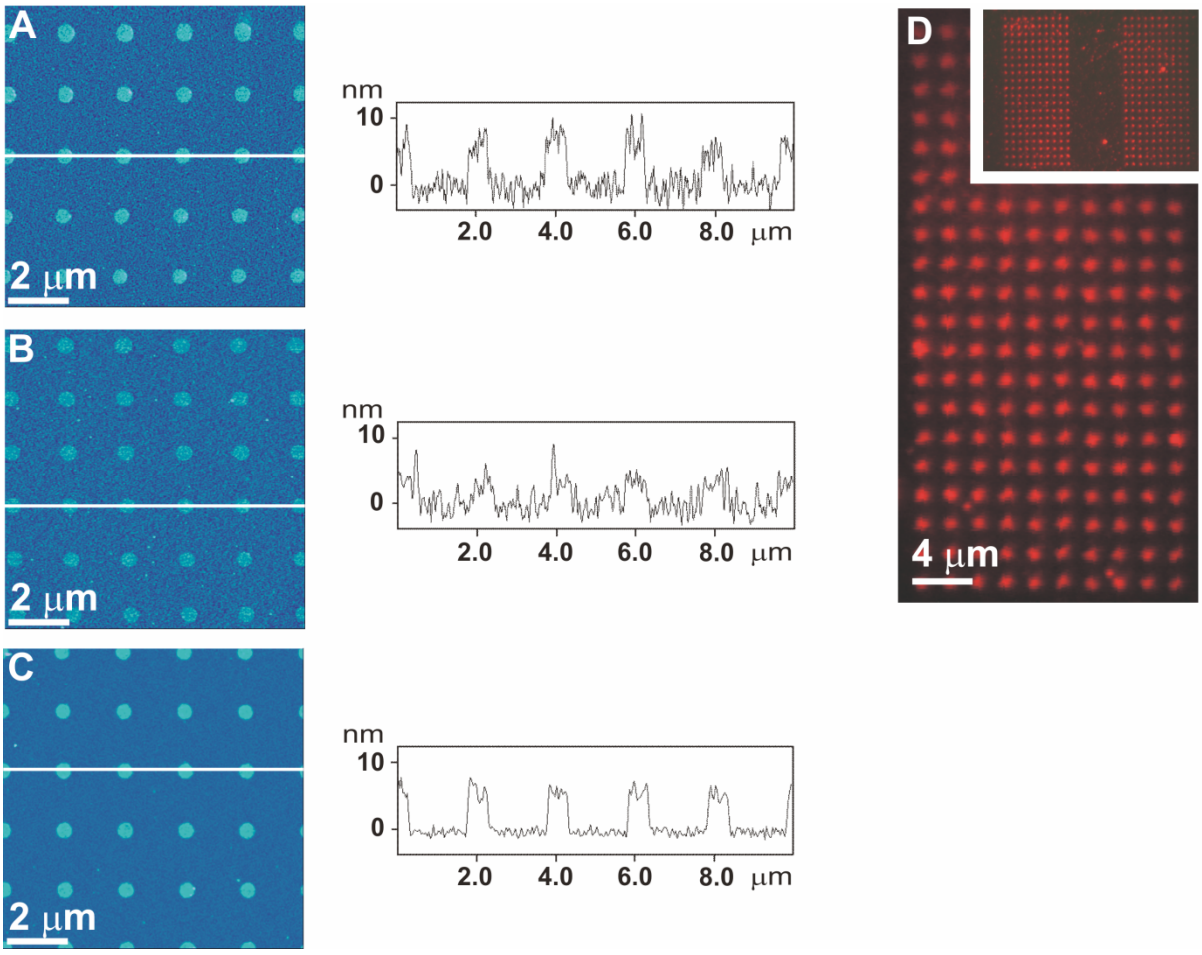
A
2 μm
nm
10
0
2.0
4.0
6.0
8.0 μm
B
2 μm
nm
10
0
2.0
4.0
6.0
8.0 μm
C
2 μm
nm
10
0
2.0
4.0
6.0
8.0 μm
D
4 μm

To verify that the antibodies bound onto the surface retained their activity and recognition capabilities, we measured the height profiles of the antibody-virus complex. Upon virus attachment, a height increase of 30 ± 5 nm is observed for all DPN-generated antibody-virus templates (**Figure 3.2A** shows viruses attached on 2F5 antibody template and its corresponding height profile). Control experiment shows that the virus does not attach to templates without immobilized antibodies. This suggests that the virus binding on the DPN-generated templates is due to the retained recognition properties of the adsorbed antibodies towards the epitopes present on the virus surface.

One of the attributes of DPN is being able to tailor feature size and probe the relationship between the number of immobilized viruses with respect to the size of a generated pattern. For instance, dot diameters of 700 and 1000 nm with 2F5 antibodies show two or more attached viruses per spot, while dot features of 300 and 500 nm have fewer than two virus particles per feature (**Figure 3.2A**). The larger dot diameters (700 and 1000 nm) exhibit >90 % virus binding (almost all of the dots have viruses attached) but the number of dots with viruses decreases with decreasing dot diameter (**Figure 3.2B**). The technique can be used to isolate and study single virus particles through the use of smaller dots (200-300 nm) **(Figure 3.3A and 3.3B**). However, with these smaller features, only 35% of the dots adsorbed the virus. Interestingly, the efficiency of capture substantially varies from antibody to antibody, and although this variation is not obvious with microarrays, it is easily observed with the nanoscale features studied herein. For example, for 2G12 antibody templates, only about 60 % of the 700 nm diameter dots contain viruses (**Figure 3.3C**) compared to the 2F5 antibody templates, which exhibit binding to 95% of the features (**Figure 3.3D**). The 2F5[16-20] and the 2G12[16, 21-22] antibodies specifically bind to

Figure 3.2. TMAFM image and corresponding height profile of 2F5 antibody patterns after incubation in a HIV solution. (B) Percent of dots containing 1 or more viruses with respect to dot diameter (300, 500, 700, and 1000 nm).

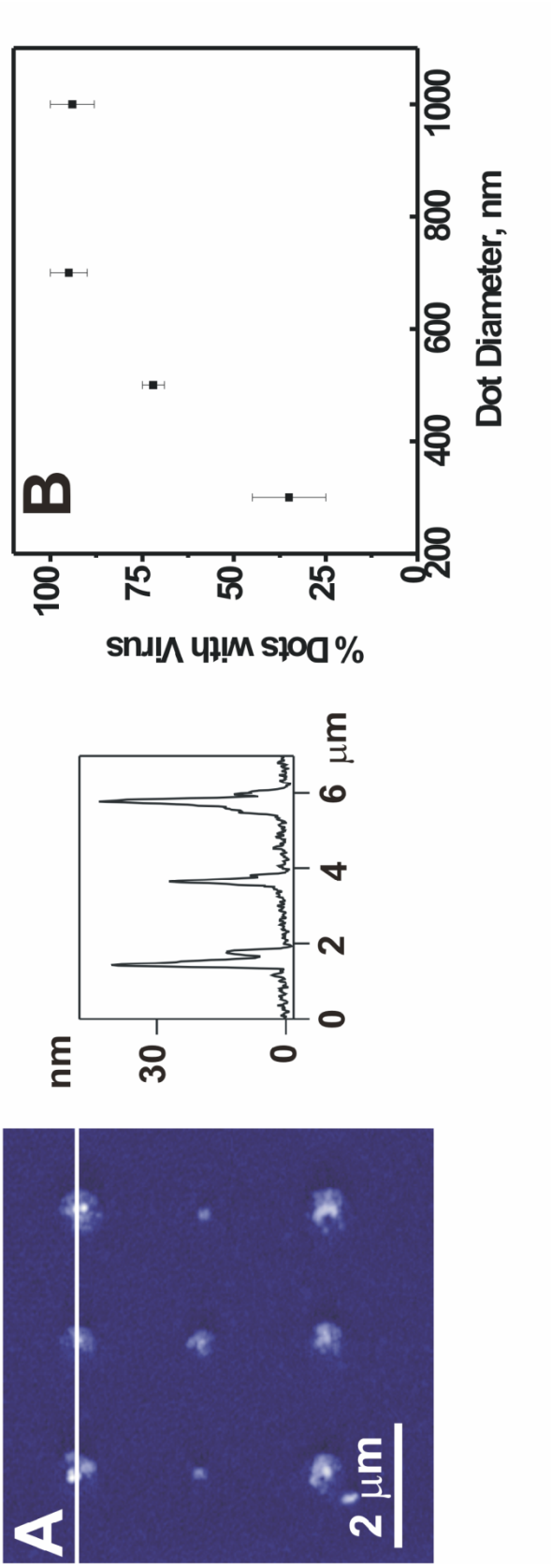
A
2 μm
nm
30
0
0
2
4
6 μm
B
% Dots with Virus
100
75
50
25
0
200
400
600
800
1000
Dot Diameter, nm

Figure 3.3. TMAFM images of (A, B, and C) 2F5 and (D) 2G12 antibody templates after incubation in a HIV solution.

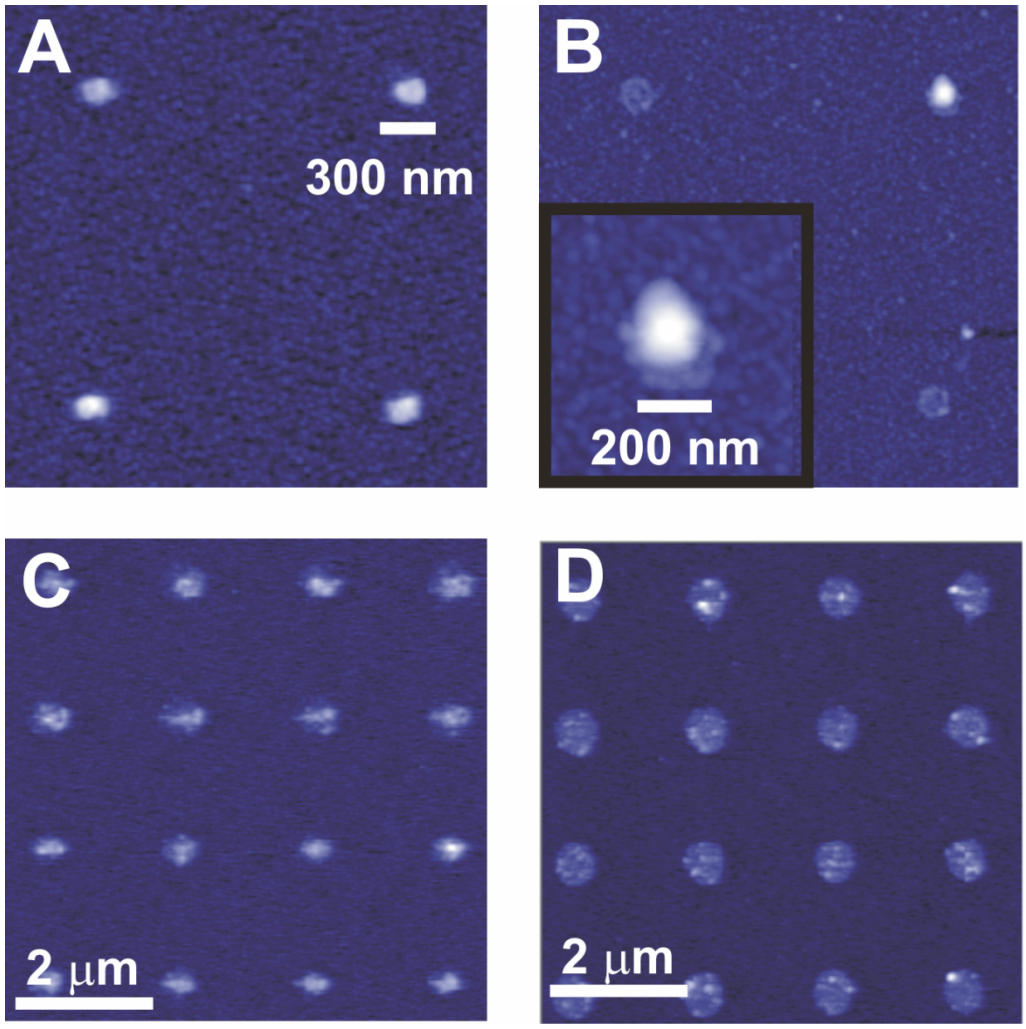
A
300 nm
B
200 nm
C
2 μm
D
2 μm

Table 3.1. Percent of dots containing 1 or more HIV particles on 700 nm features

DPN Antibody Templates	Epitope Recognized	Percent Dots[a] with HIV-1
2F5	gp41, ELDKWA (residues 662-667)	95 ± 5
2G12	gp120, base of V3 and V4 loop	62 ± 3
F105	gp120, CD4bs	27 ± 3
17B	gp120, CD4i	11 ± 5
48D	gp120, CD4i	6 ± 1
B12	gp120, CD4bs/V2	3 ± 5
F425 A1g8	gp120, CD4i	2 ± 1
No Antibody		0

[a] Dot diameter = 700 nm

epitopes at the C- terminal region of the extra cellular domain of the gp41 and the silent face of the gp120 proteins, respectively.

Other antibodies that are of even greater interest are those that target epitopes at the CD4bs (CD4 binding site) and CD4i (CD4 induced) regions of the gp120 protein of the HIV. These regions play a significant role in the binding of the virus to a cell surface. To determine how the antibodies, which target these sites, effect HIV immobilization, F105, B12, F425 AIg8, and 17B antibodies were adsorbed onto Zn ion modified MHA templates generated using DPN (**Table 3.1**) and subsequently exposed to a HIV solution. The F105 antibody templates exhibited the most dots with bound virus (<30%) while F425 A1g8 antibody templates exhibited the least (<3%). All of the additional antibody templates that were tested exhibited fewer dots with viruses than the 2G12 and 2F5 antibody templates.

The observed difference in activity for nanoscale features made by DPN versus micro- or macroscale techniques is not a consequence of the tools used to make the structures. Indeed, the difference between microscale and nanoscale features becomes exceedingly clear when one uses antibody templates made by microcontact printing and does an analogous study as a function of feature size. With large structures made by microcontact printing (10 μm diameter dots), all of the dots contained a collection of virus particles, (**Figure 3.4**). Unlike using smaller dot features, one cannot discriminate between the differences in activities of the immobilized antibodies for HIV.

To determine the total number of viruses attached on the DPN-generated templates (14560 dots, 700 nm in diameter, with center to center distance of 2 μm), lysis buffer solution

Figure 3.4. TMAFM images of (A) 2F5 and (B) 2G12 templates after incubation in a HIV solution (10 μm diameter dot features generated using microcontact printing).

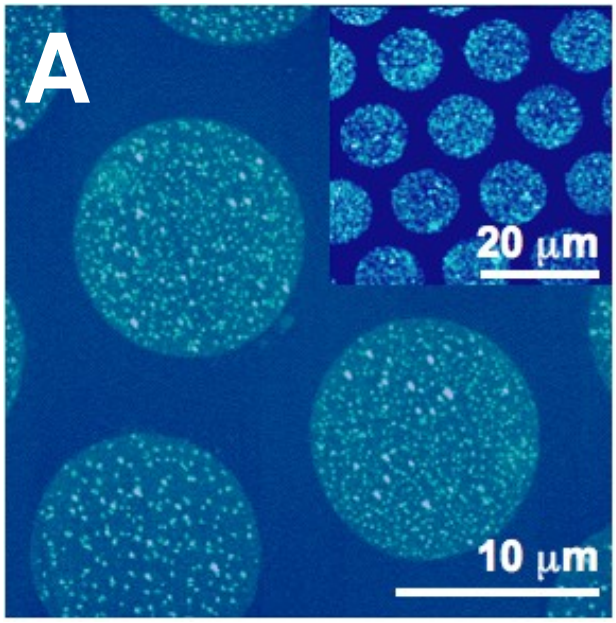
A
20 μm
10 μm

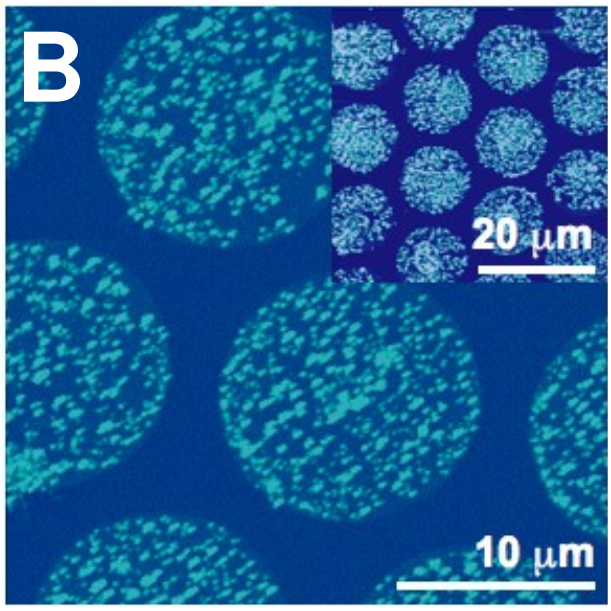
B
20 μm
10 μm

Figure 3.5. Virus count determined by RT-PCR for no antibody (control) and antibody (2F5, 2G12, F105) DPN templates exposed to HIV.

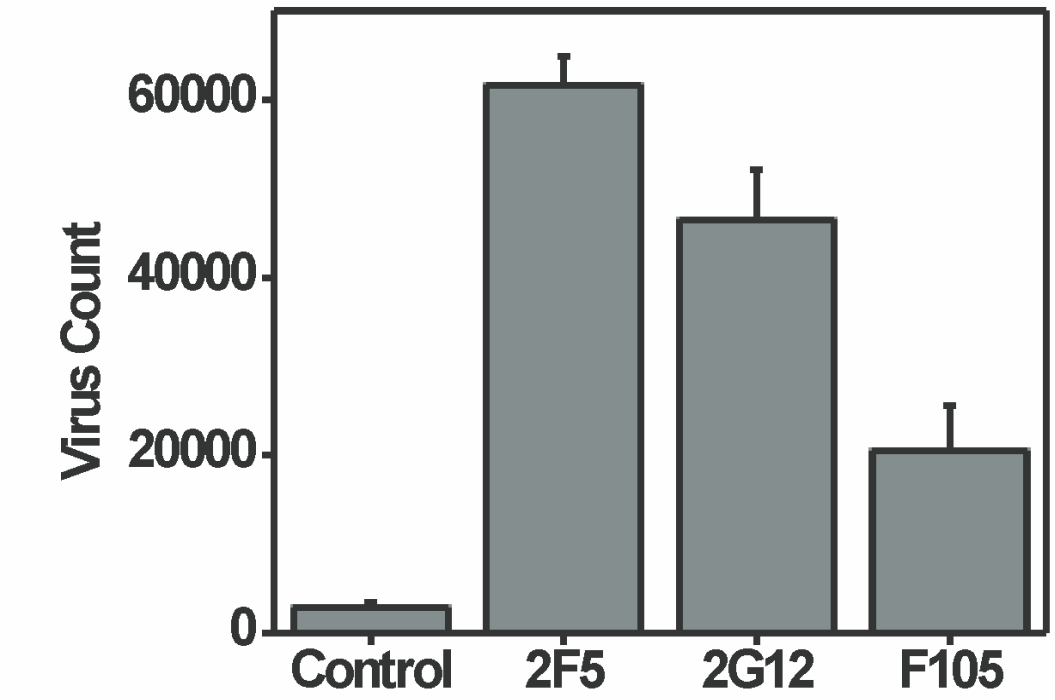
Virus Count
60000
40000
20000
0
Control
2F5
2G12
F105

was placed on the surface of the three samples containing the largest number of dots with viruses (**Table 3.1**) (2F5, 2G12 and F105), and the total number of HIV-1 RNA copies was determined using quantitative reverse transcriptase-polymerase chain reaction (RT-PCR) (**Figure 3.5**). Compared to templates containing no antibody (control), 21.8, 16.4, and 7.2 fold increases in virus count were exhibited for 2F5, 2G12, and F105 DPN templates exposed to HIV solution, respectively. The RT-PCR data exhibits the same trend observed by AFM where the 2F5 DPN templates exhibited the largest number of adsorbed viruses followed by 2G12 and F105. Although the control (a substrate without antibody) shows viruses non-specifically bound to the surface, the non-specific binding is negligible compared to the other three samples.

3.4. CONCLUSION

I have demonstrated that nanoarrays can be used to screen antibody activity and to identify differences in activity that is not easily observed with conventional microarrays. The difference in activity is pronounced with the smaller features, presumably because of the difference in immobilization states of the tethered antibodies and the fact that with inefficient immobilization strategies, there is not enough feature area to ensure the formation of an active antibody state. Using this approach we have identified substantial differences between many of the antibodies that are used for HIV neutralization and recognition. In addition, we have developed a novel RT-PCR based approach for counting the number of recognized viruses in the context of the nanoarrays, one of the most efficient ways of counting a small number of particles. Both AFM images and RT-PCR results show that the tethered 2F5 antibodies exhibit the highest virus binding compared to the other immobilized antibodies which bind to specific epitopes of the gp-120 protein on the HIV surface. Among the gp-120 antibodies, on the other hand, the 2G12 antibody templates displayed the most bound viruses, while the antibodies, which specifically bind to the CD4bs and CD4i epitopes, exhibited the least.

CHAPTER 4

Nanostructured Polyelectrolyte Multilayer Organic Thin Films Generated via Parallel Dip-pen Nanolithography

4.1. INTRODUCTION

In the field of nanoscience and nanotechnology, the development of lithographic methods for fabricating submicrometer and more recently sub-100 nm features is of great interest for both fundamental and technological purposes. Many structures, when miniaturized to the sub-100 nm length scale, possess architecture dependent chemical and physical properties. The ability to print such structures and interface them with larger architectures is opening applications in electronics,[1] optics,[2-3] catalysis,[4-5] and biosensing.[6-8] Examples of lithographic methods for making micro and/or nano scale patterns include photolithography,[9] microcontact printing,[10-12] e-beam lithography,[13] nanoimprint lithography,[14] and dip-pen nanolithography (DPN).[15-20]

The development of DPN as both a nanofabrication research and production tool has been the topic of significant interest over the past five years.[15-20] DPN, which is a direct-write scanning-probe-based lithography, utilizes a cantilever tip to deliver various reagents to nanoscopic regions of a target substrate with high resolution and registration. Although the bulk of the effort in utilizing DPN has focused on its use as a serial process, the use of multiple scanning-probe microscopy (SPM) cantilever probes as pens has been shown to increase patterning speed and array density.[17, 21] Another attribute of DPN is its substrate generality and its ability to interface soft matter with hard inorganic substrates. A wide variety of substrates, from metals to insulators, have been explored in combination with many types of inks including small organic molecules, metal ions, biomaterials, sol gels, nanoparticles, and polymers.[22-29]

The ionic layer-by-layer (LBL) assembled films, introduced by Decher,[30-31] have been widely studied because of their potential applications in electronic materials[32-37] such as photovoltaics and electrochromic thin films, as well as interfacial biological studies.[38-42] These

organic LBL films, which are often referred to as polyelectrolyte multilayer (PEM) films, can be formed by sequentially immersing substrates into solutions of oppositely charged polyions. The ease of use of the LBL methodology in the assembly of charged polymers offers one the ability to tailor important parameters such as film thickness at the nanometer-scale and the chemical functionality of the top-most layer of the PEM films. In addition, LBL organic films have been widely studied using various lithographic techniques. Hammond and co-workers have mainly focused on the LBL organic film assembly of various polyions on patterned monolayers by means of microcontact printing.[43-48] Indeed, micro-scale techniques for fabricating LBL structures using photolithography or micro-contact printing are well-established.[32-42, 49-53] Developing such capabilities for DPN not only would permit a significant reduction in feature size, but also would allow construction of chemically distinct LBL features on the nanometer length scale, and allow one to use high registration capabilities of DPN to guide the growth of LBL structures in a site-directed manner. Recently, Ivanisevic and co-workers have taken a step in this direction by demonstrating the deposition of charged polymers onto SiO_2 and polymer-coated SiO_2 films using DPN.[54-55] Small-feature-generating capabilities could open avenues for the use of the DPN-initiated LBL techniques for potential nanoelectronic applications. Herein, we report an approach to integrating LBL with DPN in the fabrication of nanometer size patterns of multilayered polyelectrolyte structures. Furthermore, through the use of multiple pen arrays, we demonstrate, for the first time, the parallel writing capabilities of DPN in the context of this LBL patterning experiment.

4.2. EXPERIMENTAL

4.2.1. Materials

11-Mercapto-1-hexadecanol (MHO), and 11-mercaptoundecyl-tri(ethylene glycol) (PEG) were purchased from ProChimia Co., Poland. Poly(diallyldimethylamonium chloride) (PDDA, MW = 100,000 ~ 200,000, 20 wt.% in water), poly(sodium 4-styrene-sulfonate) (PSS, MW = 65,000), and poly(allylamine hydrochloride) (PAH, MW = 70,000) were purchased from Aldrich (Milwaukee, WI) and used without purification. All other chemicals were ACS grade from Aldrich Chemicals and were used as received. Milli-Q water (> 18 MΩ cm), obtained using a Branstead NANOpure water system, was used for all aqueous experiments. Si (100) wafers (4 in. diameter; 3-4.9 Ωcm-1 resisitivity; 500 nm oside layer; 500-550 μm thickness) were purchased from Silicon Quest International, Inc (Santa Clara, CA).

4.2.2. Preparation of Substrates

An oxidized silicon wafer was cut into 1 × 1 cm squares. After being ultrasonicated with ethanol for 10 min and rinsed with Milli-Q water, the Si substrates were immersed into a "piranha solution" (H_2SO_4/30% H_2O_2 = 7/3 (v/v)), (Caution: Piranha solutions are extremely dangerous and should be used with extreme caution) at 80 ^oC for 10 min. The cleaned substrates were rinsed with Milli-Q water and dried with N_2, and then put into a thermal evaporator chamber. Under vacuum conditions (pressure < 1×10^{-7} Mbar), the substrates were coated with a 10 nm Ti adhesion layer via thermal evaporation and subsequently coated with 50 nm Au. Obtained Au substrates were used immediately for DPN experiments.

4.2.3. DPN Procedure

The metal substrates were patterned with MHA under ambient conditions (set point = 0.5 nN, 22 - 24 °C, 30 - 36 % relative humidity) by using a ThermoMicroscopes CP AFM (Sunnyvale, CA) or Nscriptor AFM (NanoInk, Inc., Chicago, IL) driven by custom lithography software (NanoInk, Inc., Chicago, IL) with MHA-coated tips. MHA-coated tips were prepared by immersing single Si_3N_4 cantilevers (k = 0.05 N/m, TM Microscopes, Sunnyvale, CA) or passive multi-probe arrays (k = 0.097 N/m, NanoInk, Inc., Chicago, IL) in an acetonitrile solution saturated with MHA for ~ 10 s. The substrates with the MHA arrays were then incubated into a solution containing MHO, ODT, or PEG for 1 min passivation.

4.2.4. PEM Preparation and Measurements

These substrates were alternately incubated into solutions of 40 mM PDDA (0.5 M NaCl) and 40 mM PSS for 10 minutes and successively exposed to solutions of 40 mM PAH (0.5 M NaCl) and 10 mM fluorescene sodium salt (**Scheme 4.1**). The topographies of PEM organic thin films were measured using Nanoscope IIIa with tapping mode (Digital Instruments, Santa Barbara, CA) and the fluorescence images were taken using s Zeiss Axiovert 100 microscope (Carl Zeiss Inc., Thornwood, NY).

4.3. RESULTS AND DISCUSSION

Figure 1A and B show the tapping mode AFM (TMAFM) images of PEM organic films adsorbed on dot patterns (200 nm diameter) of MHA with ODT and MHO as passivation materials, respectively. As seen in **Figure 4.1A**, the surface of the ODT back-filled area is extensively covered by nonspecifically adsorbed polyelectrolytes. On the

Scheme 4.1. Schematic representation of the process used to obtain polyelectrolyte multilayer (PEM) organic films on self-assembled monolayers (SAM) of 1-mercaptohexadecanoic acid (MHA) patterned using dip-pen nanolithography (DPN).

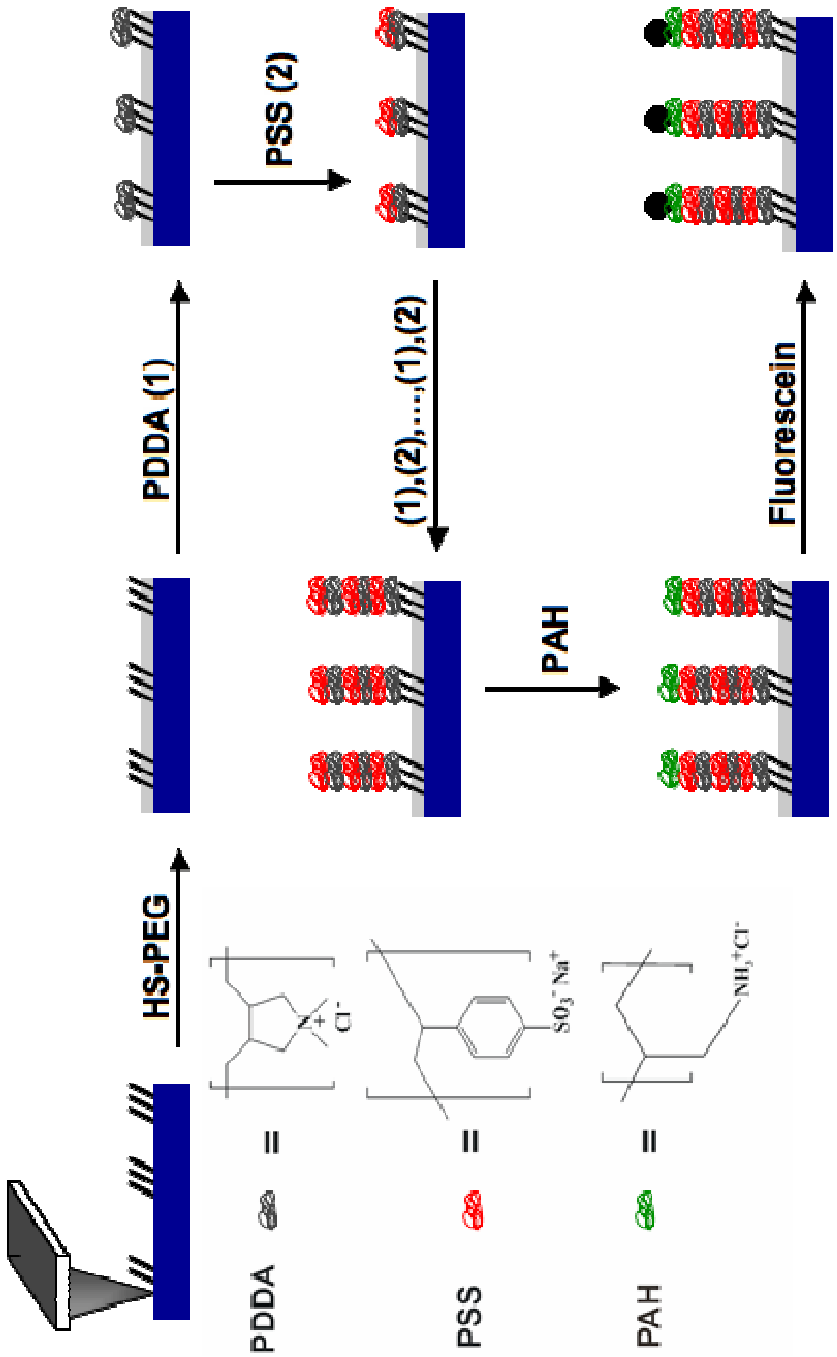
HS-PEG
PDDA (1)
PSS (2)
(1),(2),...,(1),(2)
PAH
Fluorescein
PDDA
PSS
PAH

Figure 4.1. Tapping mode topographical AFM images of PEM organic films on MHA dot arrays passivated with (A) ODT and (B) MHO.

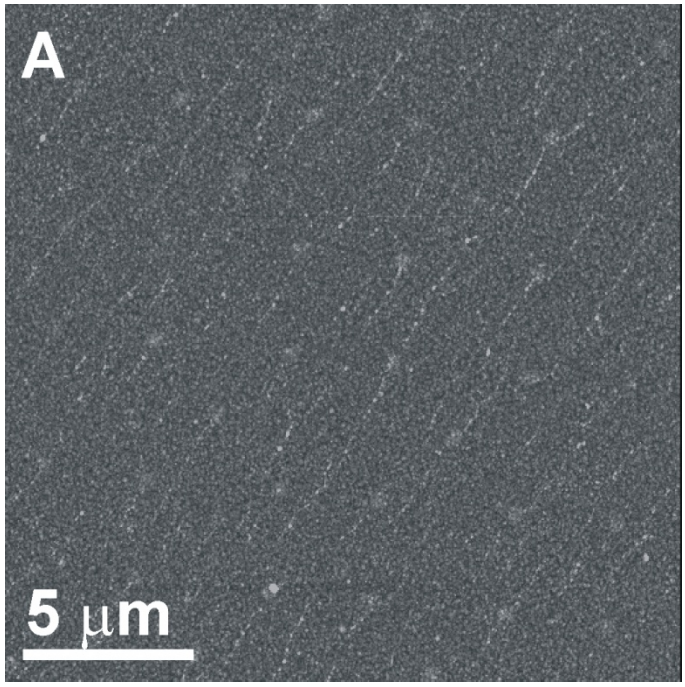
A
5 μm

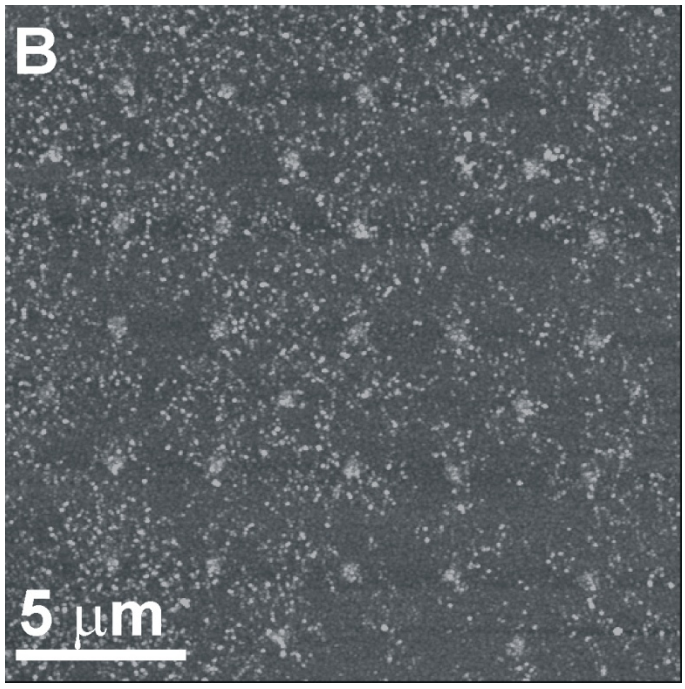
B
5 μm

other hand, substrates which were backfilled with provide surfaces more resistant to the non specific adsorption of polyelectrolytes (**Figure 4.1B**) but not as clean as the structure formed in similar patterned substrates with PEG as the adsorbate-resistant material (**Figure 4.2A**).[45, 56-59] PEG has been used extensively as a resist material for various biomolecules such as proteins, peptides, and viruses.[56-59] Dot arrays of MHA SAMs with 2 μm dot-to-dot spacing were patterned, and the bare gold regions were then back-filled using PEG, **Figure 4.2**. The diameters and heights of the dots of the MHA are 200 and 2 nm, respectively. PDDA molecules were electrostatically bound to the carboxylate moieties of the MHA dot arrays upon incubation in the aqueous polyelectrolyte solutions. The surface charge reversal, upon the addition of a positively charged polyelectrolyte, enabled the addition of a negatively charged polyelectrolyte layer (PSS). Six polyelectrolyte layers were adsorbed onto the MHA dot arrays through alternate incubation of the substrate in the charged polyelectrolyte solutions. The surfaces of the resulting PEM organic thin films bear a negative charge resulting from the adsorption of PSS as the final polyelectrolyte. There is minimal nonspecific adsorption of polyelectrolytes on the PEG passivated surface (**Figure 4.2A**). An increase in the heights of the dot arrays after depositing six layers was determined by AFM to be approximately 16.3 nm. PEM dot patterns with diameters ranging from 80 to 180 nm were also fabricated in order to demonstrate high resolution capabilities for the DPN-LBL process (**Figure 4.2B**). Although the smallest PEM dot diameter that was generated was approximately 80 nm, it is in principle possible to decrease PEM pattern features further since it has been shown that DPN can generate MHA features as small as 15nm.[15-20]

Figure 4.2. Topographical AFM image of (A) 200 nm, (B) 80 to 180 nm dot arrays of PEM (PE $_{PDDA/PSS}$ = 3) and (C) corresponding average heights of each polyelectrolyte layer.]

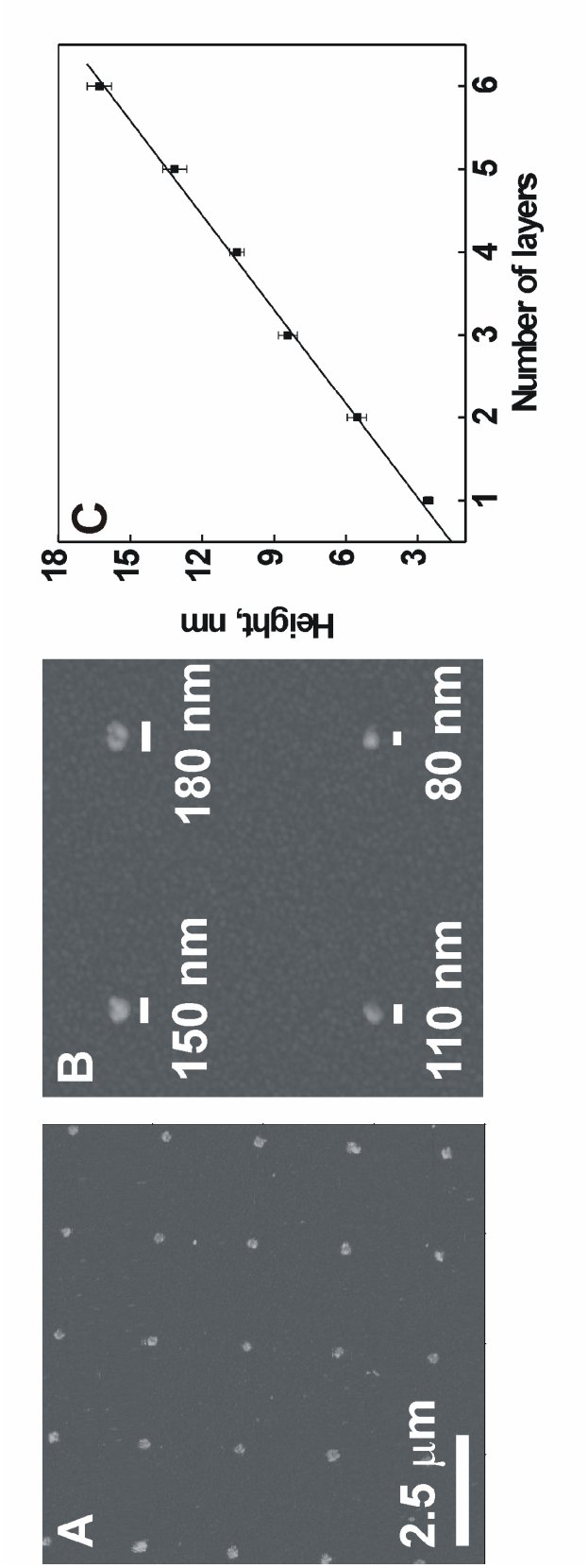
A
2.5 μm
B
150 nm
180 nm
110 nm
80 nm
C
Height, nm
18
15
12
9
6
3
1
2
3
4
5
6
Number of layers

The multilayer assembly of the polyelectrolytes onto DPN-generated MHA patterns was monitored by TMAFM by measuring the height change of the dot patterns as a function of layer number, **Figure 4.2C**. A linear increase in the height was observed, which is consistent with the uniform addition of polyelectrolyte monolayers on the patterned surface with each adsorption step. The electrostatic binding of the PDDA or PSS molecules onto the top-most layer of the pre-formed multilayer dots increased their height by approximately 2.3 nm, the slope of the line in **Figure 4.2C**. This height change is comparable to that observed for similar multiple structures prepared by microcontact printing methods, but slightly higher by 0.5 nm.[43-51] This difference may arise from different deposition conditions of polyelectrolytes and NaCl concentrations. When the concentration of the polyelectrolytes in our experiment was decreased by half (20mM polyelectrolyte solution with 0.5 M NaCl), the average height value of each layer adsorbed onto the DPN patterned features decreased by 0.5 nm. Increasing the dot sizes of the array from 200 to 500 nm did not affect the increase in height of the patterns when alternately exposed to the polyelectrolytes used, which suggests that polyelectrolyte adsorption, under these conditions, is independent of feature size.

Line arrays of MHA were also fabricated using DPN. The widths and heights of the lines of the MHA are 200 and 2 nm, respectively. The average heights of the PEM structures, determined from TMAFM show a linear increase, with values comparable to the average heights of the PEM dot arrays. The surfaces of the PEM line arrays bear a negative charge resulting from the adsorption of the final polyelectrolyte layer (PSS). These substrates were soaked in a 40 mM aqueous PAH solution with 0.5 M NaCl in order to investigate the deposition of the weak polycation onto the nanostructured strong polyanion surface. The adsorption of the weak

Figure 4.3. Topographical AFM image of PEM line arrays with $(PDDA/PSS)_3PAH$ layers (A) and its corresponding height profile (B).

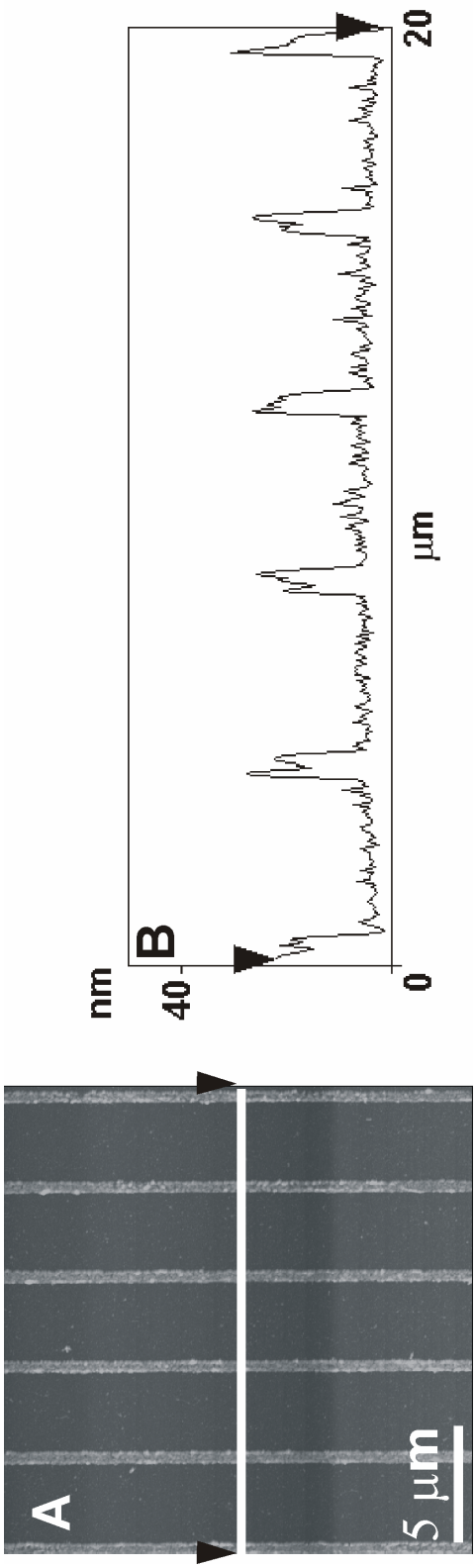
A
5 µm
B
nm
40
0
20
µm

polycation onto the PEM line array was determined by tapping mode AFM. As shown in Figure 3, the PAH was selectively deposited onto the patterned area with sharp boundary features. Furthermore, it shows that PAH was not adsorbed onto the PEG back-filled areas. The heights of the line arrays were determined to be approximately 19 nm (**Figure 4.3B**). The height increase of the PAH layer is comparable to the thickness of each PSS and PDDA layer.

In order to demonstrate the usefulness of the DPN-generated PEM organic films in surface immobilization of molecules other than polyions, fluorescein sodium salts (**Figure 4.4A**) were chosen as a test case because they can be imaged easily by fluorescence microscopy and have been incorporated into printed films.[47] Multilayers of polyelectrolytes electrostatically stacked onto DPN- generated MHA patterns were immersed in a fluorescein sodium salt solution (40mM) for 10 minutes. **Figure 4.4** shows fluorescent microscopy images of the PEM organic thin films bearing the fluorescein anion on the top-most layer. Uniform fluorescein structures on the surfaces of multilayers are observed for DPN-generated dot (**Figure 4.4B**) and line (**Figure 4.4C**) PEM organic thin film features.

Simultaneous generation of multiple near-identical structures is possible with arrays of cantilevers. To demonstrate this capability, we used a 26 probe array with a tip-to-tip distance of 35 μm. The array was coated with MHA and used to generate 200 nm dot array features (36 x 72) on a gold substrate with an interfeature center-to-center distance of 900 nm. 67,000 features could be generated in 15 min with the approach. PEMs were then generated on the MHA array template via the LBL approach and labeled with the green fluorescein dye (**Figure 4.4D**). Although there are a few defects (~4%), the reproducibility over relative large distances (mm) is remarkable.

Figure 4.4. Fluorescent images of fluorescein sodium salt, (A) structure, adsorbed onto the surface of DPN generated polyelectrolyte multilayer arrays using one (B, C) and 26 (D) AFM cantilever probe.

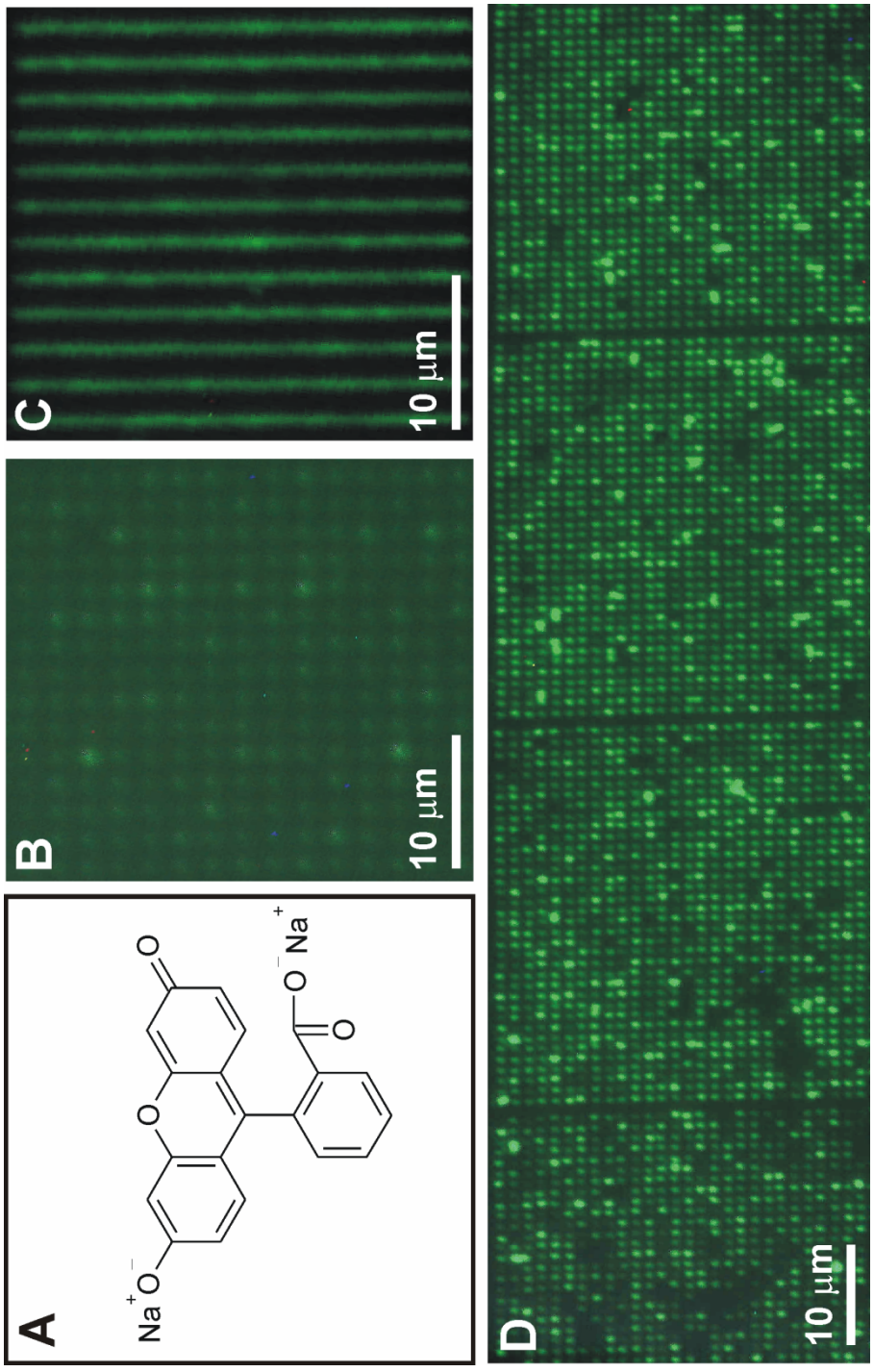
A
B
C
D
10 μm
10 μm
10 μm
O
O
O
O
Na+
O−
Na+
O−

4.4. Conclusion

We have demonstrated that PEM organic thin films can be fabricated on DPN generated MHA patterns, by alternating the exposure of the pattern features to aqueous polyelectrolyte solutions. This can be accomplished without the need of masks, e-beam lithography, or stamps. Through the use of multi-pen AFM cantilever probes, parallel fabrication of the polyelectrolyte multilayer features with nanoscale resolution can be achieved. This capability demonstrates the versatility of the approach for making many similar structures that span macroscopic distances in a relatively high throughput manner.[60-62] When one considers that DPN arrays as large as 10,000 pens have been constructed, it is conceivable that this procedure could be extended to making large area patterns for many purposes, including integrated optics, electronic devices, and sensors.

Chapter 5

Polyethylene Glycol as Resist and Sacrificial Material for Generating Positive and Negative Nanostructures

5.1. Introduction

Dip-pen nanolithography (DPN)[1,2] has emerged as a powerful tool for printing soft and hard matter on surfaces with sub-50 nm to many micrometer resolution. Indeed lithographic patterns of various small organic molecules,[3-5] polymers,[6-8] proteins,[9-12] sol gels,[13] nanoparticles,[14, 15] high melting temperature molecules,[16] and viruses[17] have been generated on a wide variety of substrates, including Au,[2, 18, 19] Ag,[20] GaAs,[21] and SiO_x.[4, 22] With the development of cantilever arrays (linear A-26 pen[23] and 2D 55,000 pen array systems[24]) the technique has evolved into a parallel methodology[25] that, in certain cases, exceeds the throughput capabilities of serial nanolithographic techniques such as e-beam lithography. Indeed, recently our group has shown that by using a 2D 55,000 pen array in conjunction with wet-chemical etching protocols, we can generate millions of solid-state nanostructures over a square centimeter area in less than 30 min.[24]

A variety of etching protocols in combination with etch resist materials have been utilized to generate solid-state metal structures for applications in electronics, catalysis, and optics.[26] For example, alkanethiols have been used extensively as etching resists because they form self-assembled monolayers (SAMs) that can protect an underlying metal surface from chemical or electrochemical oxidation and dissolution.[27-31] In fact, alkanethiols as DPN inks combined with wet-chemical or electrochemical etching protocols have been used to produce solid-state nanostructures with feature sizes ranging from 12 nm to many microns.[30-33] Typically, lithographic patterns of 1-octadecanethiol (ODT) or 16-mercaptohexadecanoic acid (MHA) are generated via DPN. Exposing the substrate containing the alkanethiol SAMs to etching solutions produces positive solid-state

nanostructures. On the other hand, hole features (negative nanostructures) can be generated through the fabrication of MHA lithographic features using DPN, subsequently backfilling the exposed gold regions with ODT, electrochemically desorbing the MHA SAMs, and incubating the substrate in an etching solution. [33]

Although alkanethiols can be excellent etch resist materials for many surfaces (e.g., Au, Pd, and Ag), they possess certain limitations. In generating negative features, two different SAMs are required (e.g. ODT and MHA), and an electrochemical set-up is necessary to selectively desorb one SAM in the presence of the other.[33,34] Pinholes can lead to non-uniform etching and lower quality structures. Finally, one must use chemical protocols to eliminate the SAM resist from the surface once the desired solid-state structures have been made. Herein, we show how polyethylene glycol (PEG), coupled with the high-resolution of DPN and wet-chemical etching methods, can be used as a novel physisorbed resist to generate high quality positive and negative nanostructures (Scheme 1). Elimination of the resist can be effected by simply rinsing the patterned substrate in dichloromethane. In this work, DPN templates of PEG features are used either as a protective or sacrificial layer to generate raised or recessed structures on surfaces, Scheme 1. Derivatives of this polymer have been used as materials to minimize non-specific adsorption of proteins and virus particles on surfaces such as Au and SiO_2.[9, 35-37]

5.2. Experimental

5.2.1. Materials

Polyethylene glycol (MW 2000) was purchased from Fluka. Thiourea and iron (III) nitrate nonahydrage were obtained from Sigma-Aldrich. All chemicals were used as received.

Scheme 5.1. Polymer-based etch-resist methodology for generating positive and negative nanostructures.

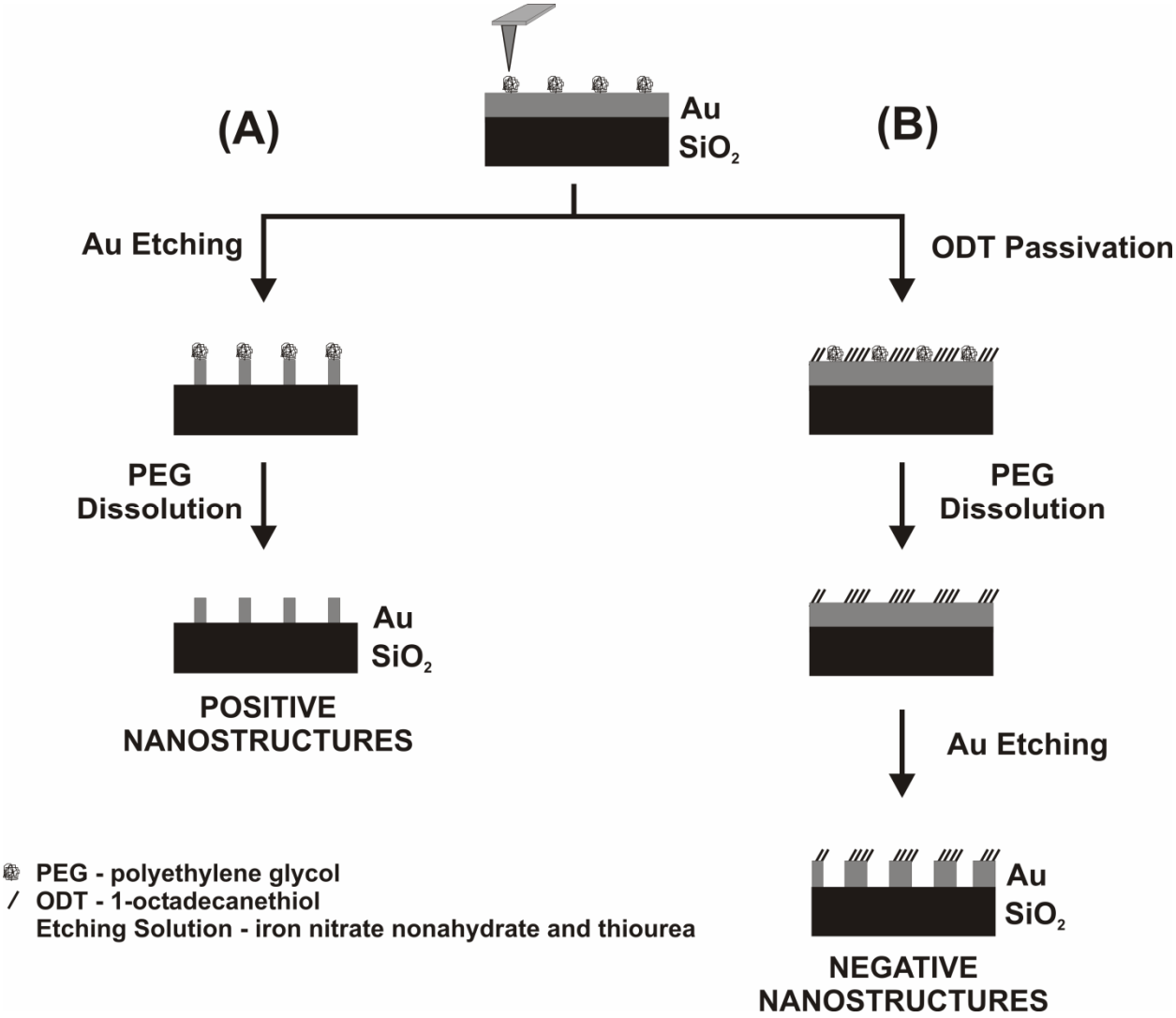
(A)
Au
SiO2
(B)
Au Etching
ODT Passivation
PEG
Dissolution
PEG
Dissolution
Au
SiO2
POSITIVE
NANOSTRUCTURES
Au Etching
PEG - polyethylene glycol
ODT - 1-octadecanethiol
Etching Solution - iron nitrate nonahydrate and thiourea
Au
SiO2
NEGATIVE
NANOSTRUCTURES

5.2.2. Fabrication of positive and negative solid state nanostructures

A cantilever array with 26 tips (A-26) was dipped into a 5 mg/ml acetonitrile solution of PEG (MW 2,000) for 10 sec, then mounted onto an NSCRIPTOR™, and used to generate dots and lines on gold surfaces. Incubating the substrate in an aqueous etching solution containing 20 mM thiourea and 30 mM iron nitrate nonahydrate generates positive solid-state nanostructures, Scheme 1A. On the other hand, substrates that were subsequently passivated with 1 mM ODT and washed with dichloromethane (to remove the PEG) before exposing to the same etching solution were used to produce negative nanoscale features, Scheme 1B. The resulting nanostructures were characterized by atomic force microscopy (AFM), scanning electron microscopy (SEM), and optical microscopy.

5.3. RESULTS AND DISCUSSION

One of the attributes of DPN is the ability to tailor feature size by varying the scan rate of the tip array and tip-substrate contact time. There is typically a feature size dependence that correlates with the square root of tip-substrate contact time.[16, 38-40] The PEG exhibits a similar dependence when deposited on a 30 nm thick Au film thermally evaporated on a SiO_2 substrate. Scan rates of 0.05, 0.10, and 0.75 μm/sec gave 175, 105, and 70 nm wide line features, respectively, Figure 1A. On the other hand, dot features can be generated by holding the tip in contact with the substrate for set periods of time. Contact times of 0.5, 1, 2, 4, and 8 sec at 80-90% humidity resulted in dot features with diameters of 100, 200, 300, 400, and 500 nm, respectively, Figure 1B.

Figure 5.1. Polyethylene glycol (A) lines and (B) dot nanostructures generated using DPN.

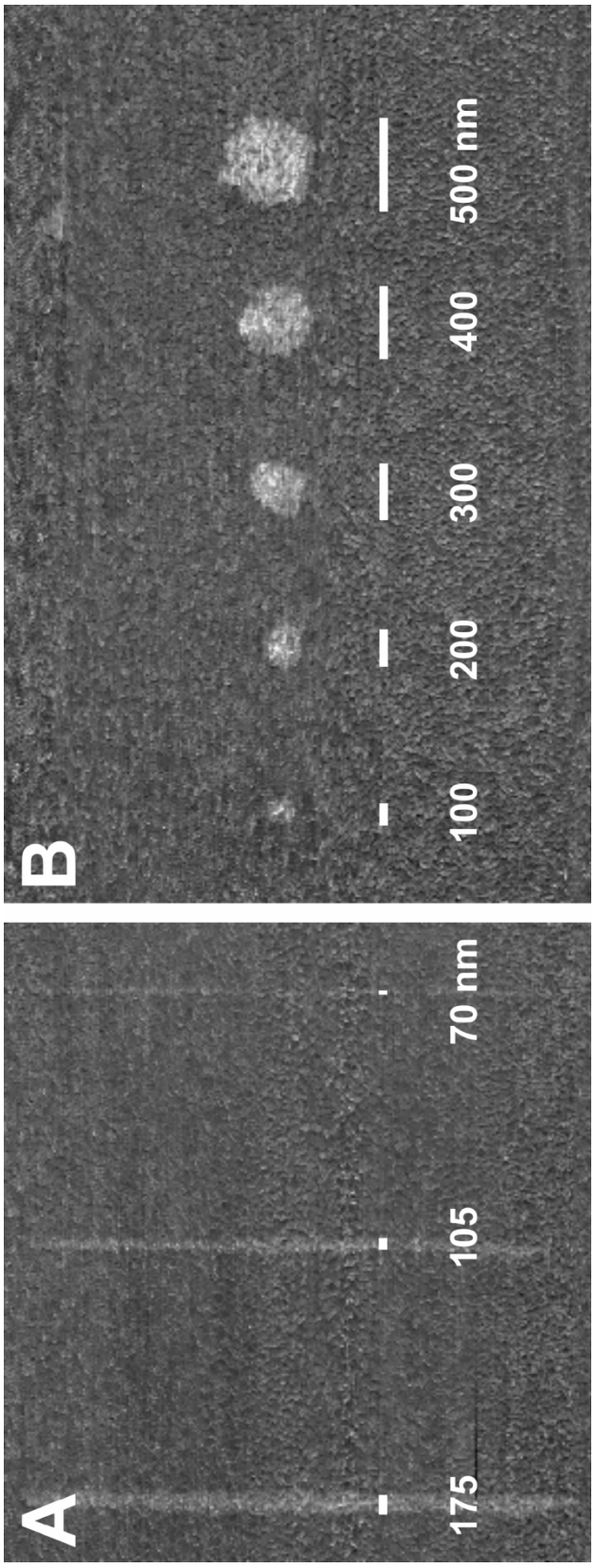
A
175
105
70 nm
B
100
200
300
400
500 nm

Figure 5.2. (A) SEM and (B) optical microscopy images of the generated positive Au nanostructures; (C) Contact mode AFM image of PEG patterns used as etch resist to make the dot features in (D); (D) Tapping mode AFM images of positive dot solid-state Au nanostructures generated from (C). One cell, which is designated by the white box in (A), is shown schematically in the inset of (A). Inset in D shows a zoomed-in AFM image of generated Au dot array.

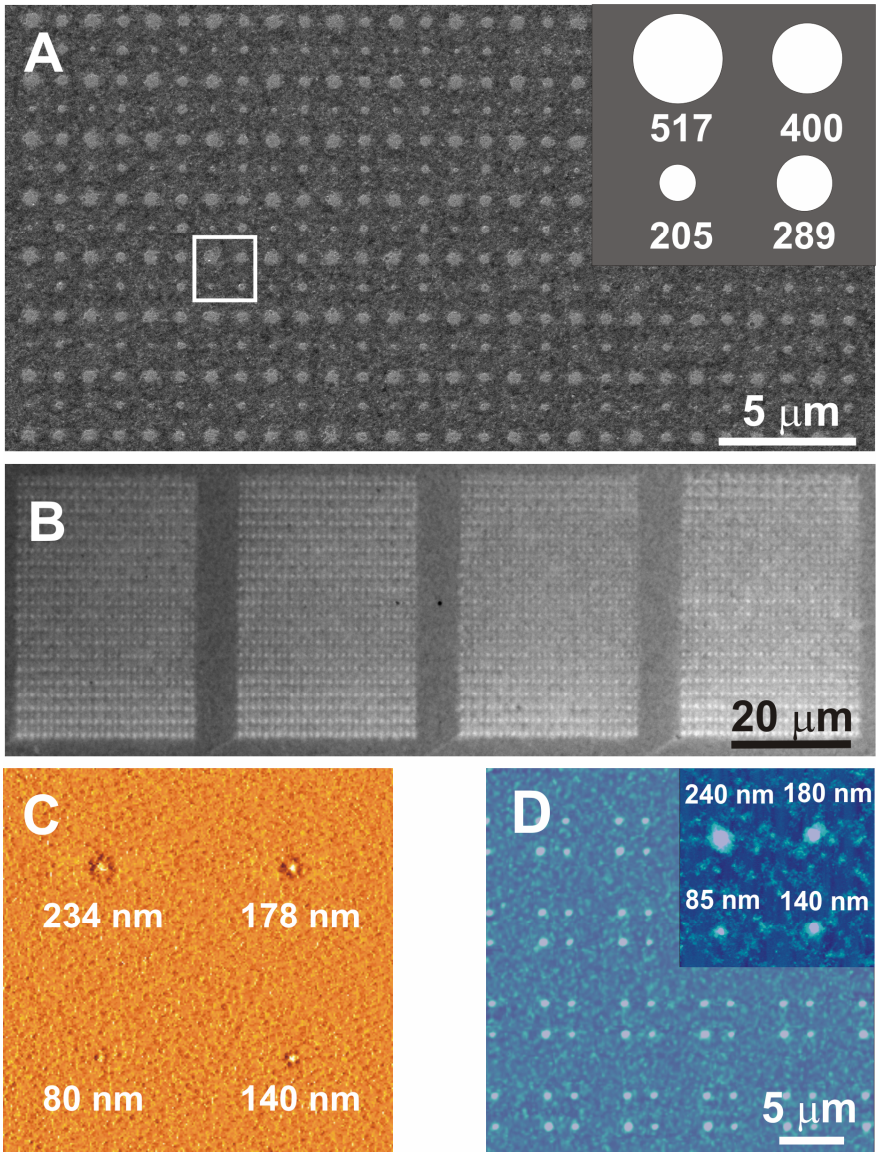
A
517
400
205
289
5 μm
B
20 μm
C
234 nm
178 nm
80 nm
140 nm
D
240 nm
180 nm
85 nm
140 nm
5 μm

After working out the protocol for patterning PEG, we evaluated the potential for using the PEG resist and wet chemical etching to generate positive solid-state features. As proof-of-concept, we used a 26-pen parallel array to generate twenty six 15 x 20 PEG dot arrays on a gold thin film surface. Each array consists of dots with deliberately generated 200, 300, 400 and 500 nm diameter features. The total time needed to generate the 26 identical PEG dot arrays was ~ 1 hr. The patterned substrate was subsequently etched using an aqueous solution of 20 mM thiourea and 30 mM iron nitrate nonahydrate to generate positive Au nanostructures with dot diameters of 205, 289, 400, and 517 nm (± 10 nm), respectively, Figure 2 A-B. Significantly, one can reduce the PEG feature size to the sub-100 nm scale simply by reducing the humidity to ~70%. For example, contact times of 1, 2, 4, and 8 sec resulted in PEG dot features with diameters of 80, 140, 178, and 234 nm, respectively (Figure 2C). We further show that Au feature size down to 85 nm thus far can be sequentially obtained using the above generated PEG features as the etch resist (Figure 2D). There is remarkably good agreement between the sizes of the PEG resist features defined by DPN and the resulting solid-state raised nanostructures. AFM analysis of the solid-state features shows that on average they are 27 nm (± 2 nm) high, which is equivalent to the thickness of the evaporated Au layer (~30 nm). These observations suggest that the PEG templates effectively protect the underlying gold regions, while the exposed gold areas were oxidized by the etching solution.

The DPN technique coupled with the novel PEG resist is quite versatile and allows one to generate very sophisticated structures, including complex shapes and patterns. As proof-of-concept, we used a digitized image of the Northwestern University logo and generated a PEG replica of it at 80 nm dot size resolution in dot matrix form (~12,000 features) on an Au thin film

Figure 5.3. (A) An SEM image of a set of positive nanostructures in the form of the NU logo (false purple color; dark purple denotes raised areas); the expanded area is a representative of the dot matrix map used to generate the structure; (B) SEM image of positive line structures generated by DPN with the PEG resist and subsequent wet chemical etching; C) AFM image of the nanostructures shown in B and its corresponding height profile.

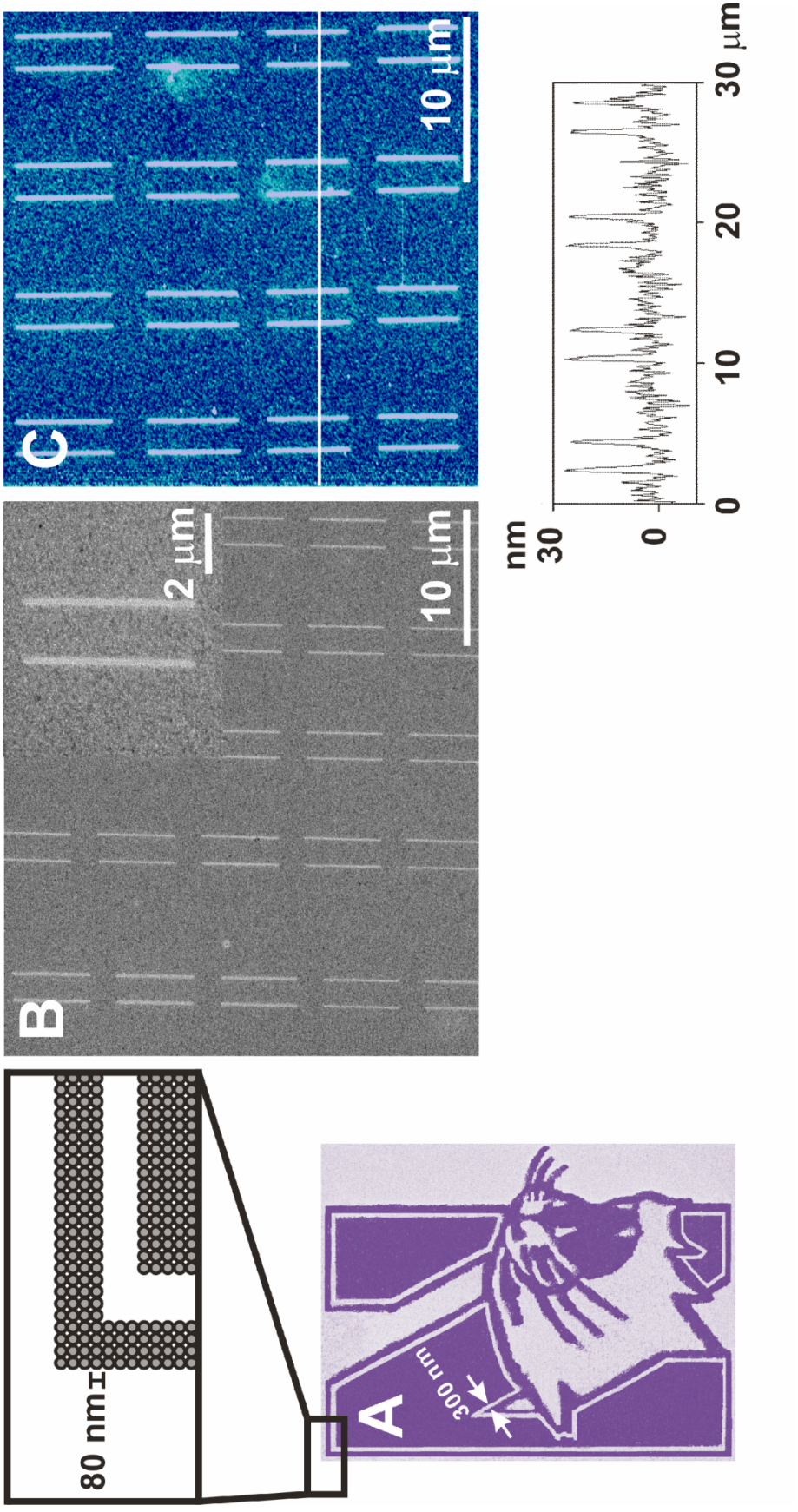
A
300 nm
80 nm
B
2 μm
10 μm
C
10 μm
nm
30
0
0
10
20
30 μm

substrate in 50 min. This structure was etched as described above for 45 min, rinsed with CH_2Cl_2, and characterized by SEM (Figure 3A). Line arrays were similarly made, and SEM and AFM analyses post-etching show the high uniformity and well-defined edges of the resulting features (Figure 3B-C). Each line, based upon AFM analysis (Fig. 3C-D) is 150 nm (± 5 nm) wide, 6 μm long, and 27 nm (± 2 nm) thick.

Interestingly, the PEG not only can be used to generate positive features but also negative ones. To generate negative features, we used the PEG as a sacrificial template (Scheme 1B). With this approach, we generate features made of PEG by DPN on a 60-70 nm thick Au film, passivate the surrounding areas with ODT by immersing the substrate for 15 min in a 1 mM ethanolic solution of ODT, and then rinse with CH_2Cl_2 which removes the PEG and residual physisorbed ODT. Subsequent etching results in the formation of negative features in the areas originally occupied by PEG. Using this approach, we have generated arrays of dot and line features, and AFM and optical analysis of the resulting structures show that they are highly uniform (4% variation in line width, 7% variation in dot diameter) (Figure 4). Height profiles show that the average depths of the generated nanostructures were similar to the thickness of the underlying gold layer (dots: ~ 65 nm, lines: ~ 58 nm). We intentionally used different Au film thicknesses (70 nm for dot and 60 nm for line, Fig. 4A and B) to evaluate the versatility of the technique and how one can control the depth of negative features using this approach. As with the positive features, the use of the cantilever arrays shows how the process can be easily scaled (Figure 4C and 4D).

Figure 5.4. AFM, height profile, and optical images of (A, C) dot and (B, D) line shaped hole nanostructures generated using the polymer-based etching methodology.

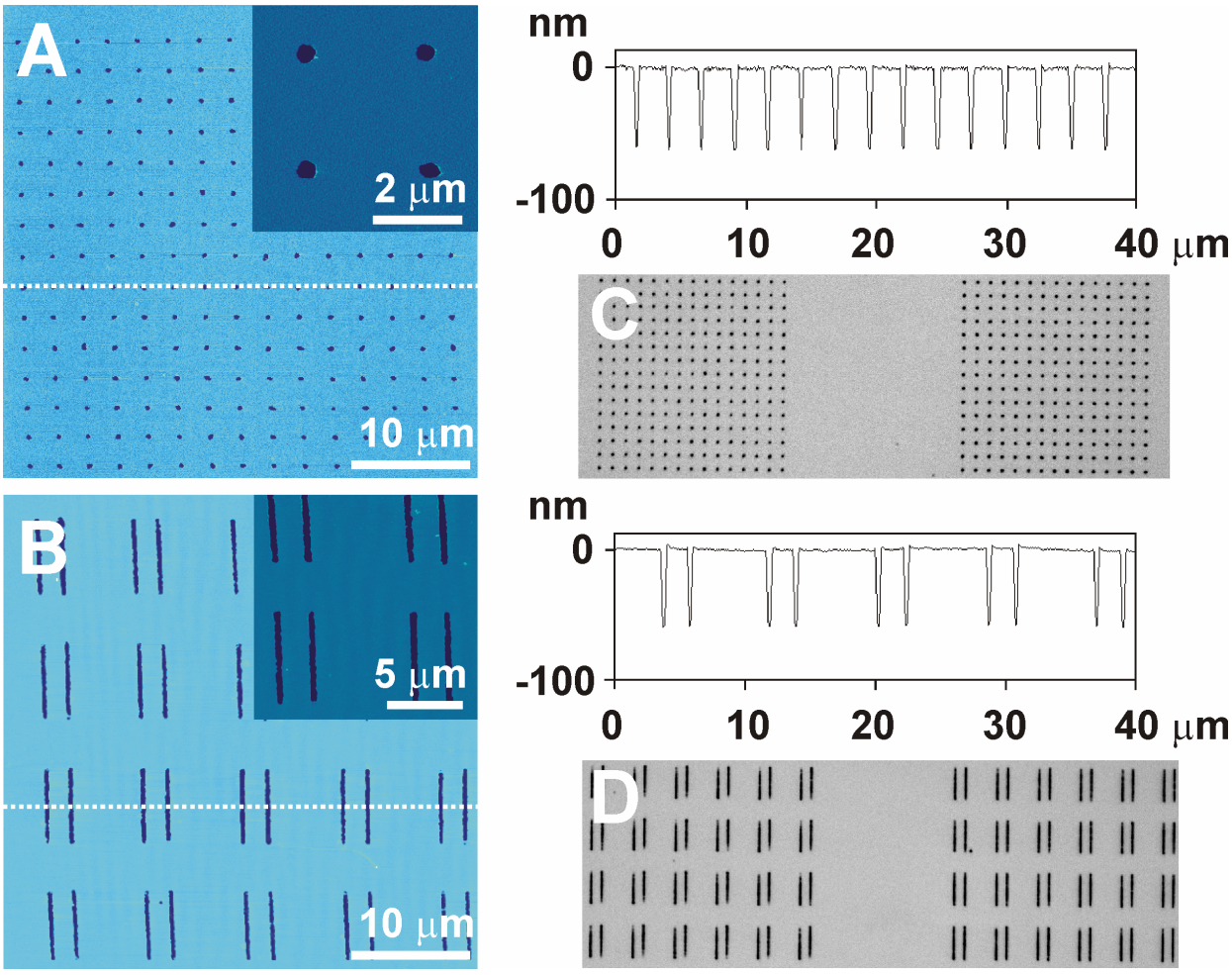
A
2 μm
10 μm
B
5 μm
10 μm
nm
0
-100
0
10
20
30
40 μm
C
nm
0
-100
0
10
20
30
40 μm
D

5.4. Conclusion

In summary, we have discovered that PEG can be used as a novel and extremely useful resist material for generating both positive and negative structures in the context of DPN. The PEG resist, when coupled with wet chemical etching, allows one to generate solid-state nanostructures in a manner that overcomes some of the limitations of the alkanethiol-based etching methods. Specifically, the polymer-based approach requires only a simple washing step to desorb materials from a substrate surface and, in principle, can be used with many types of underlying substrates (there is no requirement of chemisorption). Furthermore, the ability to generate a thick polymer layer and the elimination of the electrochemical desorption step associated with SAMs, results in less pitting of the surface due to pinholes. Finally, the process works with parallel pen arrays allowing one to pattern over relatively large areas, and it is likely extendable to other polymeric materials and perhaps other lithographic techniques.

CHAPTER 6

Seed Mediated Growth of Bimetallic Prisms

6.1. INTRODUCTION

Bimetallic alloy and core-shell nanoparticles are an interesting class of materials with unusual optical, catalytic, electronic, and magnetic properties.[1-14] Such structures have been studied for potential bioanalytical[11] and biomedical[12] applications. Synthetic strategies utilized to make such nanostructures include simultaneous chemical reduction of two or more metal ions,[1-4] reduction of one metal ion onto the surface of another metal particle,[5-11, 15-16] and γ-irradiation of a mixed solution of ionic precursors of two metal elements.[13-14, 17] The co-reduction of metal precursors and the γ-irradiation approach lead to alloy structures, and the seeding approach leads to core-shell structures. The core-shell approach is often used to stabilize an ordinarily unstable particle by coating it with a layer of material that is less reactive than the core.[8] It also has been used to optimize magnetic properties[7] and generate colorimetric labels for multiplexed DNA detection schemes.[9] The bulk of efforts aimed at producing core-shell structures have focused on isotropic spherical or pseudo-spherical structures. Other than work with nanorods,[18] very few methods have been developed for making core-shell anisotropic structures.

Recently, we[19-20] and others[21-22] have developed methods for preparing triangular nanoprisms made of silver. Using a combination of thermal and photochemical synthetic approaches, one can now control many of the architectural parameters of this interesting class of materials. These structures have striking architecture-dependent optical properties, including surface plasmon bands that are highly dependent upon edge length, thickness, and degree of truncation.[20] Their surface chemistry on the other hand is difficult to control, so one's ability to turn such structures into biological probes through surface functionalization with adsorbates has

been a challenge. Herein, we report a strategy for making silver core-gold shell nanoprisms that relies on the silver prisms as seeds and the reduction of gold ions on their surfaces via L-ascorbic acid. This is a modification of a strategy that has been used effectively in making Au nanorods and nanowires.[23-25] Interestingly, we have discovered a stoichiometry-dependent process that results in the formation of the desired core-shell prisms or nanoclusters with corrugated surface features, under one set of conditions.

6.2. EXPERIMENTAL

6.2.1. Materials

Hydrogen tetrachloroaurate ($HAuCl_4$), sodium borohydride ($NaBH_4$), trisodium citrate, silver nitrate ($AgNO_3$), cetyltrimethylammonium bromid (CTAB), sodium hydroxide (NaOH), and L-ascorbic acid were obtained from Aldrich Chemical and were used as received. Bis (p-sulfonatophenyl) phenylphosphine dihydrate dipotassium (BSPP) was purchased from Strem Chemicals . Prior to use, glassware was cleaned with aqua regia (v/v % HCl : HNO_3 = 3:1, caution: aqua regia is a very toxic chemical and should be handled carefully) and thoroughly rinsed with Millipore water (18.2 MΩ).

6.2.2. Synthesis of silver prism nanoparticles

Silver prism seeds were synthesized as previously reported.[19] Briefly, nanopure H_2O (95 mL), aqueous $AgNO_3$ (2 mL, 5 mM) and aqueous trisodium citrate (1mL, 30 mM) were were vigorously mixed in a flask immersed in an ice bath (stirred for 30 min). Aqueous $NaBH_4$ (1 mL, 50 mM) was quickly added to the ice cold mixture. The clear solution turned yellow. 3-5 drops of the aqueous $NaBH_4$ was added every two minutes over a 15 min period. BSPP (1 mL,

5 mM) and aqueous $NaBH_4$ was simultaneously added dropwise for 5 min. The resulting Ag colloid solution was continuously stirred overnight in the dark. The aged solution was then exposed to a light source to photoinduced the conversion of the Ag spheres to prism.

6.2.3. Synthesis of silver spherical nanoparticles

Spherical silver seed nanoparticles were synthesized from a modified literature procedure.[23] To a vigorously stirred aqueous solution of $AgNO_3$ (0.01 mM, 38 mL) and trisodium citrate (0.01 mM), 1.0 mL of ice-cold 0.1 M $NaBH_4$ was rapidly added. The solution was stirred for one hour prior to use.

6.2.4. Synthesis of Core-shell nanoparticles

Core-shell nanoparticles were synthesized by adding aliquots of silver seeds (prism or spherical shaped nanoparticles) (250, 500, 750, 1000, 2000, and 5000 μL) to growth solutions containing $HAuCl_4 \cdot 3H_2O$ (0.01 M, 0.25 mL), CTAB (0.05 M, 9 mL), L-ascorbic acid (0.1 M, 0.05 mL), and NaOH (0.1 M, 0.05 mL). Nanoparticle (seeds and core-shells) formation was monitored by UV-vis spectroscopy (Jasco V-530) and the products were characterized by transmission electron microscopy (TEM) (Hitachi H8100) and EDX.

6.3. RESULTS AND DISCUSSION

Gold-coated silver prisms that resemble arrowheads form from solutions where the gold content was relatively low (Ag^+/Au^{3+}=1:5), Figure 1A. Higher magnification images show that the bimetallic nanoparticles have pseudo-triangular shapes with thicker coatings on the vertex of the silver prism seed (**Figure 6.1A**, inset). As the Ag to Au ion mole ratio decreases, the general shape of the resulting nanoparticles changes from pseudo-triangular to an ill-defined structure

Figure 6.1. TEM images of (A) triangular and (B) corrugated Ag/Au core-shell nanoparticle with Ag^{+}/Au^{3+} mole ratios of 1:5 and 1:33, respectively (insets are zoomed in images).

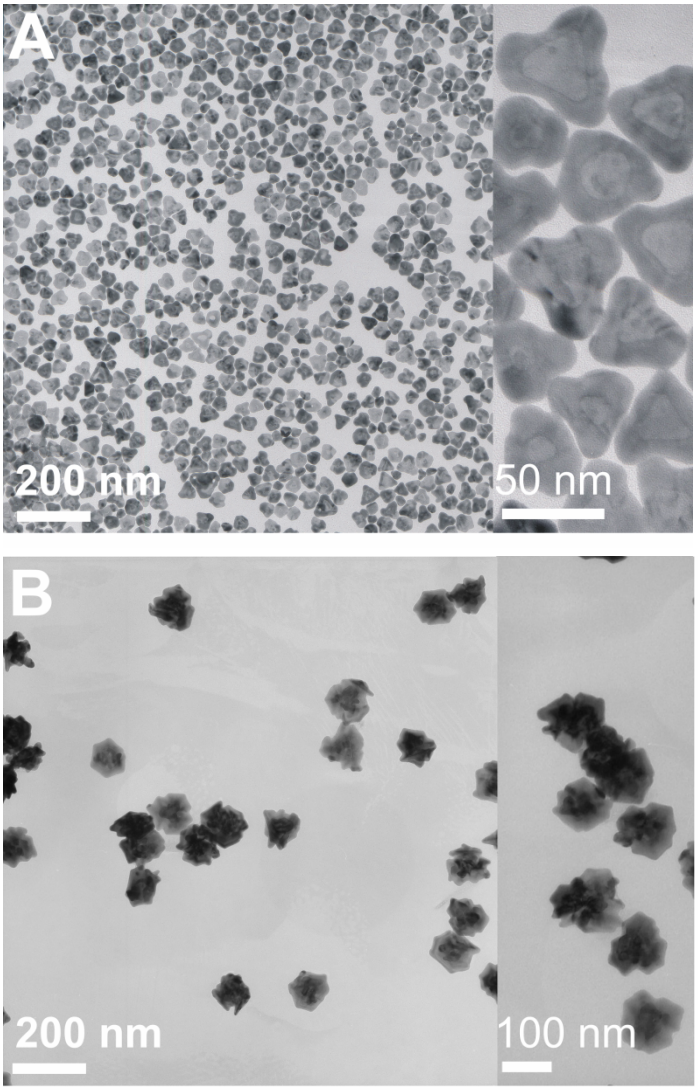
A
200 nm
50 nm
B
200 nm
100 nm

Figure 6.2. TEM images of spherical Ag/Au core-shell nanoparticles with Ag^{+}/Au^{3+} ion mole ratios of (A) 1:5, (B) 1:13, (C) 1:40, and (D) 1:100.

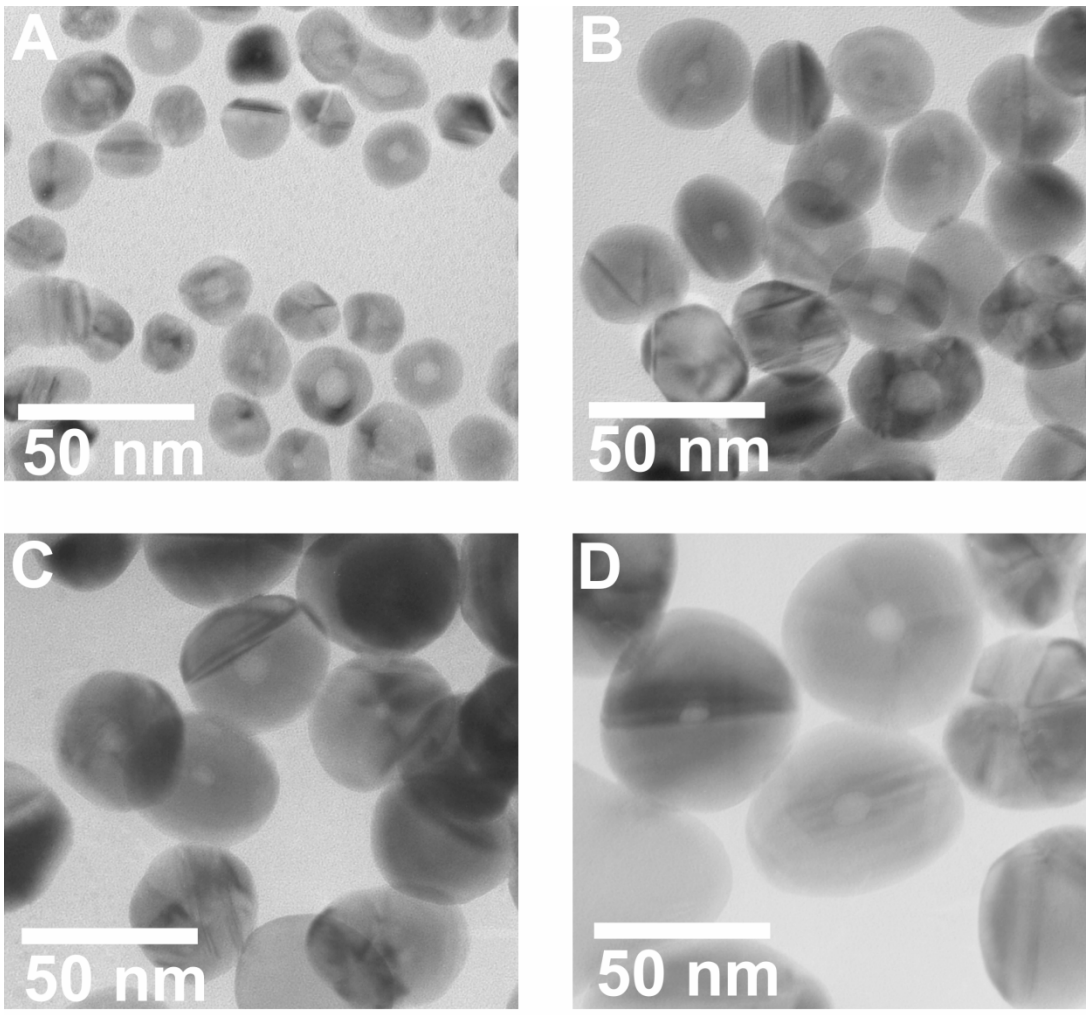
A
50 nm
B
50 nm
C
50 nm
D
50 nm

with a corrugated surface, **Figure 6.1B** and inset. The degree of roughness increases with increasing Au ion content. Others have observed similar surface morphologies with hollow alloy materials made of Ag and Au.[26] Interestingly, this effect that results in the formation of the architectures with the roughened surfaces is not observed with spherical particles, regardless of the use of comparable conditions. In such cases, only core-shell structures with smooth surface coatings are obtained, **Figure 6.2**. Unlike the spherical bimetallic core-shell nanostructures, the core and shell boundaries of the nanoparticles produced using silver prism seeds are only clearly distinguishable with solutions containing a higher silver prism content (**Figure 6.1**). Moreover, the sizes of the triangular cores are smaller compared to the Ag prism seed that was used, 25 nm and 60 nm, respectively. The decrease in size of the resulting silver cores results from the oxidation of silver by Au^{3+}.[16, 27-28] Unlike our previous report on the synthesis of triangular nanoframes,[29] wherein L-ascorbic acid was not added to the growth solution, complete dissolution of the silver prism core is not observed.

In both the cases of the structures with corrugated surfaces and the gold-coated prisms, the size of the final structures can be controlled over the 45-150 nm range, Table 1. Size in the case of the nanoprisms is determined by measuring the distance from the apex of the prism to the middle of its opposite side. In the case of the structures with corrugated surfaces, on the other hand, an average diameter was used. The size of the core-shell structure is dictated by the thickness of the coating obtained, which depends directly on the gold ion to silver prism mole ratio. A decrease in silver prism content favors structures with thicker Au coatings.

In **Figure 6.3**, we show the typical extinction spectra for the resulting triangular and corrugated shaped Ag/Au core-shell nanoparticles and Ag prism seeds. The near-instantaneous

Table 6.1. Average Sizes of Core-shell Nanoparticles.

Ag seed shape	Ag(I):Au(III)	Average Diameter (nm)	Average core (nm)	Average shell (nm)
Spherical	1:5	21.5 ± 3.6	8.0 ± 1.9	6.5 ± 1.8
	1:10	26.6 ± 3.9	8.4 ± 2.3	8.9 ± 1.6
	1:13	29.4 ± 2.4	8.2 ± 1.6	10.6 ± 1.8
	1:20	34.4 ± 2.9	8.3 ± 1.5	12.7 ± 1.6
	1:40	46.2 ± 3.9	8.3 ± 1.3	19.1 ± 2.3
	1:100	62.3 ± 6.8	8.2 ± 1.6	27.1 ± 3.6
Prism	1:5	49.3 ± 5.6	24.1 ± 6.4	11.9 ± 2.1
	1:13	87.9 ± 12.1		
	1:25	111.6 ± 10.7		
	1:33	117.7 ± 12.4		
	1:50	150.7 ± 17.2		

Ag spherical seed size = 8.1 ± 2.0
Ag prism seed size = 60 ± 15

Figure 6.3. UV-vis spectra of (A) silver prism seed solution (particle size ≈ 60 ± 15 nm), (B) time-evolution of gold shell formation on the silver prism surface (Ag^{+}/Au^{3+} = 1:5, at t = 2 min to t = 30 min with 2 min interval), (C) prism and corrugated shaped core-shell nanoparticles (increasing Au content corresponds to increasing wavelength, Ag^{+}/Au^{3+} = 1:5, 1:13, 1:25, 1:33, 1:50, 1:100) and (D) their respective absorbance growth over time.

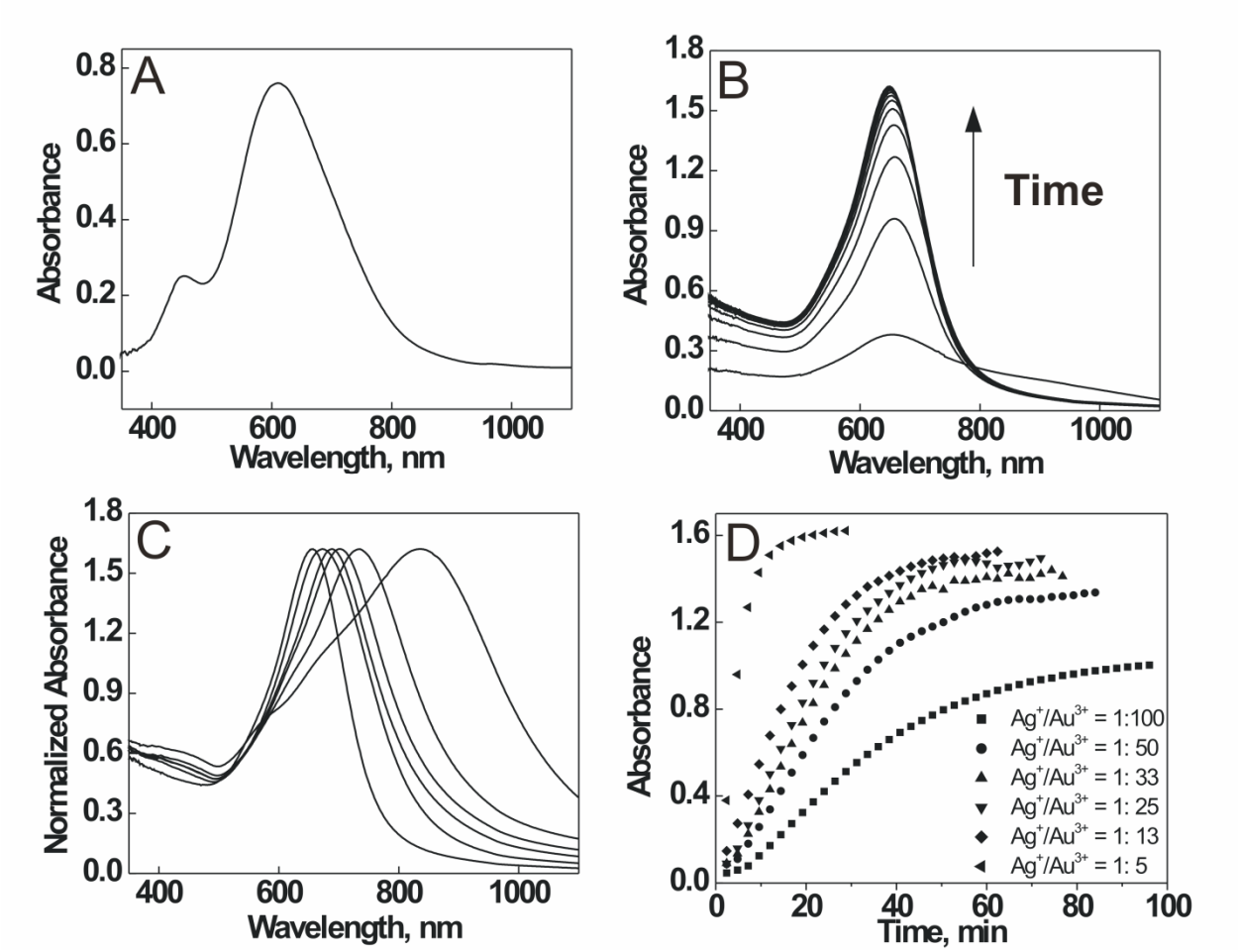
A
Absorbance
Wavelength, nm
B
Absorbance
Time
Wavelength, nm
C
Normalized Absorbance
Wavelength, nm
D
Absorbance
Time, min
Ag+/Au3+ = 1:100
Ag+/Au3+ = 1: 50
Ag+/Au3+ = 1: 33
Ag+/Au3+ = 1: 25
Ag+/Au3+ = 1: 13
Ag+/Au3+ = 1: 5

formation of the Au shell on the surface of the Ag seeds results in the dampening of the in-plane quadrupole resonance surface plasmon (SP) peak of the Ag seed at 460 nm (**Figure 6.3A**) as observed in the absorption spectra of the growth solution as a function of time (**Figure 6.3B**). An increase in the absorbance at 650 nm is observed as the nanoshell growth progresses (Ag^{+}/Au^{3+}=1:5, **Figure 6.3B**). The SP peak of particles prepared with high Ag to Au ion mole ratio lies at shorter wavelengths (Ag^{+}/Au^{3+}=1:5, 650 nm) than particles with a lower ratio (Ag^{+}/Au^{3+}=1:100, 840 nm). All of the observed spectra are red-shifted compared to the plasmon resonance of pure Au nanoparticles (d ≈13 nm) at 520 nm and the in-plane dipole resonance SP peak of pure Ag prism seeds at 600 nm. Based on the TEM images and the corresponding extinction spectra of the core-shell stuctures, the optical response of the synthesized core-shell nanoparticles produced depends upon the particle size and shape. The corrugated structures exhibit plasmon resonaces which are red-shifted from the absorbance for the gold-coated prisms (**Figure 6.3C**). This correlates well with previous reports where core-shell particles with large dimensions absorb in the visible and near-IR spectral region.[30-31] Moreover, the rates of the reactions are dependent upon the Ag/Au ratio with the fastest rates observed for higher Ag^{+}/Au^{3+} ion mole ratios (**Figure 6.3D**).

Figure 6.4 shows representative energy-dispersive X-ray spectroscopy (EDX) spectra of the Ag/Au core-shell nanoparticles. All peaks corresponding to Au increase for solutions of core-shell particles containing higher gold content. This is consistent with TEM and UV-vis data for such structures which show that an increase in the amount of Ag prism seed added to the growth solution, results in core-shell nanoparticles with smaller Au shells.

Figure 6.4. EDX spectra of Ag/Au core-shell nanoparticles prepared with (A) 5000 μL (Ag^{+}/Au^{3+} = 1:5), (B) 750 μL (Ag^{+}/Au^{3+} = 1:33) , and 250 μL (Ag^{+}/Au^{3+} = 1:100) of Ag prism seeds. Cu and Si peaks are due to Cu grid and EDX detector, respectively.

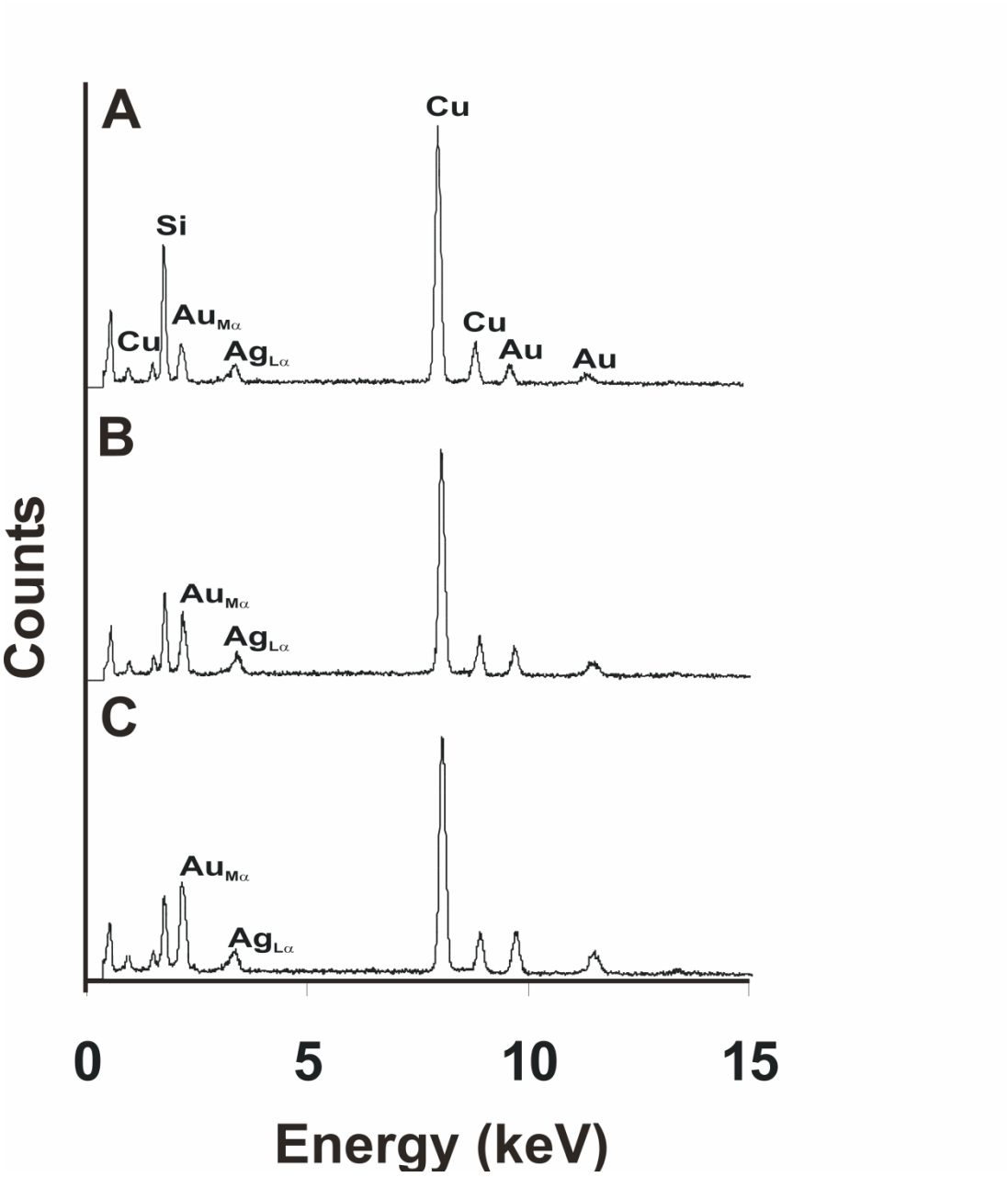
A
Cu
Si
Au$_{M\alpha}$
Cu
Ag$_{L\alpha}$
Cu
Au
Au
B
Au$_{M\alpha}$
Ag$_{L\alpha}$
C
Au$_{M\alpha}$
Ag$_{L\alpha}$
Counts
0
5
10
15
Energy (keV)

6.4. CONCLUSION

I have shown that triangular and corrugated core-shell nanoparticles can be synthesized using a seed mediated growth approach. The optical properties and physical attributes (shapes and sizes) of these core-shells can be tailored using various stoichiometric ratios of silver and gold. Owing to the highly roughened surfaces of the corrugated core-shell nanoparticles, they may exhibit better enhancement in surface enhanced raman spectroscopy (SERS) compared to other analogous nanoparticles with smooth surfaces. Moreover, these structures with gold coatings can now be studied for their potential use as building blocks for functional materials such as diagnostic labels and therapeutic agents.

REFERENCES

REFERENCES FOR CHAPTER 1

1. Love, J. C.; Estroff, L. A.; Kriebel, J. K.; Nuzzo, R. G.; Whitesides, G. M. *Chem. Rev.* **2005**, *105*, 1103.

2. Gates, B. D.; Xu, Q. B.; Stewart, M.; Ryan, D.; Willson, C. G.; Whitesides, G. M. *Chem. Rev.* **2005**, *105*, 1171.

3. Park, S. J.; Taton, T. A.; Mirkin, C. A. *Science* **2002**, *295*, 1503.

4. Elghanian, R.; Storhoff, J. J.; Mucic, R. C.; Letsinger, R. L.; Mirkin, C. A. *Science* **1997**, *277*, 1078.

5. Taton, T. A.; Mirkin C. A.; Letsinger, R. L. *Science* **2000**, *289*, 1757.

6. Jin, R.; Cao, Y. C.; Hao, E.; Metraux, G. S.; Schatz, G. C.; Mirkin, C. A. *Nature* **2003**, *425*, 487.

7. Jin, R.; Cao, Y.; Mirkin, C. A.; Kelly, K. L.; Schatz, G. C.; Zheng, J. G. *Science* **2001**, *294*, 1901.

8. Cao, R,; Jin, R.; Mirkin, C. A. *J. Am. Chem. Soc.* **2001**, *123*, 7961.

9. Bogunia-Kubik, K.; Sugisaka, M. *Biosystems* **2002**, *65*, 123.

10. Muller, W. T.; Klein, D. L; Lee, T.; Clarke, J.; Mceuen, P. L.; Schultz, P. G. *Science* **1995**, *268*, 272.

11. Li, X. M.; Paraschiv, V.; Huskens, J.; Reinhoudt, D. N. *J. Am. Chem. Soc.* **2003**, *125*, 4279.

12. Alberts, B.; Johnson, A.; Lewis, J.; Raff, M.; Roberts, K.; Walters, P. *Molecular Biology of the Cell*. 4th ed.; Garland Science: London, **2002.**

13. El-Sayed, M. A. *Acc. Chem. Res.* **2001**, *34*, 257.

14. Link, S.; El-Sayed, M. A. *J. Phys. Chem. B* **1999**, *103*, 8410.

15. Barbucci, R.; Pasqui D.; Wirsen, A.; Affrossman, S.; Curtis, A.; Tetta, C. *J. Mater. Sci. Mater. Med.* **2003**, *14*, 721.

16. Marrian, C. R. K.; Tennant, D. M. J. *J. Vacuum Sci. Tech. A* **2003**, *21*. S207.

17. Wallraff, G. M.; Hinsberg, W. D. *Chem. Rev*. **1999,** *99*, 1801.

18. Kumar, A.; Whitesides, G. M. *Science* **1994**, *263*, 60.

19. Xia, Y.; Whitesides, G. M. *Angew. Chem. Int. Ed.* **1998**, *37*, 550.

20. Binnig, G.; Rohrer, H. *Helv. Phys. Acta* **1982**, *55*, 726.

21. Binnig, G.; Quate, C. F.; Gerber, C. *Phys. Rev. Lett.* **1986**, *56*, 930.

22. Lyo, L.-W.; Avocerie, P. *Science*, **1989**, *245, 1369.*

23. Eigler, D. M.; Schweizer, E. K. *Nature* **1990**, *344*, 524.

24. Jaschke, M.; Butt, H. J. *Langmuir* **1995**, *11*, 10

25. Piner, R. D.; Mirkin, C. A. *Langmuir* **1997**, *13*, 6864.

26. Weeks, B. L.; DeYoreo, J. J. *J. Phy. Chem. B.* **2006**, *110*, 10231.

27. Liu, X.; Guo, S.; Mirkin, C. A. *Angew. Chem. Int. Ed.* **2003,** *42*, 4785-4789.

28. Lim, J.-H.; Mirkin, C. A. *Adv. Mater.* **2002,** *14*, 1474-1477.

29. Noy, A.; Miller, A. E.; Klare, J. E.; Weeks, B. L.; Woods, B. W.; De Yoreo, J. J. *Nano Lett.* **2002,** *2*, 109-112.

30. Liu, X.; Zhang, Y.; Goswami, D. K.; Okasinski, J. S.; Salaita, K.; Bedzyk, M. J.; Mirkin, C. A. *Science* **2004,** *307*, 1763-1766.

31. Lee, K.-B.; Park, S.-J.; Mirkin, C. A.; Smith, J. C.; Mrksich, M. *Science* **2002,** *295*, 1702-1705.

32. Liu, X.; Fu, L.; Hong, S.; Dravid, V. P.; Mirkin, C. A. *Adv. Mater.* **2002,** *14*, 231-234.

33. Su, M.; Liu, X.; Li, S.-Y.; Dravid, V. P.; Mirkin, C. A. *J. Am. Chem. Soc.* **2002,** *124*, 1560-1561.

34. Vega, R. A.; Maspoch, D.; Salaita, K.; Mirkin, C. A. *Angew. Chem. Int. Ed.* **2005,** *44*, 6013-6015.

35. Hong, S.; Mirkin, C. A. *Science* **2000,** *288*, 1808-1811.

36. Hong, S.; Zhu, J.; Mirkin, C. A. *Science* **1999,** *286*, 523-525.

37. Zhang, H.; Jin, R.; Mirkin, C. A. *Nano Lett.* **2004,** *4*, 1493-1495.

38. Ivanisevic, A.; Mirkin, C. A. *J. Am. Chem. Soc.* **2001,** *123*, 7887-7889.

39. Jung, H.; Kulkarni, R.; Collier, C. P. *J. Am. Chem. Soc.* **2003,** *125*, 12096.

40. Pena, D. J.; Raphael, M. P.; Byers, J. M. *Langmuir* **2003,** *19*, 9028.

41. Salaita, K.; Lee, S. W.; Wang, X.; Huang, L.; Dellinger, T. M.; Liu, C.; Mirkin, C. A. *Small* **2005,** *1*, 940.

42. Salaita, K.; Wang, Y.; Fragala, J.; Vega, R. A.; Liu, C.; Mirkin, C. A. *Angew. Chem. Int. Ed.* **2006,** *45*, 7220.

43. Miller, U. R.; Nicolau, D. V. *Microarray Technology and Its Applications.* Springer: New York, **2005.**

44. Ye, S.; Day, I. N. M. *Microarrays & Microplates*. Bios Scientific: Oxford, **2003.**

45. Vijayendran, R. A.; Leckband, D. E. *Anal. Chem.* **2001**, *73*, 471.

46. Nakanishi, K.; Muguruma, H.; Karube, I. *Anal. Chem.* **1996**, *68*, 1695.

47. Hoffman, W. L.; O'Shannessy, D. J. *J. Immunol. Meth.* **1988**, *112*, 113.

48. Lee, S. W.; Sanedrin, R. G.; Oh, B. K.; Mirkin, C. A. *Adv. Mater.* **2006**, *17*, 2749.

49. Vega, R. A.; Maspoch, D.; Shen, C. K. –F.; Kakkassery, J. J.; Chen, B. J.; Lamb, R. A.; Mirkin, C. A. *Chembiochem* **2006**, Early View.

50. Iler, R. K. *J. Colloid Interf. Sci.* **1966**, *21*, 569.

51. Decher, G. *Science* **1997**, *277*, 1232.

52. Decher, G.; Hong, J. D. *Makromol. Chem. Macromol. Symp.* **1991**, *46*, 321.

53. Decher, G.; Lehr, K.; Lowack, K.; Lvov, Y.; Schmitt, J. *Biosens. Bioelect.* **1994**, *9*, 677.

54. Kotov, N. A.; Dekany, I.; Fendler, J. H. *J. Phys. Chem.* **1995**, *99*, 13065.

55. Lee, G. S.; Lee, Y. J.; Yoon, K. B. *J. Am. Chem. Soc.* **2001**, *123*, 9769.

56. Keller, S. W.; Kim, H.-N.; Mallouk, T. E. *J. Am. Chem. Soc.* **1994**, *11*, 8817.

57. Ferreira, M.; Rubner, M. F. *Macromolecules* **1995**, *28*, 7107.

58. Tsukruk, V. V.; Rinderspacher, F.; Bliznyuk, V. N. *Langmuir* **1997**, *13*, 2171.

59. Lvov, Y.; Haas, H.; Decher, G. *Langmuir* **1994**, *10*, 4232.

60. Shi, X. Y.; Sanedrin, R. G.; Zhou, F. M. *J. Phys. Chem. B* **2002**, *106*, 1173.

61. Xia, Y.; Zhao, X.-M.; Whitesides, G. M. *Microelectron. Eng.* **1996**, *32*, 255.

62. Geissler, M.; Wolf, H.; Strutz, R.; Delamarche, E.; Grummt, U.-W.; Michel, B.; Bietsch, A. *Langmuir* **2003**, *19*, 6301.

63. Salaita, K. S.; Lee, S. W.; Ginger, D. S.; Mirkin, C. A. *Nano Lett.* **2006,** *6*, 2493-2498.

64. Jana, N. R.; Gearheart L.; Murphy, C. J. *J. Phys. Chem. B* **2001**, *105*, 4065.

65. Murphy, C. A.; Sau, T. K.; Gole, A. M.; Orendorff, C. J.; Gao, J.; gou L.; Hunyadi, S. E.; Li, T. *J. Phys. Chem. B* **2005**, *109*, 13857.

66. Millstone, J. E.; Park, S.; Shufford, K. L.; Qin, L.; Schatz, G. C.; Mirkin, C. A. *J. Am. Chem. Soc.* **2005**, *127*, 5312.

REFERENCES FOR CHAPTER 2

1. MacBeath, G.; Schreiber, S. L. *Science* **2000**, *289*, 1760.

2. MacBeath, G.; Koehler, A. N.; Schreiber, S. L. *J. Am. Chem. Soc.* **1999**, *121*, 7967.

3. Zhu, H.; Bilgin, M.; Bangham, R.; Hall, D.; Casamayor, A.; Bertone, P.; Lan, N.; Jansen, R.; Bidlingmaier, S.; Houfek, T.; Mitchell, T.; Miller, P.; Dean, R. A.; Gerstein, M.; Snyder, M. *Science* **2001**, *293*, 2101.

4. Kane, R. S.: Yakayama, S.; Ostuni, E.; Ingber, D. E.; Whitesides, G. M. *Biomaterials* **1999**, *20*, 2363.

5. Blawas, A. S.; Reichert, W. M. *Biomaterials* **1998**, *19*, 595.

6. Brooks, S. A.; Dontha, N.; Davis, C. B.; Stuart, J. K.; O'Neill, G.; Khun, W. G. *J. Am. Chem. Soc.* **1999**, *121*, 8044.

7. Ng, H. T.; Fang, A.; Huang, L.; Li, S. F. Y. *Langmuir* **2002**, *18*, 6324.

8. Falconnet, D.; Koenig, A.; Assi, S.; Textor, M. *Adv. Funct. Mater.* **2004**, *14*, 749.

9. Hergenrother, P. J.; Depew, K. M.; Schreiber, S. L. *J. Am. Chem. Soc.* **2000**, *122*, 7849.

10. Yam, C. M.; Gu, J.; Li, S.; Cai, C. *J. Colloid. Interf. Sci.* **2005**, *285*, 711.

11. Wilcop, T.; Wang, Z.; Cheng, Q. *Langmuir* **2004**, *20*, 1114.

12. Jun, Y.; Cha, T.; Guo, A.; Zhu, X.-Y. *Biomaterials* **2004**, *25*, 3503.

13. St. John, P. M; Davis, R.; Cady, N.; Czajka, J.; Batt, C. A.; Craihead, H. G. *Anal. Chem.* **1998**, *70*, 1108.

14. Tan, J. L.; Tien, J.; Chen, C. S. *J. Am. Chem. Soc.* **2002**, *18*, 519.

15. Bernard, A.; Delamarche, E.; Schmid, H.; Michel, B.; Bosshard, H. R.; Biebuyck, H. *Langmuir* **1998**, *14*, 2225.

16. Dulcey, C. S.; Georger, Jr., J. H.; Krauthamer, V.; Stenger, D. A.; Fare, T. L.; Calvert, J. M. *Science* **1991**, *252*, 551.

17. Biebricher, A.; Paul, A.; Tinnefeld, P.; Golzhauser, A.; Sauer, M. *J. Biotechnol.* **2004**, *112*, 97.

18. Xu, P.; Uyama, H.; Whitten, J. E.; Kobayash, S.; Kaplan, D. L. *J. Am. Chem. Soc.* **2005**, *127*, 11745.

19. Xu, P.; Kaplan, D. L. *Adv. Maters.* **2004**, *16*, 628.

20. Li, X. M.; Huskens, J.; Reinhoudt, D. N. *J. Mater. Chem.* **2004**, *14*, 2954.

21. Peter, M,; Li, X. M.; Huskens, J.; Reinhoudt, D. N. *J. Am. Chem. Soc.* **2004**, *126*, 11684.

22. Kenseth, J. R.; Harnisch, J. A.; Jones, V. W.; Porter, M. D. *Langmuir* **2001**, *17*, 4105.

23. Agarwal, G.; Sowards, L. A.; Naik, R. R.; Stone, M. O. *J. Am. Chem. Soc.* **2003**, *125*, 580.

24. Wadu-Mesthrige, K.; Xu, S.; Amro, N. A.; Liu, G. *Langmuir* **1999**, *15*, 8580.

25. Lee, K.-B.; Kim, E.-Y.; Mirkin, C. A.; Wolinsky, S. M. *Nano Lett*. **2004**, *4*, 1869.

26. Lee, K.-B.; Park, S.-J.; Mirkin, C. A.; Smith, J. C.; Mrksich, M. *Science* **2002**, *295*, 1702.

27. Wilson, D. L.; Martin, R.; Hong, S.; Cronin-Golomb, M.; Mirkin, C. A.; Kaplan, D. L. *Proc. Natl. Acad, Sci. USA.* **2001**, *98*, 13660. b) J.-H.

28. Lim, J.-H.; Ginger, D. S.; Lee, K.-B.; Heo, J.; Nam, J.-M.; Mirkin, C. A. *Angew. Chem. Int. Ed.* **2003**, *42*, 2309.

29. Nam, J.-M.; Han, S. W.; Lee, K.-B.; Liu, X.; Ratner, M. A.; Mirkin, C. A. *Angew. Chem. Int. Ed.* **2004**, *43*, 1246.

30. Lee, K.-B.; Lim, J.-H.; Mirkin, C. A. *J. Am. Chem. Soc.* **2003**, *125*, 5588.

31. Demers, L. M.; Ginger, D. S.; Park, S.-J.; Li, G.; Chung, S. W.; Mirkin, C. A. *Science* **2002**, *296*, 1836.

32. Vega, R. A.; Maspoch, D.; Salaita, K.; Mirkin, C. A. *Angew. Chem. Int. Ed.* **2005**, *44*, 6013.

33. Piner, R. D.; Zhu, J.; Xu, F.; Hong, S.; Mirkin, C. A. *Science* **1999**, *283*, 661.

34. Hong, S.; Zhu, J.; Mirkin, C. A. *Science* **1999**, *286*, 523.

35. Hong, S.; Mirkin, C. A. *Science* **2000**, *288*, 1808.

36. Ginger, D. S.; Zhang, H.; Mirkin, C. A. *Angew. Chem. Int. Ed.* **2004**, *43*, 30.

37. Liu, G. Y.; Xu, S.; Qian, Y. L. *Acc. Chem. Res*. **2000**, *33*, 457.

38. Liu, X.; Zhang, Y.; Goswami, D. K.; Okasinski, J. S.; Salaita, K. S.; Sun, P.; Bedzyk, M. J.; Mirkin, C. A. *Science* **2005**, *307*, 1763.

39. Salaita, K.; Lee, S. W.; Wang, X.; Huang, L.; Dellinger, T. M.; Liu, C.; Mirkin, C. A. *Small* **2005**, *1*, 940.

40. Lee, S. W.; Sanedrin, R. G.; Ho, B.-K.; Mirkin, C. A. *Adv. Mater. in press.*

41. Zhang, M.; Bullen, D.; Chung, S.-W.; Hong, S.; Ryu, K. S.; Fan, Z.; Mirkin, C. A.; Liu, C. *Nanotechnology* **2002**, *13*, 212.

42. Bullen, D.; Chung, S.-W.; Wang, X.; Zou, J.; Mirkin, C. A.; Liu, C. *Appl. Phys. Lett.* **2004**, *84*, 789.

43. Service, R. F. *Science* **2002**, *298*, 2322.

44. Aybay, C. *Immunol. Lett.* **2003**, *85*, 231.

45. Owaku, K.; Goto, M.; Ikariyama, Y.; Aizawa, M. *Anal. Chem.* **1995**, *67*, 1613.

46. Boyle, M. D. P.; Reis, K. J. *Biotechnol.* **1987**, *5*, 697.

47. Johnson, C. P.; Jensen, I. E.; Prakasam, A.; Vijayendran, R.; Leckband, D. *Bioconjugate Chem.* **2003**, *14*, 974.

48. Vijayendran, R. A.; Leckband, D. E. *Anal. Chem.* **2001**, *73*, 471.

49. Lynch, M.; Mosher, C.; Huff, J.; Nettikadan, S.; Johnson, J.; Henderson, E. *Proteomics* **2003**, *4*, 1695.

50. P-Grosdemange, C.; Simon, E. S.; Prime, K. L.; Whitesides, G. M. *J. Am. Chem. Soc.* **1991**, *113*, 12.

51. Prime, K. L.; Whitesides, G. M. *J. Am. Chem. Soc.* **1993**, *115*, 10714.

52. Smith, J. C.; Lee, K.-B.; Wang, Q.; Finn, M. G.; Johnson, J. E.; Mrksich, M.; Mirkin, C. A. *Nano Lett.* **2003**, *3*. 883.

53. Yin, H. B.; Brown, T.; Wilkinson, J. S.; Eason, R. W.; Melvin, T. *Nucleic Acids Res.* **2994**, *32*, e118.

54. Zheng, T.; Peelen, D.; Smith, L. *J. Am. Chem. Soc.* **2005**, *127*, 9982.

55. Wagner, P.; Zaugg, F.; Kernen, P.; Hegner, M.; Semenza, G. *J. Vac. Sci. Technol. B* **1996**, *14*, 1466.

56. Cabrita, J. F.; Abrantes, L. M.; Viana, A. S. *Electrichim. Acta* **2005**, *50*, 2117.

57. Degenhart, G. H.; Dordi, B.; Schonherr, H.; Vacso, G. J. *Langmuir* **2004**, *20*, 6216.

58. Cleveland, J. P.; Anczykowski, B.; Schmid, A. E.; Elings, V. B. *Appl. Phys. Lett.* **1998**, *72*, 2613.

59. Browning-Kelley, M. E.; Waud-Mesthrige, K.; Hari, V.; Liu, G.-Y. *Langmuir* **1997**, *13*, 343.

60. Waud-Mesthrige, K.; Amro, N. A.; Garno, J. C.; Xu, S.; Liu, G. *Biophys. J.* **2001**, *80*, 1891.

61. Vijay-Kumar, S.; Bugg, C. E.; Cook, W. J. *J. Mol. Biol.* **1987**, *194*, 531.

REFERENCES FOR CHAPTER 3

1. Vega, R. A.; Maspoch, D.; Salaita, K.; Mirkin, C. A. *Angew. Chem. Int. Ed.* **2005**, *44*, 6013.

2. Smith, J. C.; Lee, K.-B.; Wang, Q.; Finn, M. G.; Johnson, J. E.; Mrksich, M.; Mirkin, C. A. *Nano. Lett.* **2003**, *3*, 883.

3. Kuznetsov, Y. G.; Victoria, J. G.; Low, A.; Robinson, Jr., W. E.; Fan, H.; McPherson, A. *Scanning* **2004**, *26*, 209.

4. Kuznetsov, Y. G.; Victoria, J. G.; Robinson, Jr., W. E.; McPherson, A. *J. Virol.* **2003**, *77*, 11896.

5. Wilk, T.; Fuller, S. D. *Curr. Opin. Struc. Biol.* **1999**, *9*, 231.

6. Starcich, B. R.; Hahn, B. H.; Shaw, G. M.; McNeely, P. D.; Modrow, S.; Wolf, H.; Parks, E. S.; Parks, W. P.; Josephs, S. F.; Gallo, R. C.; Wong-Staal, F. *Cell* **1986**, *45*, 637.

7. Wyatt, R.; Sodroski, J. *Science* **1998**, *280*, 1884.

8. Huang, C.; Tang, M.; Zhang, M.-Y.; Majeed, S.; Montabana, E.; Stanfield, R. L.; Dimitrov, D. S.; Kober, B.; Sodroski, J.; Wilson, I. A.; Wyatt, R.; Kwong, P. D. *Science* **2005**, *310*, 1025.

9. Whetsell, A. J.; Drew, J. B.; Milman, G.; Hoff, R.; Dragon, E. A.; Adler, K.; Hui, J.; Otto, P.; Gupta, P.; Farzadegan, H.; Wolinksy, S. M. *J. Clin. Microbiol.* **1992**, *30*, 845.

10. Patterson, B. K.; Till, M.; Otto, P.; Goolsby, C.; Furtado, M. R.; McBride L. J.; Wolinsky, S. M.. *Science* **1993**, *260*, 976.

11. Gupta, P.; Ding, M.; Cottrill, M.; Rinaldo, C.; Kingsley, L.; Wolinsky, S.; Mellors, J. *J. Clin. Microbiol.* **1995**, *33,* 1670.

12. Ganeshan, S.; Dickover, R. E.; Korber, B. T. M.; Bryson, Y. J.; Wolinsky, S. M. *J. Virol.* **1996**, *71*, 663.

13. Patterson, B. K.; Till, M.; Otto, P.; Goolsby, C.; Furtado, M. R.; McBride, L. J.; Wolinsky, S. M. *Science* **1993**, *260*, 976.

14. Lee, K.-B.; Kim, E.-Y.; Mirkin, C. A.; Wolinsky, S. M. *Nano. Lett.* **2004**, *4*, 1869.

15. Vega, R. A.; Maspoch, D.; Shen, C. K. –F.; Kakkassery, J. J.; Chen, B. J.; Lamb, R. A.; Mirkin, C. A. *Chembiochem* **2006**, Early View.

16. Burton, D. R.; Stanfield, R. L.; Wilson, I. A. *Proc. Natl. Acad. Sci USA.* **2005**, *102*, 14943.

17. Nyambi, P. N.; Gorny, M. K.; Bastiani, L.; van der Groen, G.; Williams, C.; Zolla-Pazner, S. *J. Virol* **1998**, *72*, 9384.

18. Sattentau, Q. J.; Zolla-Pazner, S.; Poignard, P. *Virology* **1995**, *206*, 713.

19. Zwick, M. B.; Labrijn, A. F.; Wang, M.; Splenlehauer, C.; Saphire, E. O.; Binley, J. M.; Moore J. P.; Stiegler, g.; Katinger, H.; Burton, D. R. ; Parren, P. W. H. I. *J. Virol.* **2001**, *75*, 10892.

20. Fauci, A. *Nat. Med.* **2003**, *9*, 839.

21. Trkola, A.; Purtscher, M.; Muster, T.; Ballaun, C.; Buchacher, A.; Sullivan, N.; Srinivasan, K.; Sodroski, J.; Moore, J. P.; Katinger, H. *J. Virol.* **1996**, *70*, 1100.

22. Calarese, D. A.; Scanlan, C. N.; Zwich, M. B.; Ceechongkit, S.; Minura, Y.; Kunert R.; Zhu, P.; Wormald, M. R.; Stanfield, R. L.; Roux, K. H.; Kelly, J. W.; Rudd, P. M.; Dwek, R. A.; Katinger, H.; Burton, D. R.; Wilson, I. A. *Science* **2003**, *300*, 2065.

REFERENCES FOR CHAPTER 4

1. Park, S. J.; Taton, T. A.; Mirkin, C. A. *Science* **2002**, *295*, 1503.

2. Jin, R.; Cao, Y.; Mirkin, C. A.; Kelly, K. L.; Schatz, G. C.; Zheng, J. G. *Science* **2001**, *294*, 1901.

3. Cao, Y.; Jin, R.; Mirkin, C. A. *J. Am. Chem. Soc.* **2001**, *123*, 7961.

4. Muller, W. T.; Klein, D. L.; Lee, T.; Clarke, J.; Mceuen, P. L.; Schultz, P. G. *Science* **1995**, *268*, 272.

5. Li, X. M.; Paraschiv, V.; Huskens, J.; Reinhoudt, D. N. *J. Am. Chem. Soc.* **2003**, *125*, 4279.

6. Elghanian, R.; Storhoff, J. J.; Mucic, R. C.; Letsinger, L.; Mirkin, C.A. *Science* **1997**, *277*, 1078.
7. Taton, T.; Mirkin, C. A.; Letsinger, R. L. *Science* **2000**, *289*, 1757.

8. Bogunia-Kubik, K.; Sugisaka, M. *Biosystems* **2002**, *65*, 123.

9. Barbucci, R.; Pasqui, D.; Wirsen, A.; Affrossman, S.; Curtis, A.; Tetta, C. *J. Mater. Sci. Mater. Med.* **2003**, *14*, 721.

10. Kumar, A.; Whitesides, G. M. *Science* **1994**, *263*, 60.

11. Xia, Y.; Whitesides, G. M. *Angew. Chem. Int. Ed.* **1998**, *37*, 550.

12. Xia, Y.; Rogers, J. A.; Paul, K. E.; Whitesides, G. M. *Chem. Rev.* **1999**, *99*, 1823.

13. Wallraff, G. M.; Hinsberg, W. D. *Chem. Rev.* **1999**, *99*, 1801 and references therein.

14. Chou, S. Y. *MRS Bull.* **2001**, *26*, 512

15. Piner, R. D.; Zhu, J.; Xu, F.; Hong, S.; Mirkin, C. A. *Science* **1999**, *283*, 661.

16. Hong, S.; Zhu, J.; Mirkin, C. A. *Science* **1999**, *286*, 523.

17. Hong, S.; Mirkin, C. A. *Science* **2000**, *288*, 1808.

18. Ginger, D. S.; Zhang, H.; Mirkin, C. A.; *Angew. Chem. Int. Ed.* **2004**, *43*, 30.

19. Liu, G. Y.; Xu, S.; Qian, Y. L. *Acc. Chem. Res*. **2000**, *33*, 457.

20. Liu, X.; Zhang, Y.; Goswami, D. K.; Okasinski, J. S.; Salaita, K.; Sun, P.; Bedzyk, M. J.; Mirkin, C. A. *Science* **2005**, *307*, 1763.

21 Zou, J.; Bullen, D.; Wang, X.; Liu, C.; Mirkin, C. A. *Appl. Phys. Lett.* **2003**, *83*, 581.

22. Cheung, C. L.; Camarero, J. A.; Woods, B. W.; Lin, T.; Johnson, J. E.; De Yoreo, J. J. *J. Am. Chem. Soc.* **2003**, *125*, 6848.

23. Maynor, B. W.; Filocamo, S. F.; Grinstaff, M. W.; Liu, J. *J. Am. Chem. Soc.* **2002**, *124*, 522.

24. Lim, J. H.; Mirkin, C. A. *Adv. Mater.* **2002**, *14*, 1474.

25. Demers, L. M.; Ginger, D. S.; Park, S. J.; Li, Z.; Chung, S. W.; Mirkin, C. A. *Science* **2002**, *296*, 1836.

26. Wilson, D. L.; Martin, R.; Hong, S.; Cronin-Golomb, M.; Mirkin, C. A.; Kaplan, D. L. *Proc. Natl. Acad. Sci. U. S. A.* **2001**, *98*, 13660.

27. Lim, J. H.; Ginger, D. S.; Lee, K. B.; Heo, J.; Nam, J. M.; Mirkin, C. A. *Angew. Chem. Int. Ed.* **2003**, *42*, 2309.

28. Su, M.; Liu, X. G.; Li, S. Y.; Dravid, V. P.; Mirkin, C. A. *J. Am. Chem. Soc.* **2002**, *124*, 1560.

29. Zhang, H.; Li, Z.; Mirkin, C. A. *Adv. Mater.* **2002**, *14*, 1472.

30. Decher, G.; Hong, J. D. *Makromol. Chem., Macromol. Symp.* **1991**, *46*, 321.

31. Decher, G. *Science* **1997**, *277*, 1332.

32. Clark, S. L.; Handy, E. S.; Rubner, M. F.; Hammond, P. T. *Adv. Mater.* **1999**, *11*, 1031.

33. Schlenoff, J. B.; Laurent, D.; Ly, H.; Stepp, J. *Adv. Mater.* **1998**, *10*, 347.

34. Cutler, C. A.; Bouguettaya, M.; Reynolds, J. R. *Adv. Mater.* **2002**, *14*, 684.

35. Delongchamp, D. M.; Kastantin, M.; Hammond, P. T. *Chem. Mater.* **2003**, *15*, 1575.

36. Li, S. L.; Jia, Q. X.; Li, A. D. Q. *Chem. Mater.* **2002**, *14*, 1159.

37. DeLongchamp, D. M.; Hammond, P. T. *Chem. Mater.* **2003**, *15*, 1165.

38. Lvov, Y.; Ariga, K.; Ichinose, I.; Kunitake, T. *J. Chem. Soc., Chem. Commun.* **1995**, 2313.

39. Ichinose, I.; Fujiyoshi, K.; Mizuki, S.; Lvov, Y.; Kunitake, T. *Chem. Lett.* **1996**, 257.

40. Mendelsohn, J. D.; Yang, S. Y.; Hiller, J.; Hochbaum, A. I.; Rubner, M. F. *Biomacromolecules* **2003**, *4*, 96.

41. Khopade, A. J.; Caruso, F. *Biomacromolecules* **2002**, *3*, 1154.

42. Zhu, H. G.; Ji, J.; Tan, Q. G.; Barbosa, M. A.; Shen, J. D. *Biomacromolecules* **2003**, *4*, 378.

43. Jiang, X.; Hammond, P. T. *Langmuir* **2000**, *16*, 8501.

44. Jiang, X.; Clark, S. L.; Hammond, P. T. *Adv. Mater.* **2001**, *13*, 1669.

45. Hammond, P. T.; Whitsidesides, G. M. *Macromolecules* **1995**, *28*, 7569.

46. Clark, S. L.; Montague, M. F.; Hammond, P. T. *Macromolecules* **1997**, *30*, 7237.

47. Clark, S. L.; Hammond, P. T. *Adv. Mater.* **1998**, *10*, 1515.

48. Park, J.; Hammond, P. T. *Adv. Mater.* **2004**, *16*, 520.

49. Kidambi, S.; Chan, C.; Lee, I. *J. Am. Chem. Soc.* **2004**, *126*, 4697.

50. Kidambi, S.; Lee, I.; Chan, C. *J. Am. Chem. Soc.* **2004**, *126*, 16286.

51. Huck, W. T. S.; Yan, L.; Stroock, A.; Haag, R.; Whitesides, G. M. *Langmuir* **1999**, *15*, 6862.

52. Hammond, P. T. *Adv. Mater. 2004*, *16*, 1271.

53. Hammond, P. T. *Curr. Opin. Coloid Interface Sci.* **2000**, *4*, 430.

54. Nyamjav, D.; Ivanisevic, A. *Chem. Mater.* **2004**, *16*, 5216.

55. Yu, M.; Nyamjav, D.; Ivanisevic, A. *J. Mater. Chem.* **2005**, *15*, 649.

56. P-Grosdemange, C.; Simon, E. S.; Prime, K. L.; Whitesides, G. M. *J. Am. Chem. Soc.* **1991**, *113*, 12.

57. Prime, K. L.; Whitesides, G. M. *J. Am. Chem. Soc.* **1993**, *115*, 10714.

58. Lee, K.-B.; Park, S. J.; Mirkin, C. A.; Smith, J. C.; Mrksich, M. *Science* **2002**, *295*, 1702.

59. Smith, J. C.; Lee, K.-B.; Wang, Q.; Finn, M. G.; Johnson, J. E.; Mrksich, M.; Mirkin, C. A. *Nano Lett.* **2003**, *3*. 883.

60. Zhang, M.; Bullen, D.; Chung, S.-W.; Hong, S.; Ryu, K. S.; Fan, Z.; Mirkin, C. A.; Liu, C. *Nanotechnology* **2002**, *13*, 212.

61. Bullen, D.; Chung, S.-W.; Wang, X.; Zou, J.; Mirkin, C. A.; Liu, C. *Appl. Phys. Lett.* **2004**, *84*, 789.

62. Service, R. F. *Science* **2002**, *20*, 2322.

REFERENCES FOR CHAPTER 5

1. Ginger, D. S.; Zhang, H.; Mirkin, C. A. *Angew. Chem. Int. Ed.* **2004,** *43*, 30.

2. Piner, R. D.; Zhu, J.; Xu, F.; Hong, S. H.; Mirkin, C. A. *Science* **1999,** *283*, 661.

3. Liu, X.; Guo, S.; Mirkin, C. A. *Angew. Chem. Int. Ed.* **2003,** *42*, 4785.

4. Jung, H.; Kulkarni, R.; Collier, C. P. *J. Am. Chem. Soc.* **2003**, *125*, 12096.

5. Sheehan, P. E.; Whitman, L. J.; King, W. P.: Nelson, B. A. *Appl. Phys. Lett.* **2004**, *85*, 1589.

6. Lim, J.-H.; Mirkin, C. A. *Adv. Mater.* **2002,** *14*, 1474.

7. Liu, X.; Zhang, Y.; Goswami, D. K.; Okasinski, J. S.; Salaita, K.; Bedzyk, M. J.; Mirkin, C. A. *Science* **2004,** *307*, 1763.

8. Noy, A.; Miller, A. E.; Klare, J. E.; Weeks, B. L.; Woods, B. W.; De Yoreo, J. J. *Nano Lett.* **2002,** *2*, 109.

9. Lee, K.-B.; Park, S.-J.; Mirkin, C. A.; Smith, J. C.; Mrksich, M. *Science* **2002**, *295*, 1702.

10. Jung, H.; Dalal, C. K.; Kuntz, S.; Shah, R.; Collier, C. P. *Nano Lett* **2004**, *4*, 2171.

11. Li, B.; Zhang, Y.; Hu, J.; Li, M. *Ultramicroscopy* **2005**, *105*, 312.

12. Lim, J.-H.; Ginger, D. S.; Lee, K.-B.; Hoe, J.; Nam, J.-M.; Mirkin, C. A. *Angew. Chem. Int. Ed.* **2003**, *42*, 2309.

13. Su, M.; Liu, X.; Li, S.-Y.; Dravid, V. P.; Mirkin, C. A. *J. Am. Chem. Soc.* **2002**, *124*, 1560.

14. Liu, X.; Fu, L.; Hong, S.; Dravid, V. P.; Mirkin, C. A. *Adv. Mater.* **2002,** *14*, 231.

15. John, N. S.; Gundiah, G.; Thomas, P. J.; Kulkarni, G. U. *Int, J. Nanosci.* **2005**, *4*, 921.

16. Huang, L.; Chang, Y.-H.; Kakkassery, J. J.; Mirkin, C. A. *J. Phys. Chem. B* **2006**, *110*, 20756.

17. Vega, R. A.; Maspoch, D.; Salaita, K.; Mirkin, C. A. *Angew. Chem. Int. Ed.* **2005,** *44*, 6013.

18. Hong, S.; Mirkin, C. A. *Science* **2000,** *288*, 1808.

19. Hong, S.; Zhu, J.; Mirkin, C. A. *Science* **1999,** *286*, 523.

20. Zhang, H.; Jin, R.; Mirkin, C. A. *Nano Lett.* **2004,** *4*, 1493.

21. Ivanisevic, A.; Mirkin, C. A. *J. Am. Chem. Soc.* **2001,** *123*, 7887.

22. Pena, D. J.; Raphael, M. P.; Byers, J. M. *Langmuir* **2003,** *19*, 9028.

23. Salaita, K.; Lee, S. W.; Wang, X.; Huang, L.; Dellinger, T. M.; Liu, C.; Mirkin, C. A. *Small* **2005,** *1*, 940.

24. Salaita, K.; Wang, Y.; Fragala, J.; Vega, R. A.; Liu, C.; Mirkin, C. A. *Angew. Chem. Int. Ed.* **2006,** *45*, 7220.

25. Zhang, M.; Bullen, D.; Chung, S. W.; Hong, S.; Ryu, K. S.; Fan, Z. F.; Mirkin, C. A.; Liu, C. *Nanotechnology* **2002**, *13*, 212.

26. Love, J. C.; Paul, K. E.; Whitesides, G. M. *Adv. Mater.* **2001,** *13*, 604.

27. Love, J. C.; Estroff, L. A.; Kriebel, J. K.; Nuzzo, R. G.; Whitesides, G. M. *Chem. Rev.* **2005,** *105*, 1103.

28. Weinberger, D. A.; Hong, S.; Mirkin, C. A.; Wessels, B. W.; Higgins, T. B. *Adv. Mater.* **2000**, *12*, 1600.

29. Xia, Y.; Zhao, X.-M.; Kim, E.; Whitesides, G. M. *Chem. Mater.* **1995,** *7*, 2323.

30. Zhang, H.; Chung, S.-W.; Mirkin, C. A. *Nano Lett.* **2003,** *3*, 43.

31. Zhang, H.; Mirkin, C. A. *Chem. Mater.* **2004,** *16*, 1480.

32. Jang, J.-W.; Maspoch, D.; Fujigaya, T.; Mirkin, C. A. *Small* **2007,** *3, 600.*

33. Salaita, K. S.; Lee, S. W.; Ginger, D. S.; Mirkin, C. A. *Nano Lett.* **2006,** *6*, 2493.

34. Zhang, Y.; Salaita, K.; Lim, J.-H.; Lee, K.-B.; Mirkin, C. A. *Langmuir* **2004,** *20*, 962.

35. Lee, K.-B.; Lim, J.-H.; Mirkin, C. A. *J. Am. Chem. Soc.* **2003,** *125*, 5588.

36. Prime, K. L.; Whitesides, G. M. *Science* **1991**, *252*, 1164.

37. Lopez, G. P.; Biebuyck, H. A.; Harter, R.; Kumar, A.; Whitesides, G. M. *J. Am. Chem. Soc.* **1993**, *115*, 10774.

38. Manandhar, P.; Jang, J.; Schatz G. C.: Ratner, M. A.; Hong, S. *Phys. Rev. Lett.* **2003**, *90*, 1155051.

39. Cho, N.; Ryu, S.; Kim, B.; Schatz, G. C.; Hong, S. *J. Chem. Phys* **2006**, *124*, 0247141.

40. Rozhok, S.; Piner, R.; Mirkin, C. A. *J. Phys. Chem. B* **2003**, *107*, 751.

REFERENCES FOR CHAPTER 6

1. Toshima, N.; Harada, M.; Yamazaki, K.; Asakura, K. *J. Phys. Chem.* **1992**, *96*, 9927.

2. Link, S.; Wang, Z. L.; El-Sayed, M. A. *J. Phys. Chem. B* **1999**, *103*, 3529.

3. Link, S.; Burda, C.; Wang, Z. L.; El-Sayed, M. A. *J. Chem. Phys.* **1999**, *111*, 1255.

4. Mallin, M. P.; Murphy, C. J. *Nano Lett.* **2002**, *2*, 1235.

5. Chen, Y. H.; Nickel, U. *J. Chem. Soc., Faraday Trans.* **1993**, *89*, 2479.

6. Freeman, R. G.; Hommer, M. B.; Grabar, K. C.; Jackson, M. A.; Natan, M. J. *J. Phys. Chem.* **1996**, *100*, 718.

7. Aliev, F. G.; Correa-Duarte, M. A.; Mamedov, A.; Ostrander, J. W.; Giersig, M.; Liz-Marzan, L. M.; Kotov, N. A. *Adv. Mater.* **1999**, *11*, 1006.

8. Pastoriza-Santos, I.; Liz-Marzan, L. M. *Langmuir* **1999**, *15*, 948.

9. Cao, Y. W.; Jin, R.; Mirkin, C. A. *J. Am. Chem. Soc.* **2001**, *123*, 7961.

10. Cho, S.-J.; Kauzlarich. S. M.; Olamit, J.; Liu, K.; Grandjean, F.; Rebbouh, L.; Long, G. J. *J. Appl. Phys.* **2004**, *95*, 6804.

11. Lyon, J. L.; Fleming, D. A.; Stone, M. B.; Schiffer, P.; Williams, M. E. *Nano Lett.* **2004**, *4*, 719.

12. Penn, S. G.; He, L.; Natan, M. J. *Anal. Tech.* **2003**, *7*, 609.

13. Mulvaney, P.; Giersig, M.;Henglein, A. *J. Phys. Chem.* **1993**, *97*, 7061.

14. Mulvaney, P. *Langmuir* **1996**, *12*, 788.

15. Rivas, S.; Sanchez-Cortez, S.; Garcia-Ramos, J. V.; Morcillo, G. *Langmuir* **2000**, *16*, 9722.

16. Moskovits, M.; Smova-Sloufova, I.; Vlckova, B. *J. Chem. Phys.* **2002**, *116*, 10435.

17. Marignier, J. L.; Belloni, J.; Delcourt, M. O.; Chevalier, J. P. *Nature* **1985**, *317*, 344.

18. Liu, M.; Guyot-Sionnest, P. *J. Phys. Chem. B* **2004**, *108*, 5882.

19. Jin, R.; Cao, Y.; Mirkin, C. A.; Kelly, K. L.; Schatz, G. C.; Zheng, J. G. *Science* **2001**, *294*, 1901.

20. Jin, R.; Cao, Y. C.; Hao, E.; Metraux, G. S.; Schatz, G. C.; Mirkin, C. A. *Nature* **2003**, *425*, 487.

21. Callegari, A.; Tonti, D.; Chergui, M. *Nano Lett*. **2003**, *3*, 1565.

22. Chen, S.; Carroll, D. *Nano Lett*. **2002**, *2*, 1003.

23. Jana, N. R.; Gearheart, L.; Murphy, C. J. *Chem. Commun.* **2001**, *7*, 617.

24. Busbee, B. D.; Obare, S. O.; Murphy, C. J. *Adv. Mater.* **2003**, *15*, 414.

25. Gao, J.; Bender, C. M.; Murhpy, C. J. *Langmuir* **2003**, *19*, 9065.

26. Jin, Y.; Dong, S. *J. Phys. Chem. B* **2003**, *107*, 12902.

27. Sun, Y.: Xia, Y. *J. Am. Chem. Soc.* **2004**, *126*, 3892.

28. Sun, Y.; Mayers, B.; Xia, Y. *Adv. Mater.* **2003**, *15*, 641.

29. Metraux, G. S.; Cao, Y. C.; Jin, R.; Mirkin, C. A. *Nano Lett*. **2003**, *3*, 519.

30. Aguirre, C. M.; Kaspar, T. R.; Radloff, C.; Halas, N. J. *Nano Lett*. **2003**, *3*, 1707.

31. Oldenburg, S. J.; Averitt, R. D.; Westcott, S. L.; Halas, N. J. J. *Chem. Phys. Lett.* **1998**, *288*, 243.